Ministère de l'Enseignement Supérieur et de la Recherche Scientifique

Université Mohamed Khider - Biskra

Faculté des Sciences et de la Technologie

Département de Génie Électrique

Thèse

Présentée en vue de l'obtention du diplôme de doctorat LMD en Energies Renouvelables

Option : Energies Renouvelables en électrotechnique

Contribution à l'étude et la commande par les techniques avancées d'une GADA dédiée aux centrales électriques éoliennes

"Contribution to the Study and Control Using Advanced Techniques of a DFIG Used in a Wind Farm"

Présentée par :

Toufik Mebkhouta

Soutenue publiquement le : 02 / 07 /2025

Devant le jury composé de :

Zouzou Salah Eddine	Professeur Université de Biskra	Président
GOLEA Amar	Professeur Université de Biskra	Directeur
BOUMARAF Rabia	Professeur Université de Biskra	Co-directeur
Betka Achour	Professeur Université de Biskra	Examinateur
Barra Kamel	Professeur Université de Batna	Examinateur

Dedicates

To **my beloved family**,

To my **dearest mother**, my greatest source of motivation—her unwavering prayers, patience, and unconditional support have been the foundation of my success. Without her strength, I would not be where I am today.

To my **dear father**, whose wisdom and guidance have been a beacon of light throughout my journey, always illuminating my path and inspiring me to persevere.

To my **dear sisters**, whose resilience and unwavering support have brought warmth and joy into my life. Your encouragement and companionship have been invaluable, and I am forever grateful to have you by my side.

To my beloved brothers, **Said, Achraf, and Anes**, my steadfast companion and supporter at every step. Your presence has been a pillar of strength in my life.

To my cherished friends and colleagues, especially **Karboua Djelloul, Douara Ben Ouadeh, Youssef Chouiha, Boussena Abdelbaki and Khadir Abdallah**, **Hicham Sayhi**, who have always stood by me with unwavering support and encouragement thank you for being an essential part of this journey.

To my brother-in-law, **Nourddine Fedda**, whose support and friendship have been truly invaluable. Your presence has enriched my life in countless ways, and I deeply appreciate your kindness.

To my esteemed teachers, at every stage of my education, who have played a pivotal role in shaping my knowledge and skills. In particular, I extend my sincere gratitude to **Professor Toual Belgacem** from the University of Djelfa, one of my former professors, whose guidance and dedication have profoundly influenced my academic path. May God bless you all abundantly for your invaluable support and mentorship.

This dedication is a heartfelt token of love, gratitude, and appreciation to everyone who has contributed to this achievement.

Mebkhouta Toufik

Acknowledgements

With profound gratitude and great satisfaction, I conclude this work, which has been carried out with unwavering dedication and high aspirations for success.

Above all, I extend my deepest thanks to Allah, the Almighty, for His countless blessings, guidance, and the strength He has bestowed upon me throughout this academic journey. Without His divine mercy and wisdom, the completion of this work would not have been possible.

I am sincerely grateful to **Professor Golea Amar** from the University of Biskra for proposing the subject of this thesis and for his invaluable expertise, insightful guidance, and unwavering support. His extensive knowledge and control have been instrumental in shaping this research. I am truly honored to have had his mentorship throughout this journey.

My heartfelt appreciation goes to **Professor Boumaraf Rabia** from the University of Biskra, my co-supervisor, whose kindness, respect, and generosity have been a continuous source of encouragement. Her exemplary character and unwavering support have significantly contributed to my academic and personal growth.

I am also deeply thankful to Professor **Benchouia Mohamed Toufik** from the University of Biskra and Doctor **Chebaani Mohamed** from Higher National School of Renewable Energies, Environment & Sustainable Development for their exceptional guidance and unwavering encouragement. their dedication, insightful advice, and genuine support have been invaluable in the successful completion of this thesis. I am truly grateful for their invaluable contributions as a co-supervisor.

I would like to express my sincere gratitude to the committee members, **Pr. Zouzou Salah Eddine**, **Pr. Betka Achour**, and **Pr. Barra Kamal**, for their valuable remarks which significantly contributed to the improvement of this work.

Mebkhouta Toufik

TABLE OF CONTENTS

CHAPTER I

Overview Of Wind Energy Systems

CHAPTER II

Modeling and Dynamic Analysis of Wind Energy Conversion Systems

CHAPTER III

Advanced Control Strategies for DFIG-Based Wind Energy Systems

CHAPTER IV

Standalone DFIG Control and Fault Detection Using Advanced Estimation Techniques

CHAPTER V

Advanced Control and Sensorless Estimation for Standalone DFIG Systems

TABLE OF FIGURES

CHAPTER I

CHAPTER II

CHAPTER III

CHAPTER IV

CHAPTER V

LIST OF TABLES

CHAPTER III

CHAPTER V

NOMENCLATURE

Abbreviations	
HAWT	Horizontal-Axis Wind Turbine
VAWTs	Vertical-Axis Wind Turbines
SCIG	Squirrel Cage Induction Generators
DFIG	Doubly-Fed Induction Generators
MPPT	Maximum Power Point Tracking
PWM	Pulse Width Modulation
PID	Proportional-Integral-Derivative
BSC	Backstepping Control
MPC FS-MPCC	Model Predictive Control Finite-Set Model Predictive Current Control
LQR	Linear Quadratic Regulator
MRAC	Model Reference Adaptive Control
FLC	Fuzzy Logic Controllers
ANNs	Artificial Neural Networks
WECS	Wind Energy Conversion System
WT	Wind Turbine
DC	Direct Current
FOC	Filed Oriented Control
DTC	Direct Torque Control
SMC	Sliding mode control
THD	Current Total Harmonic Distortion
TB	Tolerance Band
EKF	Extended Kalman Filter
DSVC	Direct stator voltage control
RSC	rotor-side converter
MRAS	Model Reference Adaptive System

Symbols		Unit
ρ	The density of air	Kg/m³
P_{wind}	Wind kinetic power	*W*
S	The circular area swept by the turbine	m^2
v	Wind speed	m/s
C_P	The power coefficient	*Constant*
Ω_t	Wind turbine rotor speed	*Rad/second*
C_1 , C_2 , C_3 , C_4 , C_5 and C_6	The coefficients of wind turbine	*Constant*
β	Pitch angle	*degree*
λ	Tip-speed ratio	*Constant*
T_{em}	The electromagnetic torque	*N.m*
T_g	The generator torque	*N.m*
T_t	The turbine torque	*N.m*
Ω_t	The turbine rotational speed	*Rad/second*
Ω_g	The rotational speed of the generator	*Rad/second*

G	The gain of the multiplier	*Constant*
J	The total inertia referred to the generator shaft	$Kg.m^2$
f	The total friction coefficient of the mechanical coupling	*Constant*
V_{sabc}	Stator voltage	*V*
V_{rabc}	Rotor voltage	*V*
I_{sabc}	Stator current	*A*
I_{rabc}	Rotor current	*A*
R_s	Stator resistance	Ω
R_r	Rotor resistance	Ω
L_s	Stator inductance	*H*
L_r	Rotor inductance	*H*
M	Mutual inductance between stator and rotor	*H*
p	The number of pair poles	*Constant*
I_{sabc}	Stator currents of the three-phase system	*A*
I_{rabc}	Rotor currents of the three-phase system	*A*
$(v_{ds} or\ v_{rd})$ and $(v_{qs}\ or\ v_{sq}$	Stator voltages in the *d*- and *q*-axis directions	*V*
v_{dr} and v_{qr}	Rotor voltages in the *d*- and *q*-axis directions	*V*
I_{ds} and I_{qs}	Stator currents in the *d*- and *q*-axis directions	*A*
$(I_{dr} or I_{rd})$ and $(I_{qr} or I_{rq})$	Rotor currents in the *d*- and *q*-axis directions	*A*
φ_{sabc}, φ_{rabc}	Stator and rotor magnetic fluxes	*Wb*
$\varphi_{dqs}$and φ_{dqr}	Stator and rotor magnetic fluxes in the *d*- and *q*-axis directions	*Wb*
P_s	The stator active power	*W*
Q_s	The stator reactive power	*VAR*
P_r	The rotor active power	*W*
Q_r	The rotor reactive power	*VAR*
ω_r	Electrical speed of rotor	*RPM*
ω_{r_est}	Estimeted electrical speed of rotor	*RPM*
ω_{mec_est}	Estimeted mechnical speed of the rotor	*RPM*
I_{dr_est}, I_{qr_est}	Estemeted *dq* rotor currents	*A*

θ_r	Rotor position	*degree*
θ_{r_est}	Esimeted rotor position	*degree*
T_s	Sampling Time	*s*
$I_{r\_(k)}$	The rotor currents at the current sampling instant (k)	*A*
$I_{r\_(k+1)}$	The predicted rotor currents at the next sampling instant (k+1)	*A*
$I_{r(\alpha+\beta j)\_(k)}$	αβ rotor currents at the current sampling instant (k) in complex term	*A*
$I_{r(\alpha+\beta j)\_(k+1)}$	αβ predicted rotor currents at the next sampling instant (k+1)	*A*
V_{bus}	The DC bus voltage	*V*
$V_{r(\alpha+\beta j)\_(k)}$	The reference rotor voltage in the αβ stationary frame at sampling instant k	*V*
$V_{s(\alpha+\beta j)\_(k)}$	The stator voltage in the αβ stationary frame at the sampling instant k	*V*
sw	The switching signal or switch state	
V_{s_ref}	The reference stator voltage amplitude	*V*
V_s	The measured stator voltage amplitude	*V*
V_{sa}	The stator phase voltage	*V*
$(I_{sa}\ or\ I_{as})$	The stator phase current	*A*
$(I_{ra}\ or\ I_{ar})$	The rotor phase current	*A*

GENERAL INTRODUCTION

The increasing global demand for energy, coupled with the urgent need to transition away from fossil fuels due to environmental concerns, has driven significant research into renewable energy sources. Among these, wind energy has emerged as one of the most promising alternatives, offering a clean, sustainable, and inexhaustible power source. Wind energy conversion is primarily achieved through wind turbines, which convert the kinetic energy of the wind into electrical power via electromechanical generators. Over the years, technological advancements have significantly improved the efficiency and feasibility of wind energy systems, making them a key component of the global strategy to reduce carbon emissions and mitigate climate change.

Among the various types of generators used in wind energy conversion systems, the Doubly-Fed Induction Generator (DFIG) has gained significant attention due to its flexibility and efficiency in variable-speed wind applications. DFIG-based systems are widely deployed in both onshore and offshore wind farms, as they enable efficient control of active and reactive power. Their ability to operate over a wide range of wind speeds while maintaining stable power output makes them a preferred choice for modern wind energy installations. However, achieving optimal performance in DFIG-based systems requires advanced control strategies that ensure stable and reliable operation under varying wind conditions.

Precise control of both electrical and mechanical components is essential in wind energy systems to maximize energy conversion efficiency. In this regard, rotor and stator currents are key parameters in control applications, as they directly influence the system's power regulation. These currents are typically monitored using current sensors. However, sensor failures are a common issue that can significantly affect system reliability, leading to performance degradation or even complete system failure. Therefore, developing robust methods for detecting and compensating for sensor faults is crucial to maintaining the efficiency and continuous operation of DFIG-based wind energy systems.

This thesis addresses these challenges by exploring modeling and control strategies for DFIG-based systems, with a particular focus on advanced control techniques and fault detection and compensation methods.

Chapter I provides a comprehensive introduction to wind energy, outlining its historical development, the classification of wind turbines, and the various types of wind energy systems, including their applications and benefits.

Chapter II delves into the modeling of wind energy systems, with particular emphasis on wind turbine modeling and the implementation of Maximum Power Point Tracking (MPPT) technique. Where this technique is a critical strategy for maximizing energy extraction. This chapter ends with modeling of DFIG in *abc* and *dq* to reference system.

Chapter III explores advanced control strategies for DFIG-based wind energy systems, focusing on the regulation of active and reactive power at the stator. This chapter provides an in-depth analysis of nonlinear and optimal control techniques, including Backstepping Control (BSC) and Linear Quadratic Regulator (LQR), as well as their integration to leverage the advantages of both approaches. Implementing these advanced control strategies ensures optimal system performance despite variations in wind speed.

Chapter IV shifts the focus to fault detection and mitigation, particularly addressing current sensor faults through the implementation of the Extended Kalman Filter (EKF) observation. Where this observation is applied to estimate rotor and stator currents when sensor failures occur with localization of the faulty sensor, ensuring continuous system operation.

Chapter V investigates the integration of Finite Set Predictive Current Control (FSPCC) with the Model Reference Adaptive System (MRAS) to eliminate the need for a speed sensor. By removing the speed sensor, operational costs are reduced while maintaining high control accuracy.

By addressing the aforementioned issues, this dissertation contributes to the enhancement of DFIG-based wind energy systems. The research offers valuable insights into improving system reliability, optimizing energy conversion, and reducing operational costs. The integration of advanced control strategies and fault detection techniques aims to ensure the continuous and efficient operation of wind energy systems, even in the presence of sensor faults or failures. The results of this work can pave the way for more cost-effective, reliable, and robust solutions in wind energy applications.

CHAPTRE I

OVERVIEW OF WIND ENERGY SYSTEMS

I.1 Introduction

Wind energy is a key renewable energy source that has gained significant attention due to its sustainability and environmental benefits. It originates from atmospheric movements caused by solar radiation, temperature variations, and the Earth's rotation. Over time, wind energy has evolved from traditional mechanical applications to advanced electricity generation systems, making it an essential component of modern energy strategies. Algeria possesses considerable wind energy potential, particularly in coastal and desert regions where wind conditions are favorable. The country's efforts to integrate wind power into its energy mix are driven by the need for diversification and sustainability. Understanding the characteristics of wind in Algeria is crucial for identifying optimal locations and maximizing energy production efficiency.

Wind turbines, the primary technology for harnessing wind energy, come in various types, including vertical-axis and horizontal-axis designs, each with distinct operational characteristics. Additionally, wind turbines can be classified based on their speed regulation, distinguishing between fixed-speed and variable-speed systems. Their installation can be either onshore or offshore, depending on environmental and technical considerations. Beyond their structural classification, wind turbines serve different applications, including standalone systems, grid-connected configurations, and hybrid systems that integrate multiple energy sources. A critical aspect of wind energy conversion is the electromechanical process, where mechanical energy from the wind is transformed into electrical power. Among the various generator technologies, the Doubly Fed Induction Generator (DFIG) is widely used due to its efficiency and operational flexibility.

This chapter provides an overview of wind energy, covering its origins, historical development, and technological advancements. It also examines the classification, installation, and operation of wind turbines, as well as the electromechanical conversion process. Particular emphasis is placed on the Doubly Fed Induction Generator (DFIG), which is widely adopted in modern wind energy systems due to its ability to operate efficiently under varying wind conditions. The DFIG's bidirectional power flow capability, improved energy capture, and reduced converter size make it a preferred choice for large-scale wind farms. These aspects lay the foundation for a deeper understanding of wind energy systems and their role in modern power generation.

I.2 Origin of wind and its impact

Winds are a natural phenomenon that constitutes an integral part of the Earth's balance and a process interrelated with several factors in their formation. A more precise definition says that winds are movements or transfers of masses of air from one site to another caused by differences in temperature and atmospheric pressure. This fundamental unevenness lies at the root of the temperature contrasts between polar, tropical, desert, and other areas. Winds can be converted to vast amounts of energy by wind turbines, with electricity being generated very productively. Understanding the origin of winds indicates that this natural phenomenon is a sustainable source of clean energy, investment in it is essential within the context of sustainable energy and sustainable development [1- 4].

I.3 Developmental history of wind energy

The idea of wind energy has its roots in the past thousands of years. In the Middle Ages, human beings adapted to the use of wind to power sailboats by harnessing the movements of winds that push the ship.

This use of wind energy by people at that time using windmills to grind grain and pump water was widespread. Technological advancement led to the exploitation of wind energy in line with development into our modern-day world when electricity generation became the forefront aspect of development. In 1888, the first electric power generating wind turbine was built by the American scientist Charles F. Brush. After that, in 1891, the world's first ever wind power station materialized in Denmark. Following that, numerous revolutionary improvements have been made in the field of wind energy. The advancement of technology has facilitated better efficiency and modern designs in the devices used for wind energy. In recent centuries, there has been growing global interest in expanding wind energy as a sustainable and clean energy source. Wind energy plays a vital role in today's electricity generation in many countries and is regarded as one of the most essential and valuable renewable energy sources [5-8].

I.4 Characteristics of winds in Algeria

Establishing a wind farm in an area is critical in determining what quantum of wind energy the area receives. The first and most important is to estimate the availability of wind resources for a region under study, which technically involves preparing a wind atlas or, in other words, wind energy mapping.

The work conducted by S. Boudia in his doctoral thesis in 2013 represents the latest effort in creating a wind atlas in Algeria. As outlined in figure I.1, the average annual wind speed in Algeria at a height of 10 meters above ground level was recorded at more than 20 stations distributed across the Algerian borders from the year 2000 to 2010 [10].

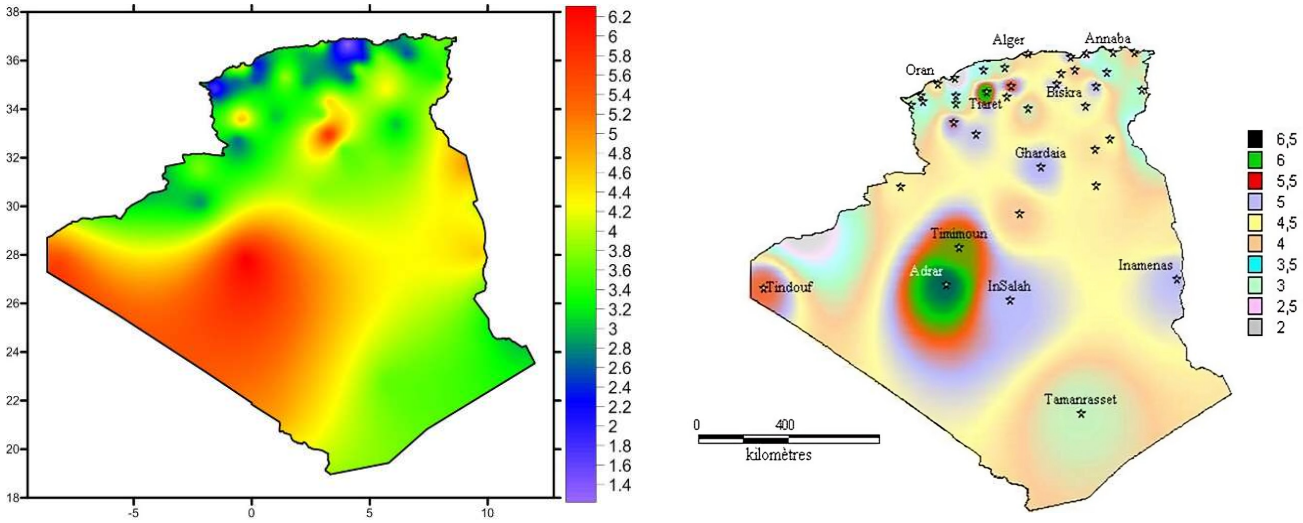

Figure I.1 Algeria ventilation map at 10m altitude (m/s) [10, 11].

Local climatic variations are evident in coastal regions like Oran, Bejaia, Annaba, and other northern areas, where wind speeds tend to be low. In contrast, the high plateaus experience average wind speeds ranging between 2.8 and 5 m/s. Furthermore, the most elevated wind speeds are typically observed in the southern remote areas, particularly in Adrar province, where speeds surpass 6 m/s [10].

I.4.1 Development of wind energy in Algeria

Since the first oil crisis in the late 1980s, Algeria has been investing large amounts in the research and development of wind power stations. This policy course gave a substantial growth in the use of wind in electricity generation. Scientific progress has made wind power stations more effective and reliable. Electricity production through wind energy in Algeria has enhanced by up to 10 megawatts in Adrar. A station had been provided with 12 turbines in 2014. The country has also developed two-phase plans to build wind projects. The first phase is expected between 2015 and 2020, in which 1000 megawatts of electricity is to be produced. Phase two is the period between 2020 to 2030 for producing electricity to a capacity of 5000 megawatts. This program including all stations hooked up to the electric grid [12-16].

I.5 The different types of wind turbines

Wind turbines are classified according to the geometric arrangement of the shaft on which the rotor is installed. There are primarily two major families: those with a vertical axis and those with a horizontal axis.

I.5.1 Vertical axis wind turbine

Vertical axis Wind turbines rotate around a vertically oriented axis, as implied by their name. These turbines can extract energy from low-speed winds and, therefore can perform well even in low wind conditions. Their design allows for the use of less land area compared to horizontal axis turbines. They can also work efficiently in any wind direction, thus contributing to a high degree of versatility upon implementation. Their electricity production is, however deficient compared to the horizontal axis ones [17-19].

I.5.1.1 Darrieus-type vertical axis wind turbine

The Darrieus wind turbine, as shown in Figure I.2, is a vertical axis wind turbine where the central rotor shaft is placed transverse to the wind flow and the blades are disposed vertically. This design of turbine can be implemented in high winded areas without much noise and sound pollution, unlike other types of turbines. However, a major drawback to the Darrieus turbine is that it requires a significant wind force to initiate rotation, and therefore, energy production [20-22].

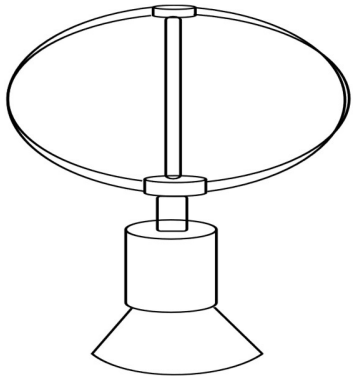

Figure I.2 Vertical Axis Wind Turbine Darrieus-Type [18].

I.5.1.2 Savonius-Type Vertical Axis Wind Turbine

Similar to the previous one, Figure I.3 shows second type of wind turbine which is named after its inventor, S.J. Savonius. The configuration and the shape of the blades are formed by

half-cylinders attached to a central axis. This type of wind turbine uses the principle of the drag force of wind. In this case, there are a few fundamental shortcomings: modest performance, low efficiency, and relatively low rotation speed. But on the positive side, concerning the previous variant, this one allows for an automatic start to rotate [20, 22].

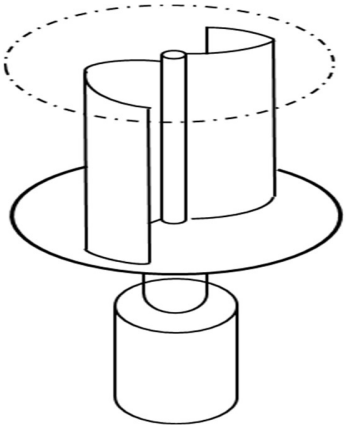

Figure I.3 Vertical Axis Wind Turbine Savonius -Type [18].

I.5.1.3 Advantages

Vertical Axis Wind Turbines (VAWTs) offer several advantages, including [23-27]:

- VAWTs can easily adapt to changing wind directions as they operate independently of wind orientation;
- Their simple design facilitates easier maintenance and operation;
- They often feature a compact structure, making them suitable for installation in densely populated areas;
- Certain designs incorporate self-starting capabilities due to their aerodynamic properties.

I.5.1.4 Inconvenient

Disadvantages of Vertical Axis Wind Turbines (VAWT) [23-27]:

- At moderate to high wind speeds, VAWTs are generally less efficient compared to Horizontal Axis Wind Turbines (HAWTs) due to aerodynamic limitations;
- VAWTs tend to experience higher levels of vibration and mechanical stress compared to HAWTs, which can lead to increased noise, especially in fluctuating wind conditions;
- They can be sensitive to environmental conditions such as turbulence (wind disturbances), affecting their performance;
- VAWTs can be more expensive to produce than horizontal axis turbines;

- They need more area to produce the same amount of energy than some horizontal axis turbines;
- The placement of the energy sensor near the ground exposes it to turbulence and gradient.

I.5.2 Horizontal Axis Wind Turbines

Horizontal axis wind turbines are the most common and widely used type compared to vertical-axis turbines. This is a type whereby the turbine has numerous blades as shown in Figure I.4 (Single blade, two-blade, three blade, Multi blade), and it is to a horizontal rotation axis of the turbine. Fans are fitted at the tower's top and swivel along a fixed horizontal axis. Horizontal axis turbine efficiency depends on the speed and height of the wind, the blades design, and energy transmission efficiency. Usually, these types have a large fan used to capture the wind and then convert it into mechanical energy [16,18, 26, 28, 29, 30].

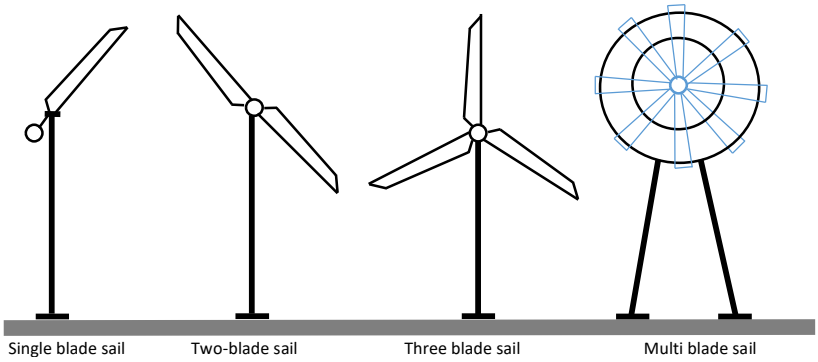

Figure I.4 Horizontal Axis Wind Turbine [31].

I.5.2.1 Low-speed wind turbines

The configuration of low-speed wind turbines involves a notable feature of having a number of blades ranging from 20 to 40, which is a drastic change compared to the fast-running version. Because this type of turbine is high in blade number, it usually limits its diameter to around 8 meters. These turbines will be on a scale where the power coefficient increases speedily with speed, but then it also falls off speedily. A turbine of such a type is most suitable for low wind speeds. These turbines start working at wind speeds ranging from 2 to 3 meters per second and exhibit high starting torque. However, the turbines remain less efficient as compared to the high-speed wind turbines, and their main field of application lies in various applications, such as water pumping [32-35].

I.5.2.2 High-speed wind turbines

High-speed wind turbines typically have a small number of blades, usually between two and four, which makes them widely used for electricity generation due to their high efficiency and lightweight design compared to slow-speed turbines of similar power. However, they face challenges such as higher cut-in wind speeds, making start-up more difficult. These turbines rotate at significantly higher speeds than their slow-speed counterparts, with rotational speed increasing as the number of blades decreases.

It is well known that wind turbine sizes vary depending on their capacity and intended application. Due to the intermittent and variable nature of wind as an energy resource, there is a growing preference for larger turbines to maximize energy capture and improve efficiency [32-35].

I.5.2.3 Advantages

Some of the key advantages of Horizontal Axis Wind Turbines (HAWTs) include [6, 24, 25, 36, 37]:

- Horizontal Axis Wind Turbines (HAWT) are, as a general rule, more efficient in converting wind power into electrical power than vertical axes;
- HAWTs perform efficiently under variable wind speeds while maintaining relatively stable performance characteristics;
- HAWTs can also easily integrate with the modern electrical grid to generate electricity in places with infrastructure;
- HAWTs are much more suitable for large-scale energy production within wind farms and offshore;
- This tower captures wind at higher altitudes, hence it is stronger and more consistent in power availability at all times.

I.5.2.4 Inconvenient

Some of the key disadvantages of Horizontal Axis Wind Turbines (HAWTs) include [6, 24, 25, 36, 37]:

- It’s very expensive to build;

- The equipment is located so high in the tower that access becomes impractical in case of problems;
- HAWTs may produce significant visual and noise effects in local communities due to the heights of towers and the size of blades;
- They might have an impact on wildlife, especially in areas with migratory birds or high biodiversity;
- Some horizontal axis turbines may face bending issues due to dynamic forces, requiring additional maintenance;
- HAWTs may rely more on wind speed for energy generation, making them less effective at low wind speeds;
- Installation of HAWTs requires a large footprint, especially in connection with large-scale projects.
- HAWTs often rely on a gearbox to match the low rotational speed of the blades with the higher rotational speed required by the generator. These gearboxes are subject to high mechanical stress and wear, leading to frequent maintenance, potential failures, and increased downtime. This not only raises operational costs but also complicates maintenance due to the elevated location of the nacelle.

I.6 Main components of a wind turbine

Figure I.5 describe the wind turbines are composed of numerous components, including the tower, the generator, as well as the nacelle, the rotor, and the blades … etc. Which are considered essential parts of wind turbines.

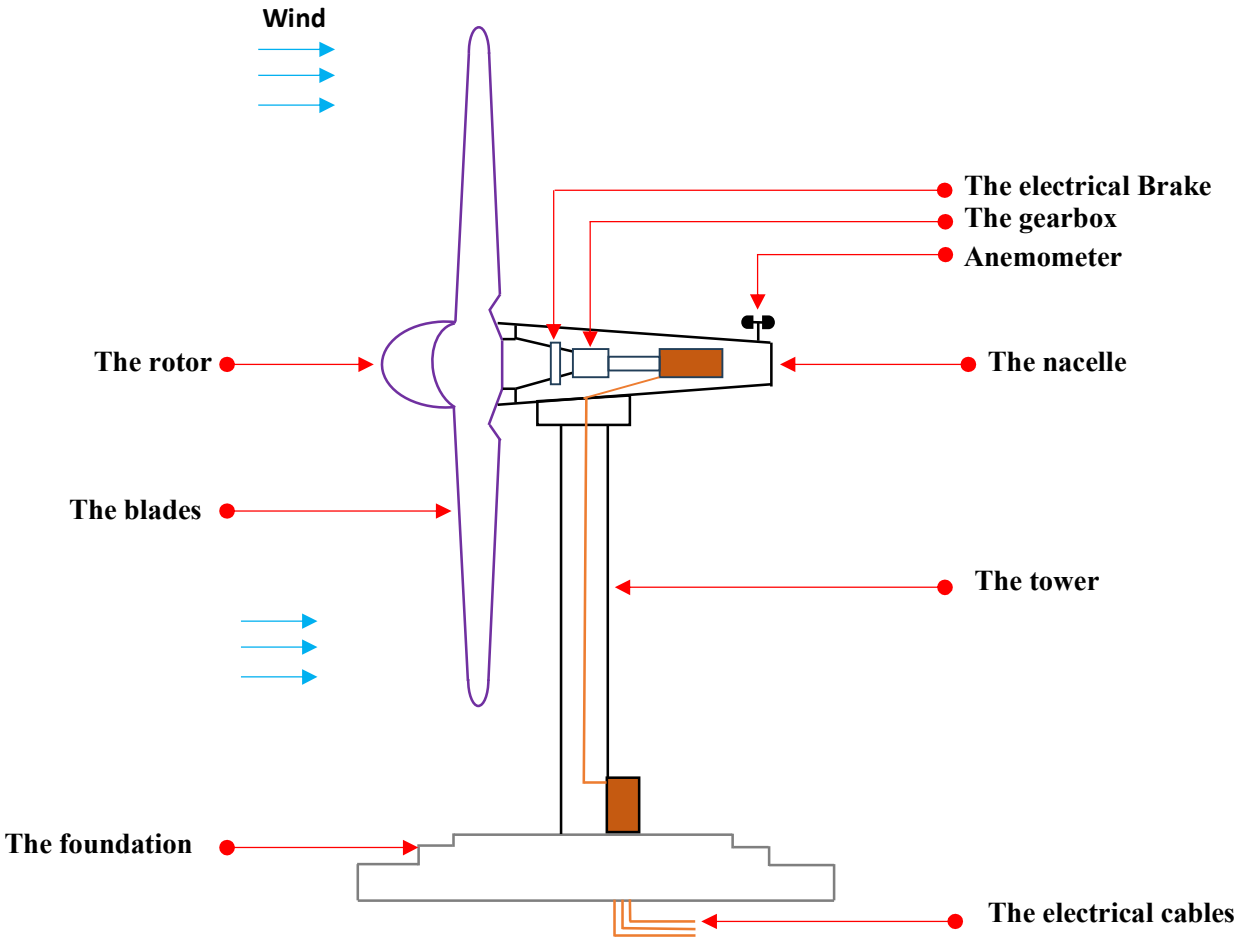

Figure I.5 Wind turbine components [40]

A. The tower: one of the main components of a wind power system is the tower, which holds up the floating surface or nacelle and the rotor. The height of towers varies from 50 to 90 meters, having a conical trunk. It is usually designed vertically with materials such as aluminum or stainless steel, these are very resistant to wear and tear under environmental conditions and operational stress. The tower is rigidly fixed into a ground foundation, which can be guaranteed stability and shielded from the adverse effects of wind forces [38, 39, 40].

B. The generator: is considered the fundamental element in the process of converting mechanical energy into electrical energy. This generator can be either synchronous or asynchronous (non-synchronous) [38, 39, 40].

C. The nacelle: Comprises all mechanical and electrical components aimed at converting wind energy into electrical power, and it ensures communication between the wind

turbine blades and the electric generator. The nacelle includes several elements such as the gearbox, sensors, generator, etc [40, 41, 42].

D. **The gearbox:** is a system comprising a series of gears that transmit mechanical energy, allowing the adjustment of the generator's rotation speed. The gearbox is typically employed as a means to match the rotational speed between the turbine and the generator in a wind power generation system [40, 41, 42].

E. **The rotor**: It is the rotating part of the wind turbine. It consists of the blades and is connected to the nacelle through the turbine's axis. The power of the wind turbine is directly proportional to the square of the rotor diameter [41, 42].

F. **The blades**: It is a specific number of blades designed to capture wind energy and transfer it to the rotor [41, 42].

I.7 Types of installations

Wind energy is tapped by planting wind turbines in two main places, which include offshore and onshore.

I.7.1 Offshore wind turbines

This is a category whereby wind turbines are grown on the seabed or on floating platforms (Figure I.6) to tap wind energy across vast water expanses. In these locations, wind speeds are typically higher and more stable compared to onshore sites, enhancing energy production efficiency. Although these systems require higher initial investments for installation and maintenance, the benefits of generating greater energy output offset these costs [43-45].

Figure I.6 Offshore wind turbines [46].

I.7.2 Onshore wind turbines

Onshore wind turbines are installed on land (Figure I.7) to exploit wind energy. These systems have relatively lower initial and operational costs than the offshore turbines, and onshore turbines are primarily considered for harnessing wind energy. On the other hand, such turbines experience potential environmental effects because they can be placed in areas with different terrains, including human impacts, such as buildings and trees [43-45].

Figure I.7 Onshore wind turbines [47].

I.8 Classification of wind turbines

There are fundamentally two technologies for wind turbines: fixed-speed and variable-speed. The following section broadly describes how these technologies operate:

I.8.1 Fixed-speed wind turbines

The concept behind "Fixed-Speed Operation" in generating wind energy is a generator generally based on a Squirrel cage induction generator directly coupled to the grid without a power converter (Figure I.8). The mechanical speed of the generator is fixed according to the electrical grid frequency and/or the number of pole pairs of the generator. To ensure operation near synchronism, it is essential to have a guidance system for the wind turbine blades. Additionally, a speed multiplier is employed to adjust the turbine speed so that it aligns with the generator's speed. The figure below illustrates the method of connection to the grid [18, 48-50].

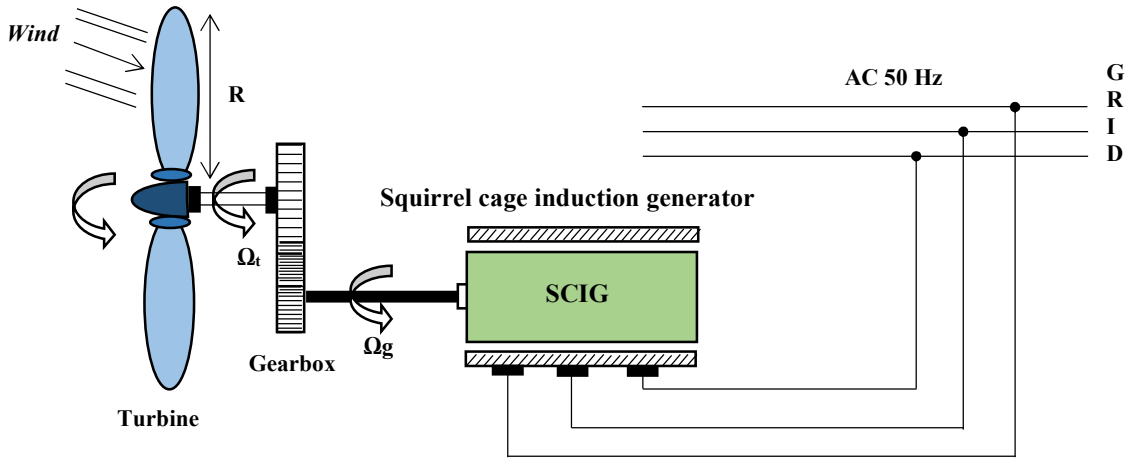

Figure I.8 Fixed-speed wind turbines [48].

I.8.1.1 Advantages

The main advantages of this operating mode are [49,51-53]:

- Simple structure;
- Absence of power converters;
- Cost-effective due to the absence of converters;
- No need for electronic systems, making it more reliable and requiring less maintenance.

I.8.1.2 Inconvenient

This strategy poses several challenges in the exploitation of the extracted energy [49,51-53]:

- Suboptimal extracted power, missing theoretical peaks;
- Very low efficiency for moderate and low winds;
- Necessity for periodic gearbox maintenance;
- Loss of control over reactive power;
- Uncontrolled magnetization of the generator;
- Inability to control the output power generation.

I.8.2 Variable-speed wind turbines

Given the issues caused by fixed-speed operation (orientation systems, periodic maintenance, poor efficiency, etc.), efforts have been made to optimize the extraction of power from the kinetic energy of the wind. To achieve this, it is necessary to continuously adjust the generator speed to the wind speed (Figure I.9). This optimization of the desired production can be carried out through controls on the turbine and on the electro technical part (the electric generator itself and/or control parameters of the power electronics converter) [39, 50, 53-55].

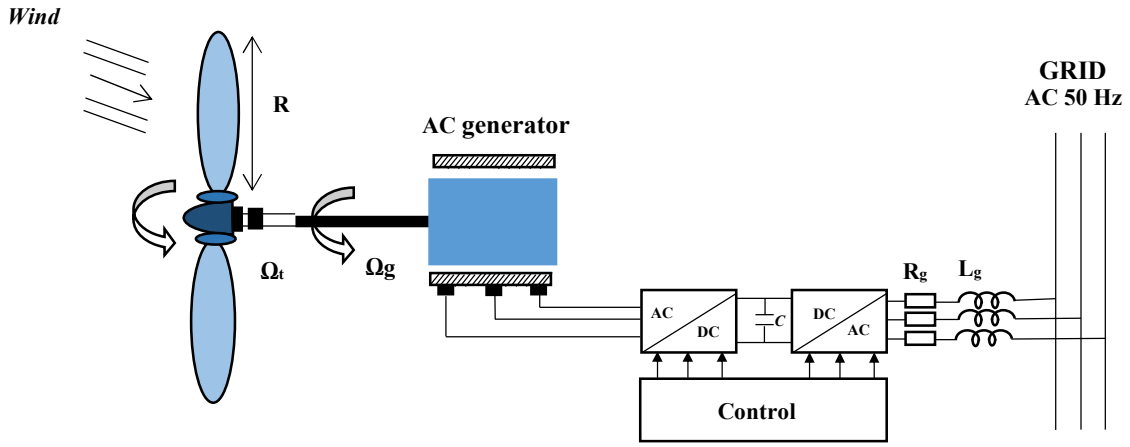

Figure I.9 Variable-speed wind turbines [55].

The static converter's mission is to decouple the frequency of the electrical distribution network from the rotational speed of the generator. It acts as an electronic interface for regulating the frequency and amplitude of various types.

I.8.2.1 Advantages

Variable-speed wind turbines provide several advantages that set them apart as a superior option compared to other types, such as [39, 49, 52]:

- Optimization of captured energy through the ability to control the rotor speed;

- Control of power transfer and clean energy sent to the grid;
- Reduction of mechanical constraints experienced by the powertrain. Turbulences and wind gusts can be absorbed. The absorbed wind energy is stored in the mechanical inertia of the turbine, thereby reducing torque oscillations;
- Generation of higher-quality electrical power;
- This type of machines offers a larger time constant for the pitch angle control system, reducing its complexity;
- Reduction of acoustic noise.

I.8.2.2 Inconvenient

Despite their many advantages, variable-speed wind turbines come with certain challenges that can impact their efficiency and operational costs [39, 49, 52]:

- Utilization of specialized machines;
- Higher additional costs (converter, control, etc.);
- Complexity of the power converters used;
- Management of power transfer between converters and optimal power point tracking of the wind turbine.

I.9 Applications of wind turbines

A wind energy system can be utilized in three distinct applications:

I.9.1 Standalone systems

Standalone wind turbine serves as a crucial resource for supplying power to remote locations, such as islands, fields requiring water pumping, and installations like sailboats, lighthouses. These isolated systems often rely on energy storage solutions, typically employing batteries. Effective management of these batteries is facilitated by charge controllers, essential for safeguarding against potential damage from overcharging or deep discharging, thereby optimizing the longevity and reliability of the battery systems the Figure below represent a standalone system based on wind turbine [54, 56-58].

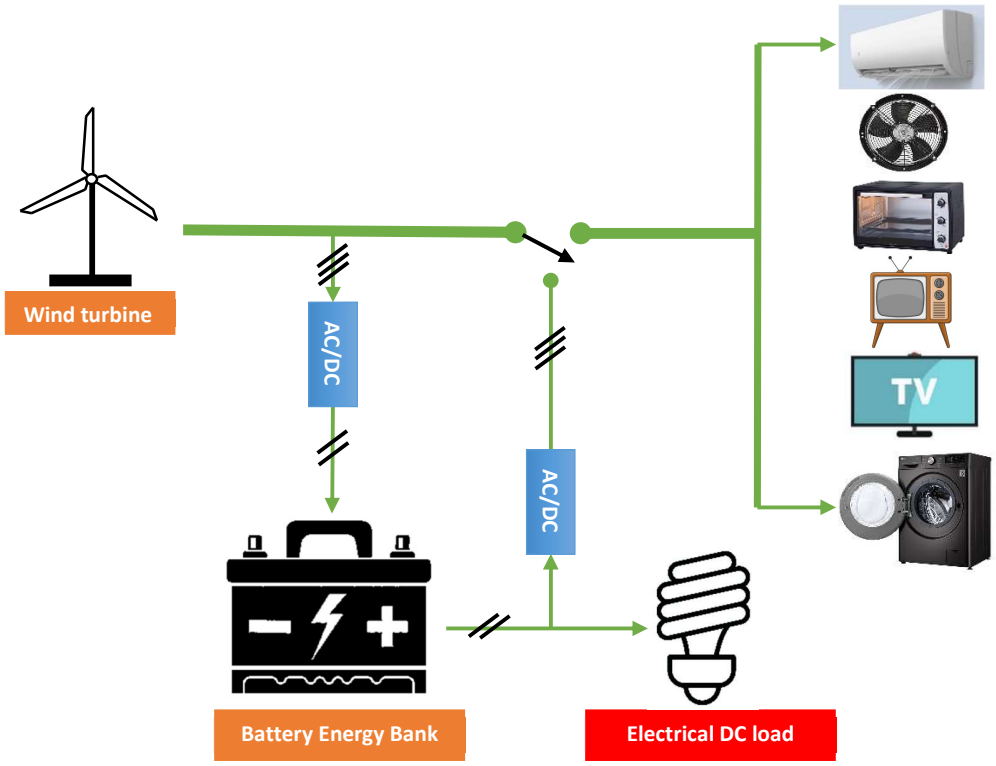

Figure I.10 A standalone system based on wind turbine [59].

I.9.2 Grid-connected systems

Grid-connected systems operate without the need for energy storage, as all generated power is directly supplied to the electrical grid. In the context of wind energy systems linked to the grid (Figure I.11), a static converter is essential for converting the variable output of wind turbines into stable electrical signals suitable for grid integration. This converter plays a critical role in ensuring the reliability and compatibility of wind generated electricity with grid infrastructure [54, 56-58].

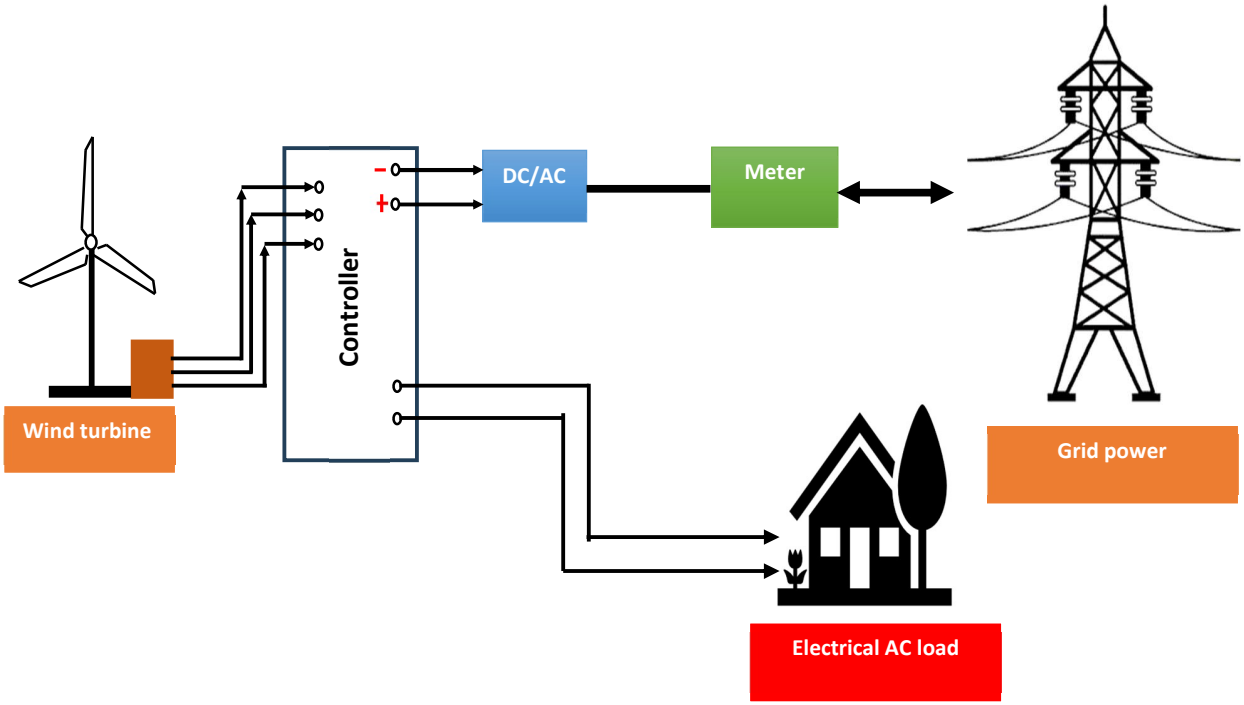

Figure I.11 A grid-connected systems based on wind turbine [60].

I.9.3 Hybrid systems

Wind turbines can be utilized in hybrid systems that integrate multiple energy sources, such as wind turbines, diesel generators, and photovoltaic units, where the Figure I.12 represent the hybrid system based on different power sources. To enhance overall energy reliability and efficiency. This combination introduces complexity, necessitating optimal management of each energy source to maximize output. Effective control of all sources is crucial to ensure efficient energy delivery. Hybrid systems are typically deployed in small-scale applications serving diverse user needs and also include converters to accommodate AC loads, facilitating seamless integration into various electrical environments [57, 58, 61-63].

These systems adhere to a basic configuration: they require a power control unit and, in some cases, an energy storage unit.

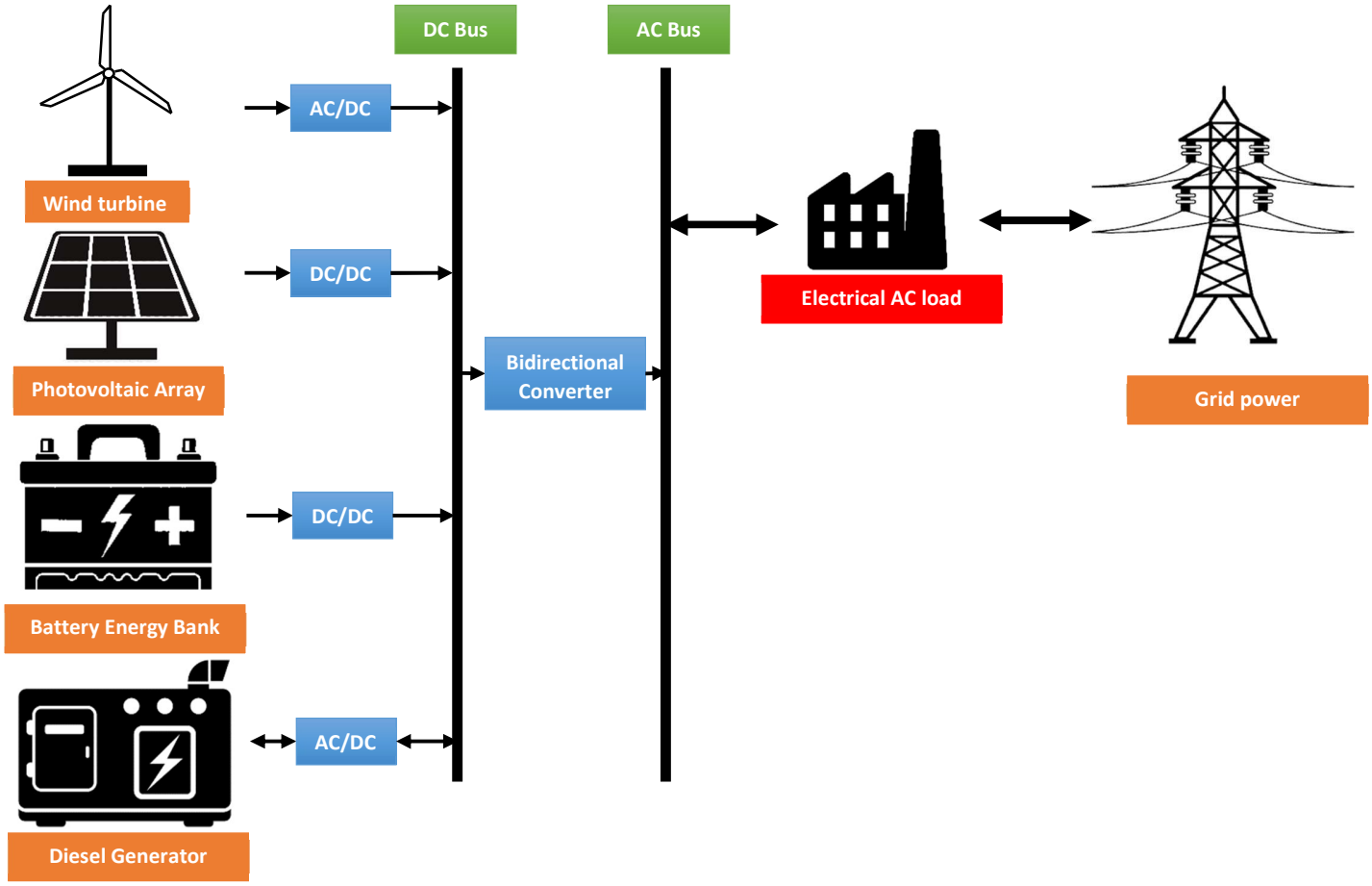

Figure I.12 A hybrid systems based on wind turbine [63].

I.10 Advantages and Inconvenient of wind energy

Wind energy is one of the most prominent renewable sources of power, offering numerous benefits and challenges that impact its widespread adoption. In this section, we will explore the key advantages and disadvantages associated with this renewable energy source:

I.10.1 Advantages

Among the main advantages offered by wind energy [6, 23, 57, 58, 64, 65]:

- Wind energy is a natural, renewable, and sustainable resource, ensuring its availability without the risk of depletion, unlike fossil fuels;
- It is a clean and environmentally friendly energy source, producing no harmful emissions or radioactive waste, making it a safer alternative to nuclear energy;
- Wind energy utilization can be intermittent due to the ease of wind turbine shutdown using controls (pitch control);

- Its utilization does not generate direct emissions of carbon dioxide (CO_2) or pollutants responsible for acid rain, such as sulfur dioxide (SO_2) and nitrogen oxides (NOx), thereby reducing air pollution;
- It is a cost-effective option in remote areas with high wind speeds, offering profitable investment opportunities and stimulating economic growth, particularly in rural regions;
- Wind energy is locally sourced, minimizing transmission losses and enhancing energy independence for nations and communities;
- Among renewable energy sources, wind power is one of the most cost-effective, with relatively low installation and operational costs, facilitating its integration into existing electrical grids;
- It creates more jobs per unit of electricity produced compared to traditional energy sources, contributing to economic and social development, especially in developing countries;
- Wind farms can be easily dismantled without leaving lasting environmental impacts, ensuring the preservation of natural resources;

I.10.2 Inconvenient

Despite its advantages, wind energy also faces several challenges [6, 23, 57, 58, 64, 66, 67]:

- The noise generated by the rotation of wind turbine blades is one of the most significant issues causing disturbances, leading to public complaints, particularly in densely populated residential areas;
- The visual impact of wind turbines is a significant factor that can influence public acceptance of wind energy projects;
- Electromagnetic interference from the components of a wind turbine should be managed appropriately;
- The tall towers supporting wind turbines may affect wildlife and surrounding ecosystems;
- Wind farms impact agricultural areas by occupying large land spaces, potentially reducing the available area for farming and affecting crop production, especially if turbine locations are not carefully planned;
- Some studies indicate that birds tend to avoid wind turbines, and placing wind farms along migration routes may increase the risk of collisions, necessitating careful site selection;

I.11 The electromechanical conversion

Electrical machines play a crucial role in harnessing mechanical energy generated by wind movement and converting it into electrical energy, primarily using synchronous and asynchronous machines. These machines differ in their operating principles and characteristics, which significantly impact their performance in wind power generation systems. The configuration of the electrical machine greatly affects its performance, determining whether the system operates at a fixed or variable speed, thereby influencing energy conversion efficiency and grid compatibility. The main characteristics of each type are as follows [56, 68, 69]:

I.11.1 Synchronous generator

In traditional electricity generation processes, these machines are commonly used, especially in large power stations such as thermal, hydraulic, or nuclear plants. Synchronous generators used in wind power generation are costlier than induction generators of the same capacity. When directly connected to the grid, their speed remains constant and synchronized with the grid frequency, leading to torque fluctuations transmitted through the power chain to the electrical energy produced. Therefore, synchronous generators are not typically used in directly grid-connected wind turbines, instead they are employed via power converters that separate the grid frequency from the machine's rotational speed. This separation allows for adjusting the rotational speed to achieve maximum aerodynamic efficiency and reduce torque fluctuations in the power chain. Some types of synchronous generators can operate at low rotational speeds, reducing the need for speed multipliers and lowering maintenance requirements [70-73].

I.11.2 Induction generator

Induction machines are commonly used in directly grid connected wind turbines due to their robust construction, low cost, and ease of integration. Their ability to operate at a fixed speed is attributed to the slip between the stator flux and rotor speed, which simplifies synchronization with the electrical grid. In the 1990s, Danish engineers introduced a two speed configuration utilizing an additional electrical machine, significantly improving wind turbine efficiency under varying wind conditions. The evolution of power electronics has enabled variable-speed operation by decoupling the generator's rotational speed from the grid frequency. This advancement not only enhances aerodynamic efficiency but also reduces torque ripple within the drivetrain. Additionally, the use of converters addresses common drawbacks of induction machines, such as reactive power consumption. [72, 74, 75].

I.11.3 Doubly fed induction generators

DFIGs play a pivotal role in renewable energy systems, especially in wind power generation, due to their efficiency over variable speeds and precise control of active and reactive power. This section provides a concise overview of their structure, types, operating modes, applications, and key advantages and inconvenient:

I.11.3.1 The structure of doubly fed induction generator

The doubly fed induction generator (DFIG) features a three-phase stator identical to that of conventional asynchronous machines. Its rotor, distinct due to the absence of a squirrel cage, is equipped with three windings connected in a star configuration and accessible via slip rings brushed by brushes. This configuration allows external access to the rotor's three-phase windings, thereby facilitating control and management of energy flows. The stator typically consists of stacked magnetic laminations with slots for inserting the windings, highlighting a structure similar to conventional three-phase machines [23, 76].

I.11.3.2 Different types of Doubly Fed Induction Generator

DFIGs can be implemented in various configurations, each designed to meet specific operational and efficiency needs. These configurations primarily differ in the methods used to manage rotor power and the type of power electronics employed. The main types include:

A. Doubly Fed Induction Generator with Rotor Power Dissipation

In this variable speed configuration depicted in figure I.13, the stator is directly connected to the electrical grid, while the rotor is connected to a rectifier. A resistive load is placed at the output of the rectifier via an IGBT or GTO chopper. Control of the IGBTs allows modulation of the energy dissipated by the rotor winding, enabling variable speed operation while keeping the asynchronous machine within the stable region of its torque/speed characteristic. The slip is adjusted according to the machine's rotational speed. As slip becomes significant, the power extracted from the rotor increases, all of which is dissipated in the resistor R [30, 77, 78].

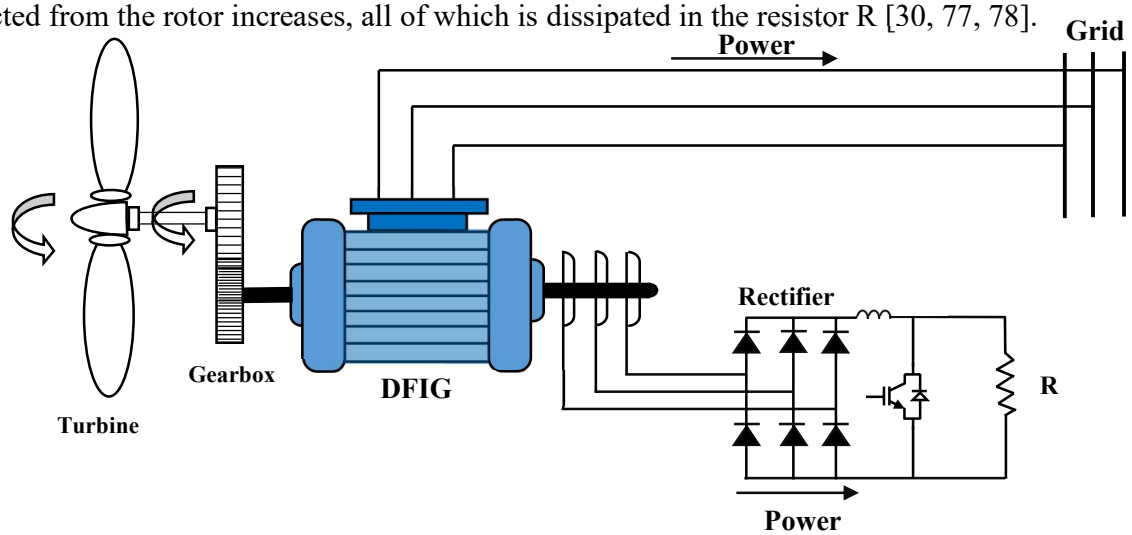

Figure I.13 Wind turbine system based on the DFIG approach with rotor energy dissipation [77].

B. Doubly Fed Induction Generator: Kramer Structure

To reduce energy losses associated with the previous structure, the chopper and resistor are replaced with an inverter that feeds slip energy back into the grid. This configuration, known as the "Kramer configuration," employs a diode bridge for rectification and a transistor bridge for inversion. The diode bridge rectifies the voltages between the slip rings, while the non-autonomous transistor inverter adjusts the variable voltage applied to the rectifier by controlling the firing angle (Figure I.14).

This design enables precise control over the diodes conduction range, allowing variability in the power extracted from the rotor circuit and consequently adjusting the slip of the asynchronous generator. One of the key advantages of this approach is that the non-autonomous inverter utilizes commutations provided by the network, making it more economical compared to alternative solutions [6, 77, 79, 80].

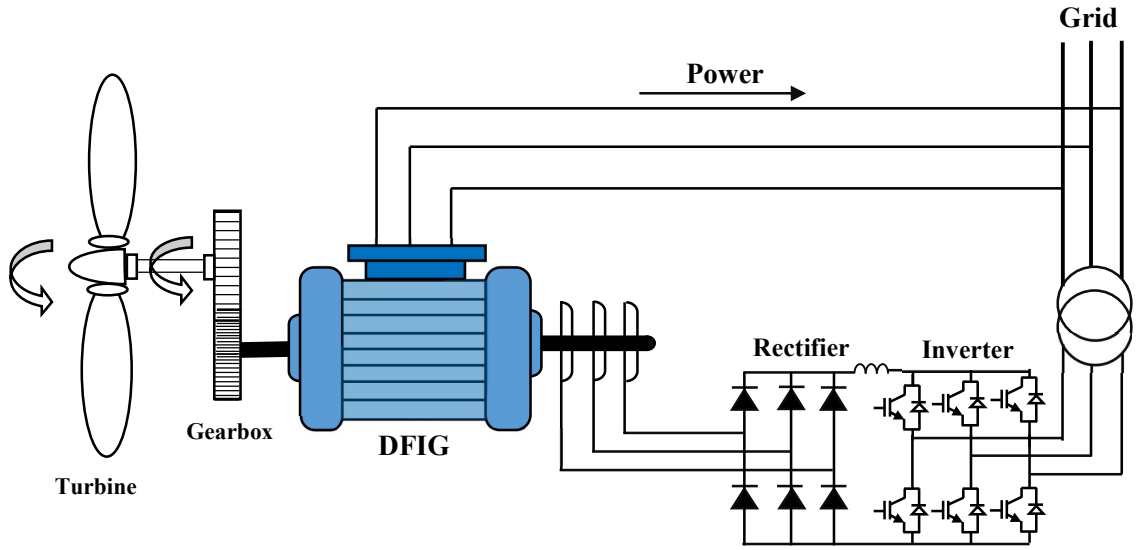

Figure I.14 Wind turbine system based on DFIG Kramer structure [77].

C. Doubly Fed Induction Generator: Scherbius Structure with Cycloconverter

To enable bidirectional energy flow between the grid and the rotor, a cycloconverter is used. This configuration, known as the Scherbius structure and illustrated in Figure I.15, allows for doubling the speed variation range compared to alternative configurations. Although the use of thyristors in this setup introduces significant harmonic components, which negatively affect the power factor quality, this topology, referred to as the static Scherbius topology, is advantageous for rotor frequency values significantly lower than those of the electrical grid. By allowing for positive or

negative slip variation, which must remain below 30% to maintain system efficiency, it ensures effective speed control. Additionally, the use of thyristors is cost-effective [79, 81-83].

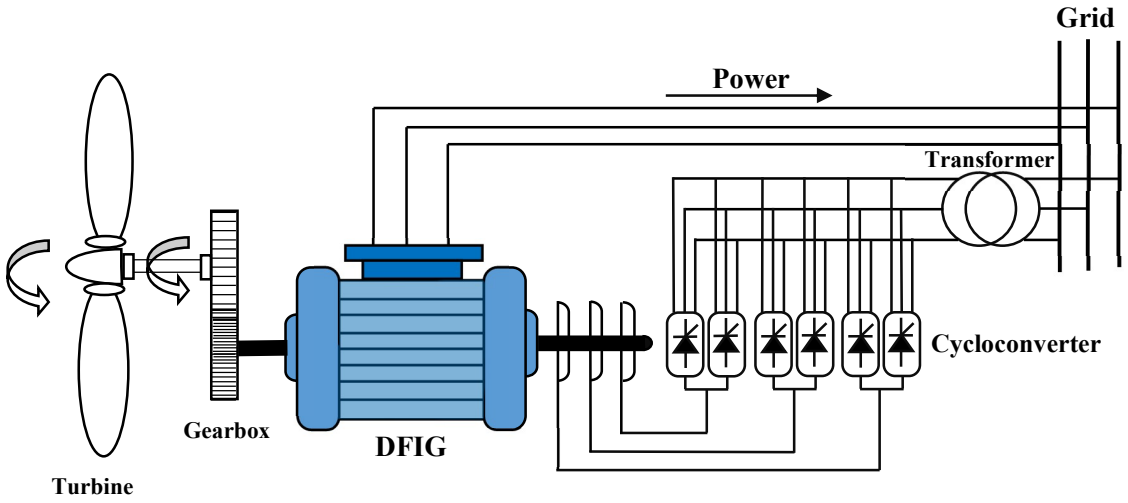

Figure I.15 DFIG-Based Wind Turbine with Cyclo Converter System [81].

D. Doubly Fed Induction Generator: Scherbius Structure with PWM Converter

Insulated Gate Bipolar Transistors (IGBTs) are power semiconductor devices capable of high-speed switching, with significantly higher switching frequencies compared to Gate Turn-Off Thyristors (GTOs). This feature allows for efficient implementation of Pulse Width Modulation (PWM) techniques, which enhance signal quality by shaping the frequency spectrum and minimizing electromagnetic interference. The configuration typically consists of two voltage source converters incorporating IGBTs, interconnected via a DC-link (Figure I.16). This arrangement facilitates precise control of generator speed, bidirectional power flow, and independent regulation of active and reactive power exchanged with the grid. Additional advantages include reduced harmonic distortion in voltage and current waveforms and stable dynamic performance, particularly near synchronous speed [16, 41, 84, 85].

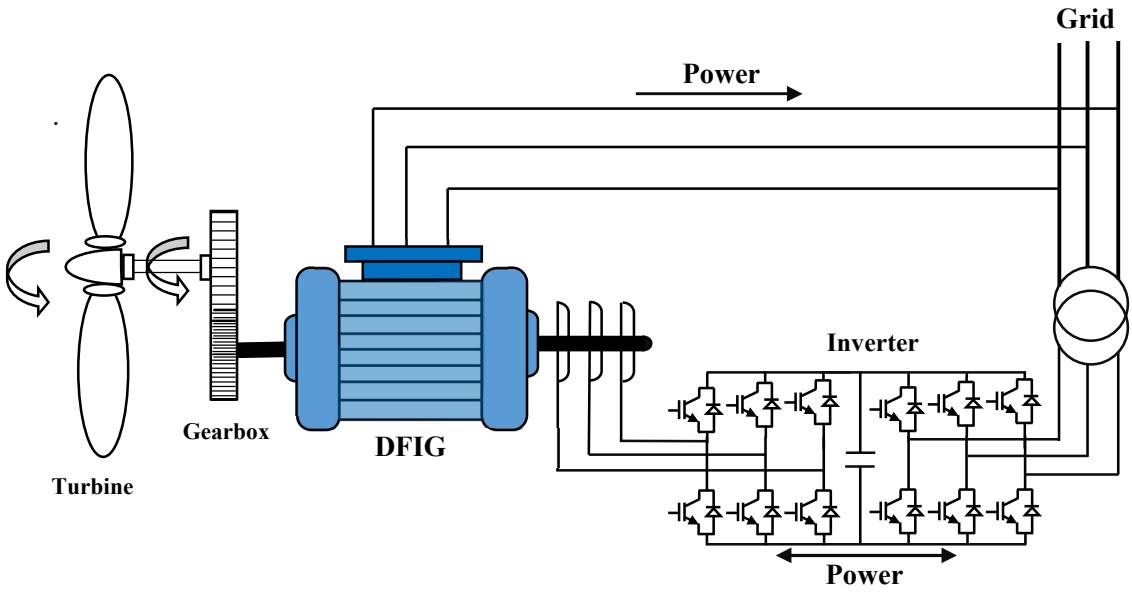

Figure I.16 Wind turbine system based on DFIG PWM structure [16].

I.11.3.3 Operating mode of the Doubly Fed Induction Generator

The Doubly Fed Induction Machine (DFIM) differs in operating characteristics from other kinds of machines. Operating unlike the squirrel-cage induction machines, which allow the motor mode to run at speed lower than the synchronous speed and the generator mode at speed higher than the synchronous speed, the DFIM controls the inner magnetic field using its rotor voltage. This offers much flexibility not just to the motor and generator modes but also to the Hypo-synchronous and Hyper-synchronous operation modes [19, 86].

In generator mode, specifically for the Doubly Fed Induction Generator (DFIG), two distinct operating modes can be distinguished:

A. Operating in Hypo-synchronous generator mode with g > 0

The figure below illustrates the transfer of electrical power between the Doubly Fed Induction Generator (DFIG) and the grid. In this setup, power is supplied to the grid via the stator (Ps) where Ps <0, while a portion of the grid's power is absorbed through the rotor as slip power (Pr) where Pr>0. This configuration indicates the operation of the DFIG in generator mode at a speed Hypo-synchronous [54, 69, 81, 87].

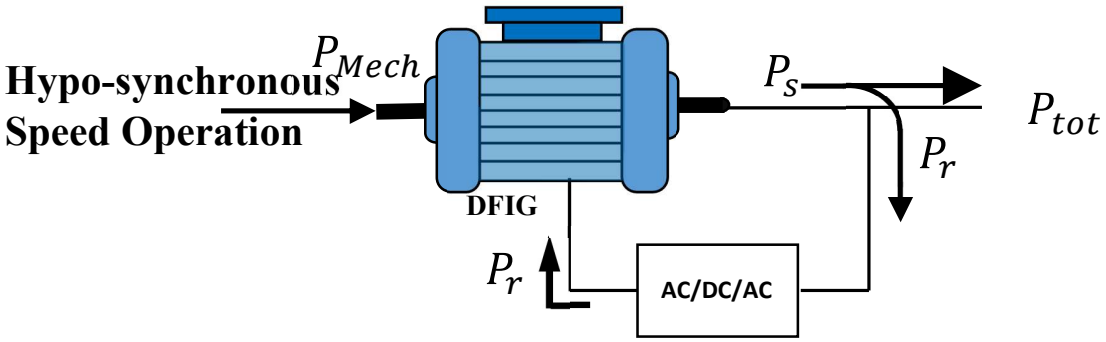

Figure 1.17 Hypo-synchronous operation of the DFIG [87].

B. Operating in Hyper-synchronous generator mode with g < 0

When the machine operates in Hyper-synchronous mode, as illustrated in Figure I.18, the electrical power generated by the DFIG is transmitted to the grid through both the stator and rotor where Ps<0 and Pr<0. This distinguishes the operation of the DFIG in Hyper-synchronous mode [54, 69, 81, 87].

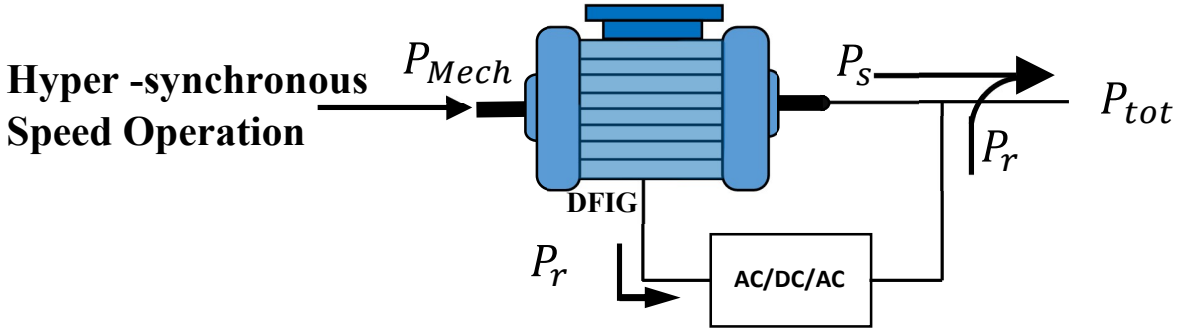

Figure I.18 Hyper -synchronous operation of the DFIG [87].

I.11.3.4 Applications Fields of doubly fed induction generator

Operating the doubly fed induction generator (DFIG) in generator mode allows for numerous applications of this machine, including [16, 69, 81-82]:

- Embedded electrical systems in ships and aircraft, where compact and flexible power generation is essential,
- Hydropower plants with variable water flow rates and rotational speeds, requiring adaptable generation systems,
- Wind and tidal energy systems, which operate under fluctuating environmental conditions affecting rotational speed,

Variable speed generator sets, which operate at reduced speeds during low demand periods, thereby improving fuel efficiency and minimizing operational costs.

I.11.3.5 Advantages and Inconvenient of doubly fed induction generator

This paragraph examines the benefits and certain limitations of the Doubly Fed Asynchronous Machine (DFIG) when operating at variable speeds [16, 23, 81, 88-89].

A. Advantages

Among the main advantages of DFIGs:

- Operation at variable speed;
- Active and reactive power can be independently controlled using the static converter connected to the rotor of the DFIG, thereby enhancing the quality of power delivered to the electrical grid;
- The ability to operate at constant torque beyond the rated speed;
- Bidirectional transfer of rotor power;
- Power converters used are approximately 70% smaller, reducing their cost and noise compared to those traditionally employed with squirrel cage or permanent magnet machines.

B. Inconvenient

Despite their numerous advantages, Doubly Fed Induction Generators (DFIGs) also present several challenges and limitations, including:

- One of the primary drawbacks of the Doubly-Fed Induction Generator (DFIG) is its pronounced sensitivity to grid disturbances;
- Utilizing an increased number of converters;
- The machine is bigger than the squirrel cage machine;
- The additional maintenance costs resulting from the use of a speed multiplier and the slip ring-brush, compared to Permanent Magnet Synchronous Generator (PMSG).
- Due to continuous mechanical stress, the gearbox in DFIG systems is prone to wear and degradation, requiring regular maintenance.

I.12 Conclusion

Wind energy has proven to be a viable and increasingly adopted renewable energy source, offering significant environmental and economic benefits. This chapter has provided an in-depth exploration of the fundamental aspects of wind power, including its origins, historical advancements, and development in Algeria. The classification of wind turbines, their deployment configurations, and their diverse applications highlight the technological diversity and adaptability of wind energy systems.

A key focus of this chapter has been the electromechanical conversion process, particularly the role of different generator technologies, with special emphasis on the Doubly Fed Induction Generator. Its operational flexibility and efficiency make it a critical component in modern wind farms.

As global energy demands continue to rise, the integration of wind power into national grids and hybrid systems and standalone will play a pivotal role in sustainable energy transitions. The knowledge presented in this chapter establishes a solid foundation for further exploration of wind energy technologies, optimization strategies, and their impact on future energy systems.

REFERENCES BIBLIOGRAPHIQUES

[1] MEZIANE, F. ,''Utilisation des Modèles CFD pour la Simulation de l'Ecoulement du Vent sur un Terrain Complexe'', Thèses DOCTORAT Sciences, UNIVERSITE M'HAMED BOUGARA-BOUMERDES, 2021.

[2] MEDDANE Fatima, Etude d'une éolienne à axe vertical, Thèse de Doctorat, département génie martime, USTO, 2018.

[3] Hurley, B. (2012). D'où vient le vent. *Wind Site Evaluation Ltd*.

[4] HASSAD, Mohamed Amine. Influence de la commande d'une GADA des systèmes éoliens sur la stabilité des réseaux électriques. Diss. 2016.

[5] …, ''L'ÉNERGIE ÉOLIENNE'', Website Available at: https://www.eolien-valais.ch/energie-eolienne/historique, Accessed September 01, 2024 at 8 p.m.

[6] Mourad, L. (2016). Synthèse de lois de commande non-linéaires pour le contrôle d'une machine asynchrone à double alimentation dédiée à un système aérogénérateur (Doctoral dissertation, Ph. D. Thesis, Université Aboubakr Belkaid–Tlemcen–Faculté de Technologie).

[7] TARFAYA, A. Etude d'un système aérogénérateur couplé au réseau électrique (modélisation et simulation) (Doctoral dissertation, Université de Annaba-Badji Mokhtar).

[8] Azzouz, T. (2015). *Modélisation et commande d'un système de conversion d'énergie éolienne à base d'une MADA* (Doctoral dissertation, Université Mohamed Khider-Biskra).

[9] S. Boudia, ''Carte du Gisement Eolien en Algérie'', Website Available at: https://www.cder.dz/spip.php?article1442, Accessed September 01, 2024 at 8 p.m.

[10] Boudia, S. M. (2013). Optimisation de l'évaluation temporelle du gisement énergétique éolien par simulation numérique et contribution à la réactualisation de l'atlas des vents en Algérie (Doctoral dissertation, Université de Tlemcen-Abou Bekr Belkaid).

[11] LAKHDAR, S. Contribution à la Commande Robuste Non Linéaire Sans Capteur d'unSystème Eolien à Base d'une Génératrice Asynchrone à Double Alimentation (GADA) (Doctoral dissertation, Université de Béchar-Mohamed Tahri).

[12] Ouahiba GUERRI, ''L'Energie éolienne en Algérie : Un bref aperçu'', Website Available at: https://www.umc.edu.dz/images/ber37_6_7.pdf , Accessed September 01, 2024 at 8 p.m.

[13] S. Ghoudelbourk, ''Etude et modélisation des convertisseurs statiques dans une chaine éolienne à base de la GADA'', PhD Thesis, Université de Annaba, 2016.

[14] Z. Chabani, ''La part des énergies renouvelables dans le bilan énergétique national à l'horizon 2030'', Mémoire de Magister, Université de Boumerdes, 2014.

[15] LAKHDARA, Amira. *Contribution à la gestion d'énergie dans un système hybride à énergies renouvelables*. Diss. 2022.

[16] Yahdou, A. ‘‘*Commande hybride par mode glissant d’ordre 2 d’un systéme éolien à double rotor’’,* Doctoral dissertation, Alger, Ecole Nationale Polytechnique, 2017.

[17] …, ‘Quelle est la différence entre une éolienne verticale et une éolienne horizontale ?’’, Website Available at: https://www.quelleenergie.fr/questions/difference-eolienne-verticale-horizontale, Accessed September 01, 2024 at 8 p.m.

[18] GASMI, Hamza. *Contribution à l'amélioration de la commande des chaines de conversion éoliennes*. 2023. Thèse de doctorat.

[19] Boyette, A. (2006). *Contrôle-commande d'un générateur asynchrone à double alimentation avec système de stockage pour la production éolienne* (Doctoral dissertation, Université Henri Poincaré-Nancy I).

[20] Dawoud HAMANE ‘’Contribution à la caractérisation de l’écoulement dans le sillage d’une éolienne’’. Thèse de Doctorat en Sciences, ECOLE NATIONALE POLYTECHNIQUE D’ALGER.2021.

[21] …, ‘‘Éoliennes à axe vertical et horizontal : types, avantages et inconvénients’’, Website Available at: https://www.terrafutura.info/eoliennes-a-axe-vertical-et-horizontal-types-avantages-et-inconvenients/, Accessed September 01, 2024 at 8 p.m.

[22] Adeline M, ‘‘Quels sont les différents types d’éoliennes ?’’, Website Available at: https://www.totalenergies.fr/particuliers/parlons-energie/dossiers-energie/energie-renouvelable/quels-sont-les-differents-types-d-eoliennes#:~:text=En%20développement%2C%20cette%20énergie%20renouvelable, horizontale%20ou%20encore%20éolienne%20domestique, Accessed September 01, 2024 at 8 p.m.

[23] Mansouri F. Z. , ‘’Commande de la Génératrice Asynchrone Double Alimentation pour La Production de L’énergie Eolienne’’, Doctoral dissertation, Université des Sciences et de la Technologie d'Oran Mohamed-Boudiaf USTOMB, 2021.

[24] Latreche, M. T. (2018). *Commande Floue de la Machine Synchrone à Aimant Permanant (MSAP) utilisée dans un système éolien* (Doctoral dissertation).

[25] Idjdarene, K. (2010). *Contribution à l’étude et la commande de génératrices asynchrones à cage dédiées à des centrales électriques éoliennes autonomes* (Doctoral dissertation, Lille 1).

[26] KSENTINI, A. (2016). *Gestion et optimisation du site idéal des éoliennes en Algérie pour une zone autonome* (Doctoral dissertation, Université de Batna 2).

[27] Ghennam, T. (2011). *Supervision d’une ferme éolienne pour son intégration dans la gestion d’un réseau électrique, Apports des convertisseurs multi niveaux au réglage des éoliennes à base de machine asynchrone à double alimentation* (Doctoral dissertation, Ecole Centrale de Lille; École Militaire Polytechnique (Alger)).

[28] M. Oussama, C. Abdelghani ‘‘Contrôle Hybride et Analyse de la Performance d'un Système de Puissance Eolien en Utilisant Différentes Approches\Hybrid Control and Analyse of the Wind Power System Performance Using Different Approaches’’, PhD Thesis in Electrical Engineering, University of Amar Telidji – Laghouat, 2021.

[29] …, ‘‘Quelle est la différence entre une éolienne verticale et une éolienne horizontale ?’’, Website Available at: https://www.quelleenergie.fr/questions/difference-eolienne-verticale-horizontale, Accessed September 01, 2024 at 8 p.m.

[30] CHEMIDI, Abdelkarim. *Analyse, modélisation et commande avancée d'une éolienne utilisée dans une ferme*. Diss, (Doctoral dissertation). université de Tlemcen), 2015.

[31] HardikPatel and SanatDamania. "PERFORMANCE PREDICTION OF HORIZONTAL AXIS WIND TURBINE BLADE." *International Journal of Innovative Research in Science, Engineering and Technology* 2 (2013): 1401-1406.

[32] Yilmaz, O. (2023). Low-speed, low induction multi-blade rotor for energy efficient small wind turbines. *Energy*. https://doi.org/10.1016/j.energy.2023.128607

[33] Beltran, Brice. *contribution à la commande robuste des éoliennes à base de génératrices asynchrones double alimentation: du mode glissant classique au mode glissant d'ordre supérieur*. Diss. Université de Bretagne occidentale-Brest, 2010.

[34] N. Akermi, ‘‘Etude des performances aérodynamiques d'une éolienne Darrieus par un model instationnaire à six degrés de liberté’’, Thèse de doctorat, Université de science et technologie, Département de génie mécanique, Oran, 2018/2019.

[35] …, ‘‘Étude théorique d'une éolienne Modifier’’, Website Available at: https://eolienne.f4jr.org/eolienne_etude_theorique,, Accessed September 01, 2024 at 8 p.m.

[36] Ashglaf, Mohmed Omran. *Development of Hybridization concept for horizontal axis wind/tidal systems using functional similarities and advanced real-time emulation methods*. Diss. Normandie Université, 2019.

[37] Benamor, Afaf. *Contribution à la Modélisation, à la Commande et au Contrôle des Systèmes de Production de l'Energie Électrique Renouvelable*. Diss. Université Mohamed Khider-Biskra, 2019.

[38] M. LARABI Abdelkader, "Conception de la commande d'une machine asynchrone destinée à l'énergie renouvelable « Application de la commande par mode de glissement à une éolienne basée sur la Machine Asynchrone a Double Alimentation » " Memoire de Magister, 2018

[39] CHEIKH RIDHA Etude et Commande d'une Eolienne à base d'une Machine Synchrone à Aimants Permanents et d'une Machine Asynchrone à Double Alimentation Doctorat a - Khider Mohamed Universiy, 2018.

[40] FADDA MOHAMED, L. ‘‘*Contribution à la modélisation et au diagnostic intelligent des systèmes de production d'énergie électrique à base d'énergies renouvelables’’,* Doctoral dissertation, 2017.

[41] Riachy, L. (2017). *Contribution à la commande d'un onduleur multiniveaux, destinée aux énergies renouvelables, en vue de réduire le déséquilibre dans les réseaux électriques* (Doctoral dissertation, Normandie Université).

[42] TARFAYA, A. *Etude d'un système aérogénérateur couplé au réseau électrique (modélisation et simulation)* (Doctoral dissertation, Université de Annaba-Badji

Mokhtar).

[43] Hevia-Koch, P., & Jacobsen, H. K. (2019). Comparing offshore and onshore wind development considering acceptance costs. *Energy policy*, *125*, 9-19.

[44] Bilgili, M., Yasar, A., & Simsek, E. (2011). Offshore wind power development in Europe and its comparison with onshore counterpart. *Renewable and Sustainable Energy Reviews*, *15*(2), 905-915.

[45] Merzouk, N. K. (2006). *Evaluation du gisement énergétique éolien contribution à la détermination du profil vertical de la vitesse du vent en Algérie* (Doctoral dissertation, Thèse de doctorat d'état en physique énergétique, Université de Tlemcen).

[46] …, ''France commits to 40 GW offshore wind by 2050'', Website Available at: https://windeurope.org/newsroom/news/france-commits-to-40-gw-offshore-wind-by-2050/, Accessed September 01, 2024 at 8 p.m.

[47] …, ''Repowered wind farms show huge potential of replacing old turbines'', Website Available at: https://windeurope.org/newsroom/news/repowered-wind-farms-show-huge-potential-of-replacing-old-turbines/, Accessed September 01, 2024 at 8 p.m.

[48] Elgharib, A. (2022). *Different Control Strategies for PMSG Connected Wind Turbine System* (Doctoral dissertation, Aix-Marseile Université).

[49] MOUMNA, M. (2022). *Contribution à l'amélioration de la qualité de l'énergie d'une chaine de conversion éolienne à la base d'une GSAP* (Doctoral dissertation, Rachid TALEB/Zinelaabidine BOUDJEMA).

[50] Davigny, A. *Participation aux services système de fermes d'éoliennes à vitesse variable intégrant du stockage inertiel d'énergie* (Doctoral dissertation, Thèse de doctorat, Hautes Études d'Ingénieur, 2007.(Fra)).

[51] Fateh, L. (2016). Modélisation et simulation d'une chaine de conversion d'énergie éolienne à base d'une machine synchrone à aimant permanent. *Mémoire Doctorat*.

[52] BENSAADI, H. (2020). *contribution à la commande d'un aérogénérateur basé sur un GSAP* (Doctoral dissertation, Université de Batna 2).

[53] FRIKH, M. L. *Contribution à l'étude d'un système de production d'énergie éolienne* (Doctoral dissertation, Université de Annaba-Badji Mokhtar).

[54] BOUROUINA A. ''Commande par mode glissant d'une éolienne de forte puissance basée sur une GADA avec observateur''

[55] EL AIMANI, S. ''Modelisation de differentes tecnologias d'eoliennes intégrées d'un un réseau mouyenne tension'', Doctoral dissertation Université de science et technologie de lille, 2004

[56] MOUALDIA, Abdelhafidh. *Stratégies de commande DTC-SVM et DPC appliquées à une MADA utilisée pour la production d'énergie éolienne*. 2014. Thèse de doctorat. Alger, Ecole Nationale Polytechnique.

[57] TOUAL, B. (2019). *Contribution à la Commande et la Gestion des Sources Hybrides d'Energie Electrique* (Doctoral dissertation, Université de Batna 2).

[58] T. Douiadi, "Etude et Commande d'une Systeme Eolien à Base d'un Générateur

Asynchrone, Mémoire de Magister, Université de Batna 2, 2010.

[59] Salas, V. (2017). Stand-alone photovoltaic systems. In *The Performance of Photovoltaic (PV) Systems* (pp. 251-296). Woodhead Publishing.

[60] …, '' GRID-CONNECTED WIND POWER SYSTEM'', Website Available at: https://www.tycorun.com/blogs/news/grid-connected-wind-power-system, Accessed September 01, 2024 at 8 p.m.

[61] Mahgoun, M. S. (2022). *Commande non conventionnelle de la machine synchrone à aimant permanant (MSAP) dédiée à la conversion éolienne* (Doctoral dissertation).

[62] MAHBOUB, M. A. (2017). *Commande Robuste d'un Système de Génération Eolien à base de Génératrice Double Alimentée sans Balais* (Doctoral dissertation, Université de Batna 2).

[63] Shafi, I., Khan, H., Farooq, M. S., Diez, I. D. L. T., Miró, Y., Galán, J. C., & Ashraf, I. (2023). An Artificial Neural Network-Based Approach for Real-Time Hybrid Wind–Solar Resource Assessment and Power Estimation. *Energies*, *16*(10), 4171.

[64] Yamina, T. (2011). *Detection de Défauts de la génératrice asynchrone à double alimentation (DFIG)* (Doctoral dissertation, Université Mohamed Boudiaf des sciences et de la technologi).

[65] Senani, F. *La Machine Asynchrone à Double Alimentation: Stratégies de Commande et Applications*. Diss. Thèse de doctorat, université des frères Mentouri de Constantine, 2018.

[66] Soltane Soltane BELAKEHAL Conception & Commande des M Commande des Machines achines à Aimants Permanents Dédiées aux Energies nergies nergies Renouvelables NIVERSITE DE CONSTANTINE 2010

[67] DOUADI Tarek Modélisation et stratégie de Commande de la Génératrice Asynchrone intégrée à un Système Eolien Université Batna 2 – Mostefa Ben Boulaïd 2019

[68] TOUAM, M. (2012). *MODÉLISATION ET COMMANDE DE LA GÉNÉRATRICE ASYNCHRONE A DOUBLE ALIMENTATION MONTÉE DANS UN SYSTÈME ÉOLIEN* (Doctoral dissertation, Ecole nationale polytechnique d'Oran-Maurice Audin).

[69] Hamane, B. (2018). *Commande robuste d'un aérogénérateur à base de machine asynchrone à double alimentation pilotée par un convertisseur matriciel* (Doctoral dissertation, Université du Québec à Trois-Rivières).

[70] MAYOUF, M. (2014). *Etude comparative des architectures et stratégies de contrôle d'un aérogénérateur synchrone a aimants permanents* (Doctoral dissertation, Université de Batna 2).

[71] RAHOUA, N. (2021). *Contribution aux Contrôles des Générateurs Synchrones à Aimants Permanents* (Doctoral dissertation, Université Mohamed Khider–Biskra).

[72] Hamecha, S. (2013). *Etude et commande d'une éolienne à base d'une machine synchrone à aimants permanents* (Doctoral dissertation, Université Mouloud Mammeri).

[73] Issam, A. (2015). *Contribution au diagnostic de défauts d'une génératrice asynchrone dans une chaine de conversion d'énergie éolienne* (Doctoral dissertation, Université Badji Mokhtar de Annaba).

[74] Mojumdar, M. R. R., Himel, M. S. H., Rahman, M. S., & Hossain, S. J. (2016). Electric machines & their comparative study for wind energy conversion systems (WECSs). *Journal of Clean Energy Technologies*, *4*(4), 290-294.

[75] Rihani, L. (2012). *Modélisation et commande de la génératrice à induction double alimentée couplée sur un réseau electrique* (Doctoral dissertation, Université de Batna 2).

[76] Bennani, H. (2011). Machine asynchrone à double alimentation: Les lois de commande en régime permanent. Québic

[77] Hamzaoui, I. (2008). *Modélisation de la machine asynchrone à double alimentation en vue de son utilisation comme aérogénérateur* (Doctoral dissertation, Alger, Ecole Nationale Polytechnique).

[78] MellouL, A. (2018). *Simulation et diagnostic d'une machine asynchrone à double alimentation d'une éolienn* (Doctoral dissertation).

[79] Poitiers, F. (2003). *Etude et commande de génératrices asynchrones pour l'utilisation de l'énergie éolienne-machine asynchrone a cage autonome-machine asynchrone a double alimentation reliée au réseau* (Doctoral dissertation, Université de Nantes).

[80] AZIZI, A. (2019). *Modélisation et optimisation d'un système de production d'énergie photovoltaïque avec un système de stockage hybride* (Doctoral dissertation, Université de Annaba-Badji Mokhtar).

[81] [81] BOUKHAMKHAM, H. (2011). *Diagnostique des défaillances dans une machine asynchrone utilisée dans une chaine éolienne* (Doctoral dissertation, Université Mohamed Khider Biskra).

[82] Zerzouri Nora, ''ETUDE DE L'EFFET DE DEFAUT SUR LE COMPORTEMENT DYNAMIQUE DE LA MACHINE ASYNCHRONE'' Doctora, UNIVERSITE BADJI MOKHTAR ANNABA, 2016.

[83] DJERIRI, Y. (2015). *Commande directe du couple et des puissances d'une MADA associée à un système éolien par les techniques de l'intelligence artificielle* (Doctoral dissertation).

[84] Contribution à l'étude de la génératrice asynchrone à double alimentation : modélisation, commande et structure (ABDELLI Houaria)

[85] DJILALI, L. *COMMANDE ROBUSTE D'UN SYSTÈME ÉOLIEN* (Doctoral dissertation, Ecole nationale polytechnique d'Oran-Maurice Audin).

[86] Bennani, Hakim. "Machine asynchrone à double alimentation: Les lois de commande en régime permanent." (2011).

[87] Chaiba, A. (2010). *Commande de la machine asynchrone à double alimentation par des techniques de l'intelligence artificielle* (Doctoral dissertation, Université de Batna 2).

[88] Idrissi, Imane. *Contribution au Diagnotic des Défauts de la Machine Asynchrone Doublement Alimentée de l'Eolienne à Vitesse Variable*. Diss. Normandie Université; Université Sidi Mohamed ben Abdellah (Fès, Maroc), 2019.

[89] Phan, T. T., Nguyen, V. L., Hossain, M. J., To, A. N., Tran, H. T., & Phan, T. N. (2016, November). Transient responses of the doubly-fed induction generator wind turbine under grid fault conditions. In 2016 International Conference on Advanced Computing and Applications (ACOMP) (pp. 97-104). IEEE.

CHAPTRE II

MODELING AND DYNAMIC ANALYSIS OF WIND ENERGY CONVERSION SYSTEMS

II.1 Introduction

Generators are a fundamental component of wind energy systems, playing a crucial role in converting mechanical energy into electrical power. Among these, the Doubly Fed Induction Generator (DFIG) stands out as one of the most important due to its high efficiency and advanced control capabilities over the generated power. This chapter provides a comprehensive description of the wind system based on DFIG, starting from wind modeling to turbine control. The dynamic laws governing the process of aerodynamic energy conversion will be analyzed, focusing on Betz's law and the power coefficient Cp, as well as the importance of the relative tip speed. Additionally, a mechanical modeling of the turbine shaft and the speed multiplier device will be presented, leading to the control strategies used to optimize turbine performance, such as Maximum Power Point Tracking (MPPT). Finally, the transition from three-phase modeling to two-phase modeling using the Park transformation it will explain, which represents an essential part of the analysis of Doubly Fed Induction Generators.

II.2 Description of the wind system based on DFIG

The wind system consists of a turbine, a speed multiplier, a generator, electronic converters, and the electrical grid. Figure II.1 presents the wind system based on the Doubly-Fed Induction Generator (DFIG). The kinetic energy of the wind is captured by the turbine, causing it to rotate. The mechanical energy generated by the turbine is passed to a speed multiplier, which increases the rotational speed to match the speed of the DFIG generator. Subsequently, this mechanical energy is converted into electrical energy by the DFIG, with a significant portion of this energy being directly transmitted to the electrical grid via the stator, while the remaining portion is transmitted through the rotor to the grid via electronic converters. These converters allow control of the energy produced by the DFIG generator, enabling adaptation to the random changes of the wind [1-3-7].

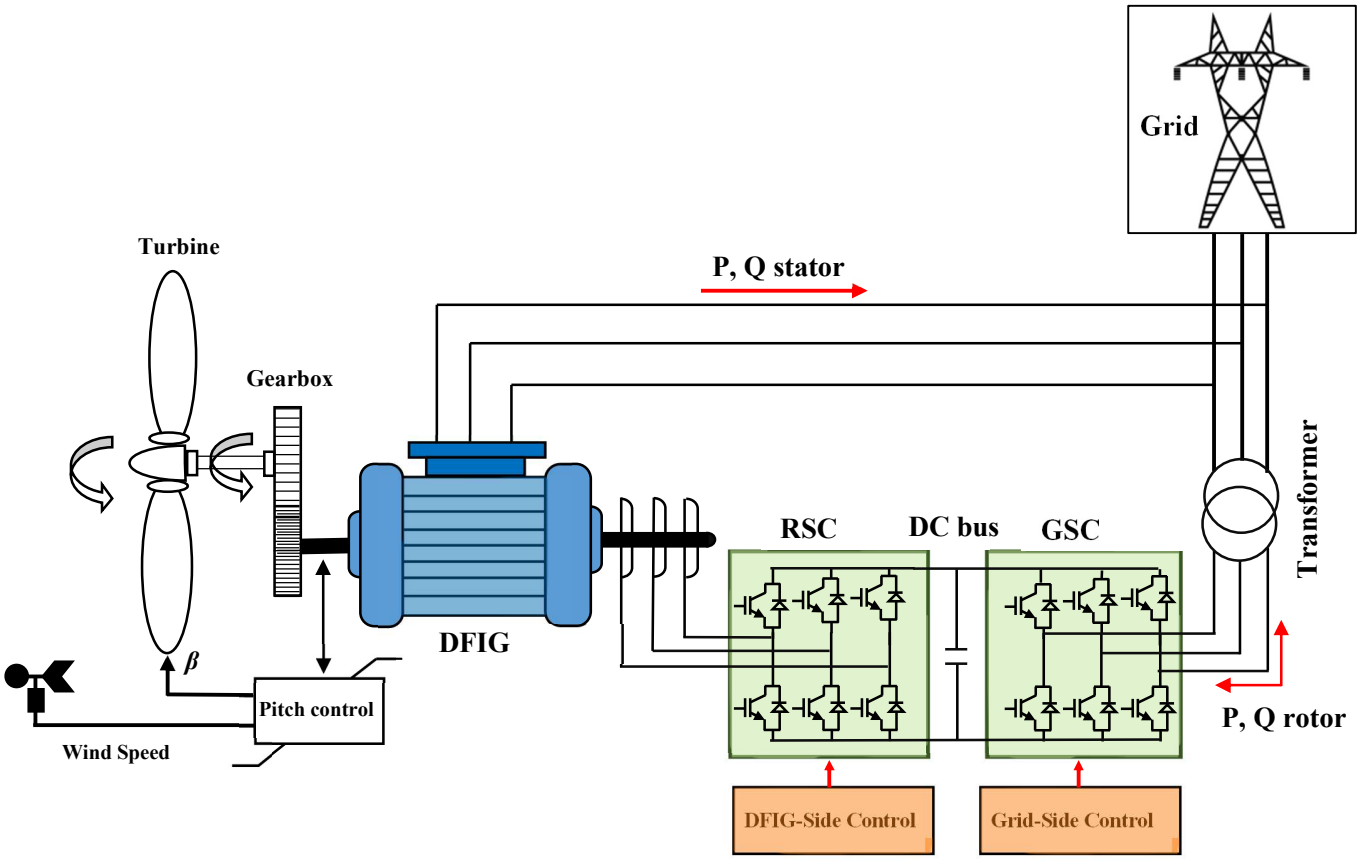

Figure II.1 Description of the wind system based on DFIG.

II.3 Wind modeling

Wind energy is an important input to wind turbine systems, the effectiveness of which varies with wind speed changes. Understanding the overall characteristics of wind is indispensable in the study of dynamic properties of the overall energy conversion system, as power generation from wind is proportional to the cube of its speed, and accurate wind speed prediction is one of the major requirements to optimize turbine performance and profitability. In mathematical terms, the random wind speed can be expressed in terms of time-dependent functions that include a number of harmonics, hence representing a clear expression of temporal variation.

A model in this case goes from a simple exponential law to a complex spectral and spatial distribution taking into account turbulent phenomena. In theoretical simulations, the duration of the wind profile must necessarily be kept limited to cut down simulation time, and the profile needs to reflect all the characteristics that are specific to a given site including intensity, variability, and statistical distribution.

Although wind speed is a three-dimensional vector, the direction of this vector is not considered for vertical-axis turbines; whereas for small horizontal-axis three-blade turbines, it is corrected by the tail of the turbine. In the present work, the evolution of wind speed is taken as an analytical function changing in time and determined by several harmonics. One importance of the model is not only allowing the definition of wind turbines operational conditions but also quantifying the potential of usable energy, thereby establishing proper machine placement. [8, 9-10].

$$V(t) = 8 + 2\,sin(\omega t) - 1.750 + 1.5\,sin(5\omega t) - 1.25\,sin(10\omega t) - 0.5sin(50\omega t) - 0.25\,sin(100\omega t)$$

$With\ \omega = 2\pi/10$

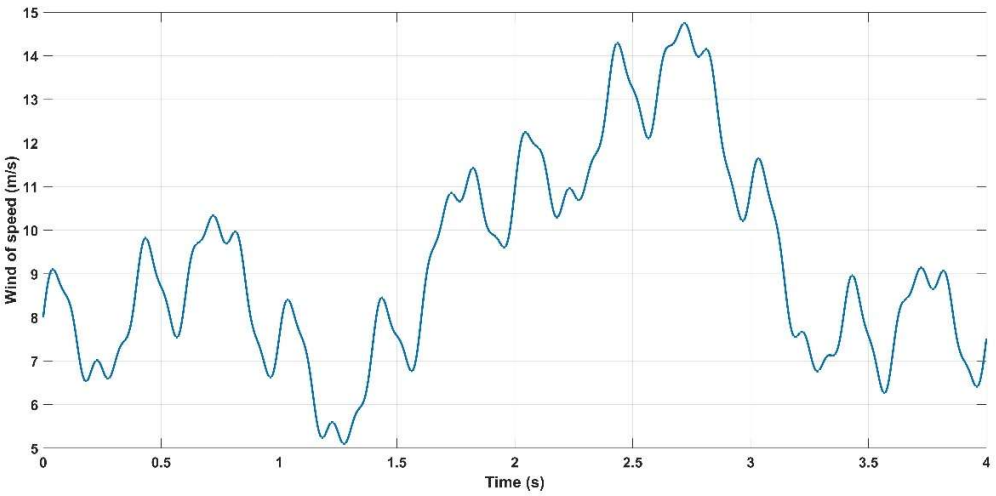

Figure II.2 A Random wind speed profile.

II.4 Modeling of the wind turbine

Dynamic modeling of a wind turbine involves the use of various equations to describe the behavior and operation of the turbine under changing operating conditions. The input and output variables of the turbine primarily depend on wind speed, as this variable significantly influences the amount of energy produced. Additional influential parameters include the turbine's geometric characteristics, expressed as a function of the rotor radius and the span of the turbine blades, the rotational speed of the turbine, the blade pitch angle, and the blade tilt angle. These equations can be aerodynamic, mechanical, or electrical in nature and are expressed in terms of the forces acting on the turbine blades and the control parameters of the generator [11,12].

The wind power equation is considered one of the basic equations in wind turbine modeling, as it expresses the available air power that can be extracted from the wind. This capacity is calculated using the following equation:

$$P_{wind} = \frac{1}{2}\rho\pi R^2 v^3 \quad \text{(II.1)}$$

Where: ρ: air density and wind speed (kg/m^3); R: represents the radius of the sail (m); v wind speed (m/s).

II.4.1 Aerodynamic power

The aerodynamic power at the turbine rotor represents the mechanical power captured by a wind turbine. This power is contingent upon the power coefficient, which is a function of the wind speed which is given by [13]:

$$P_{\text{Aero}} = \frac{1}{2}C_p(\lambda,\beta)\rho\pi R^2 v^3 \quad \text{(II.2)}$$

Where: C_p Coefficient of power; λ is Tip speed ratio; β is the pitch angle.

II.4.2 Power coefficient Cp

The important factors that have influence on the power coefficient $C_p$are the number of rotor blades and their geometric and aerodynamic shapes, like the length and profile of the sections. These designs are site adapted for characteristics, desired nominal power, type of regulation (pitch control or stall regulation), and operational mode (fixed or variable speed). The power coefficient, denoted as $C_p(\lambda,\beta)$, shows the aerodynamic efficiency of the wind turbine. It is a function of tip-speed ratio, λ, and the pitch angle of the blade, β.

The efficiency of the wind turbine blades' power coefficient (C_p) can be estimated analytically. Empirical and nonlinear the following equations model the variation of the power coefficient concerning the specific speed and blade pitch angle [14-16].

$$C_p(\lambda,\beta) = C_1\left(\frac{C_2}{\lambda_i} - \beta C_3 - C_4\right)e^{-\frac{C_5}{\lambda_i}} + C_6 \quad \text{(II.3)}$$

Where:

$$\lambda_i = \frac{1}{\lambda + 0.08.\beta} - \frac{0.035}{\beta^3 - 1} \quad \text{(II.4)}$$

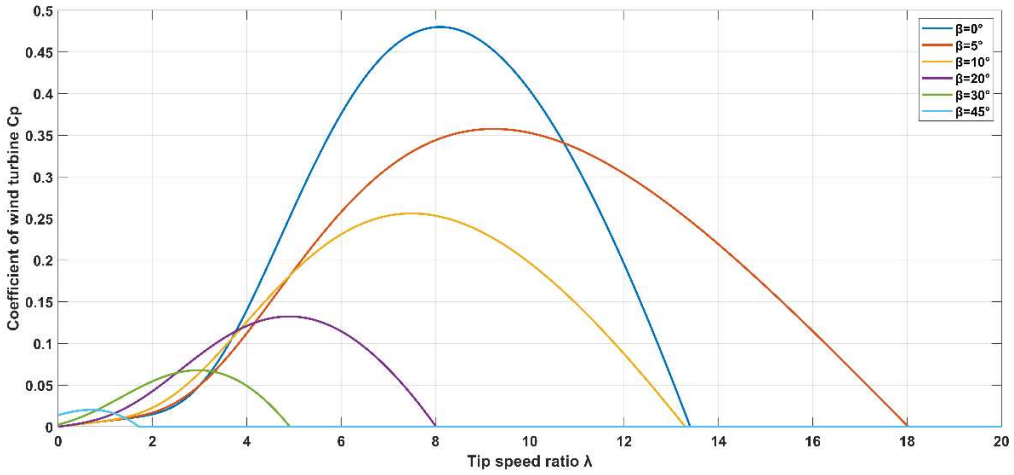

Figure II.3 Variation of the $\boldsymbol{\lambda}$ and $\boldsymbol{Cp}$- curve depending on the pitch angle of the blades ($\boldsymbol{\beta}$).

II.4.3 The specific speed (Tip-Speed-Ratio)

The specific speed, often denoted as λ, is defined as the ratio between the linear speed at the tip of the turbine blades (Ω_t , R) and the instantaneous wind speed. This relationship is expressed by the following equation [17-20]:

$$\lambda = \frac{\Omega_t R}{v} \tag{II.5}$$

II.4.4 Betz's Law

Betz's law was first formulated in 1929 and is named after the German scientist Albert Betz, who determined that wind turbines cannot capture and convert more than 59% of the kinetic energy of the wind into mechanical energy. The model shown in Figure II.4 illustrates the flow tube system surrounding a horizontal-axis wind turbine. The upstream wind speed of the generator is denoted by the symbol V_1, while V_2 represents the speed in the downstream direction [17,20-22].

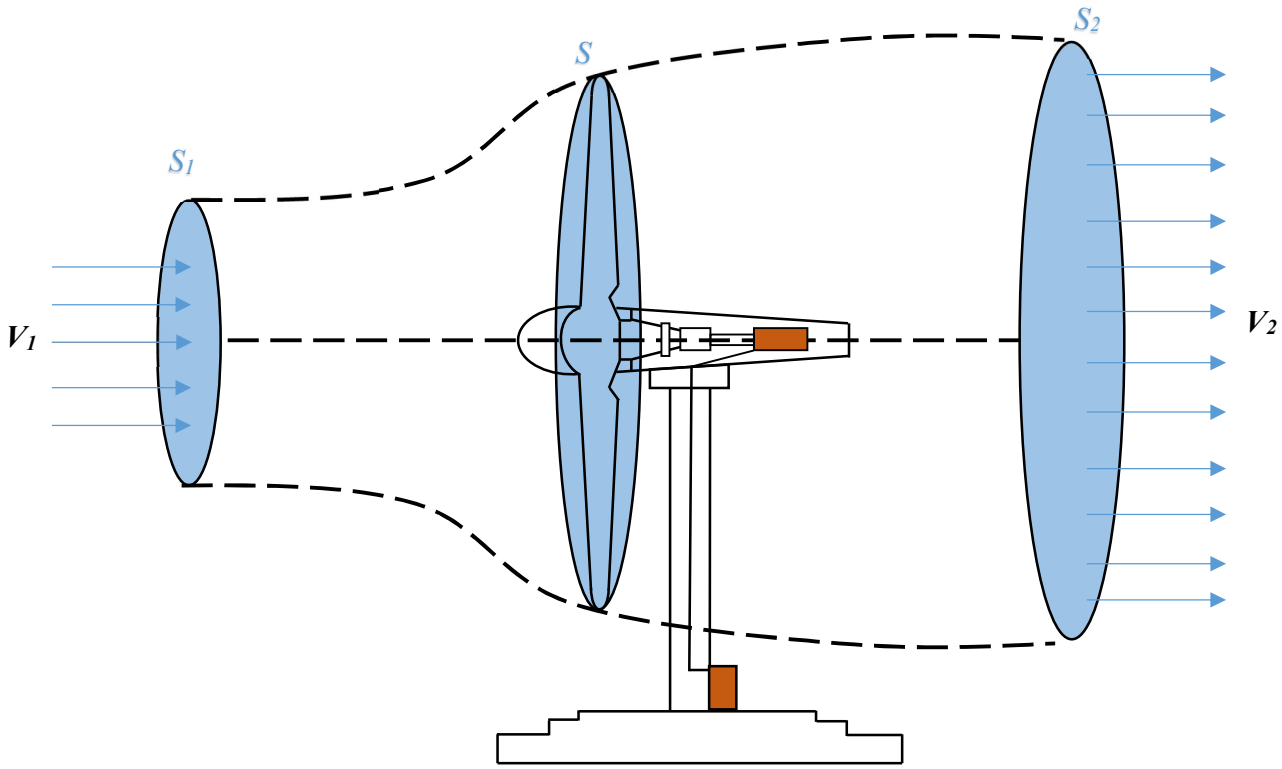

Figure II.4 Illustration of Betz's law.

When the air crosses the rotor at speed V_2, the average speed across the rotor can be expressed as $(V_1 + V_2)/2$. The moving air mass with density ρ that crosses the surface of the turbine blades in one second equals the product of the density ρ, the area S, and the average speed. So that is:

$$m = \frac{\rho S (V_1+V_2)}{2} \tag{II.6}$$

The difference between the upstream and downstream power represents the actual power extracted by the rotor blades:

$$P_{\text{Aero}} = \frac{m (V_1^2-V_2^2)}{2} \tag{II.7}$$

By substituting equation, 6 into equation 7, we find:

$$P_{\text{Aero}} = \frac{\rho S (V_1+V_2) (V_1^2-V_2^2)}{4} \tag{II.8}$$

The total power theoretically available on the surface S is extracted without reduction in wind speed by putting $V_2 = \frac{V_1}{3}$ in the expression (8):

$$P_{Aero} = \frac{\rho S V_1^3}{4}\left(1+\frac{1}{3}\right)\left(1+\frac{1}{9}\right) = \frac{\rho S V_1^3}{2}\left(\frac{16}{27}\right) \tag{II.9}$$

II.4.5 Model of the speed multiplier

Due to the slow speed of the turbine compared to the generator, a speed multiplier is used to match the turbine speed Ω_t with the speed required by the generator Ω_g. multiple the turbine speed results in a reduction of the generator torque T_g, according to the following mathematical equations [22-24]:

$$\begin{cases} \Omega_t G = \Omega_g \\ \frac{T_t}{G} = T_g \end{cases} \quad \text{(II.10)}$$

Where:

T_g is the generator torque;

T_t is turbine torque;

Ω_g is the rotational speed of the generator;

Ω_t is the turbine rotational speed;

G is the gain of the multiplier.

II.4.6 Mechanical shaft modeling

The fundamental equation of dynamics is essential for determining the evolution of the mechanical speed of a wind turbine's rotor based on the total mechanical torque applied to it. By taking into account the mechanical torque T_g exerted on the rotor shaft as well as the electromagnetic torque T_{em}, this equation allows the analysis of the variation in mechanical speed [20,25-27]:

$$J \frac{d\Omega_g}{dt} = T_g - T_{em} - F\Omega_g \quad \text{(II.11)}$$

Where:

J: is the total inertia referred to the generator shaft;

F : The total friction coefficient of the mechanical coupling;

T_{em}: The electromagnetic torque developed by the generator.

The following diagram represents the wind turbine model connected to the shaft through the gearbox:

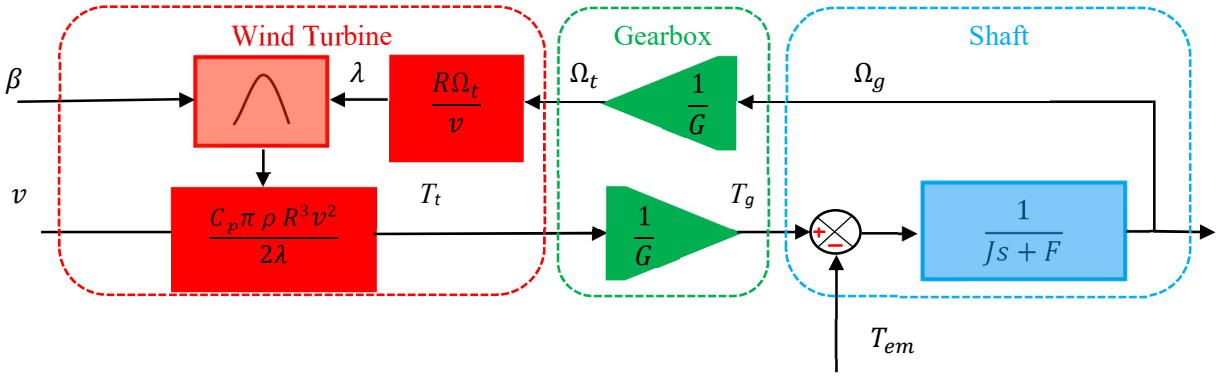

Figure II.5 The block diagram of wind turbine.

II.5 Wind turbine control

II.5.1 Operating zones of wind turbines

Given the fluctuating and random nature of the wind, the generated power in strong wind conditions can be very high. Therefore, control strategies are adopted to ensure optimal and high performance of wind turbines across a wide range of wind speeds. Accordingly, the operating regions are determined based on wind speed. Figure II.6 shows the power development as a function of wind speed, where the operating range of the variable-step wind system can be divided into four regions as follows [28-31]:

Zone 1: In this zone, the wind turbine activates when the mechanical speed exceeds a determined threshold Ω_{in} at this stage, the power delivered by the turbine is zero Pt=0 because the wind speed is insufficient to produce electrical energy;

Zone 2: The goal of this zone is to extract the maximum power available. In this zone, the power transmitted to the shaft depends on the wind speed *v*. So, when the generator speed reaches a certain threshold, a control algorithm, such as Maximum Power Point Tracking (MPPT), is used to optimize the extraction of maximum power;

Zone 3: In this region, the speed of the wind turbines is constant, making the power generated from the turbine equal to the nominal power;

Zone 4: In the fourth region, the wind turbines are stopped for safety purposes when the wind speed becomes too high and poses a risk to the turbines. The blade pitch angle is set at 90 degrees, which stops the turbine operation until the wind speed decreases.

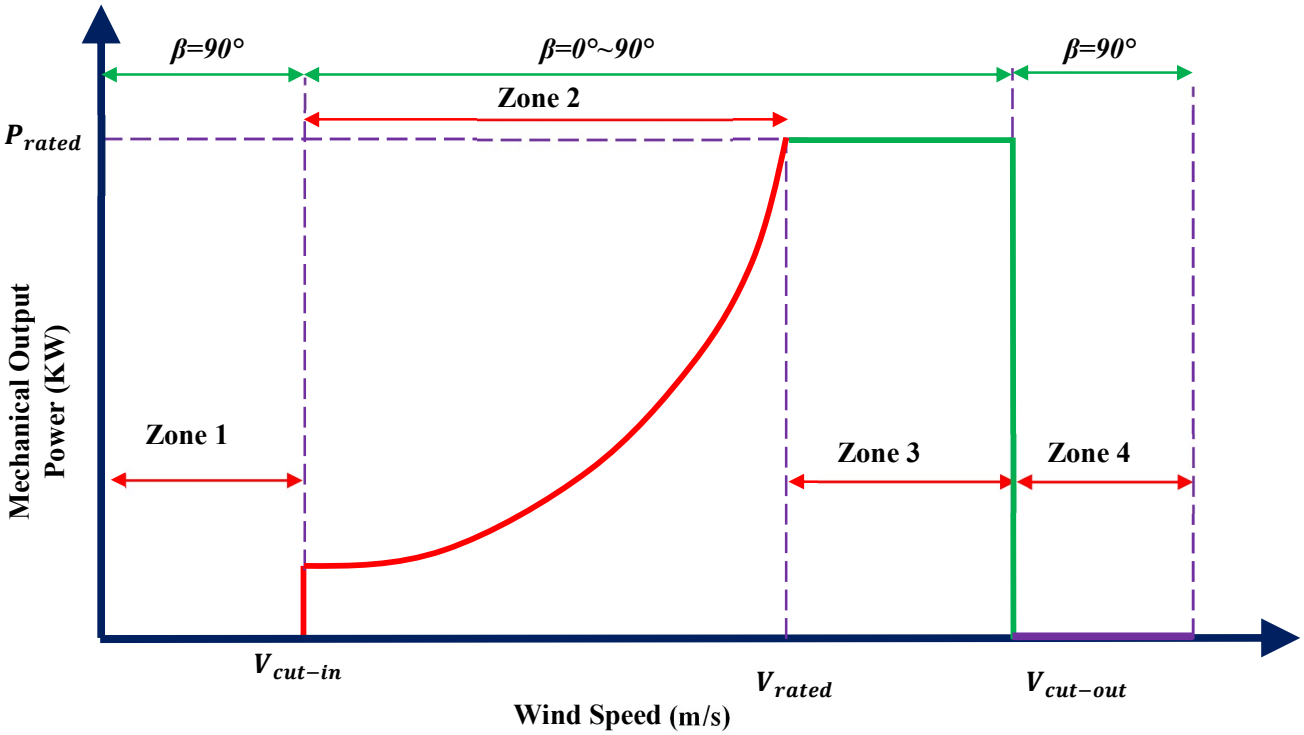

Figure II.6 Operating zones of the wind turbine.

II.5.2 Control of the wind turbine by using Maximum Power Point Tracking (MPPT) for maximizing the extracted power (Speed Control)

To ensure optimal power output from wind turbines, the rotor speed must be continuously adjusted to the maximum power point (MPP) using an MPPT algorithm, which adapts to changes in wind speed and speed ratio over time. Given the stochastic nature of wind and its impact on power variability, this approach assumes ideal performance of the electrical machine and its converter, maintaining the electromagnetic torque at its reference value for efficient power conversion where [32-34]:

$$T_g = T_{em\_ref} \tag{II.12}$$

The fundamental equation of dynamics, which describes the evolution of mechanical speed as a function of the total mechanical torque applied to the rotor, allows this speed to be adjusted relative to a reference value. This adjustment is achieved through appropriate speed control, aiming to establish a reference electromagnetic torque:

$$T_{em\_ref} = K_p\left(\Omega_{g_{ref}} - \Omega_g\right) + K_i \int (\Omega_{g_{ref}} - \Omega_g) \tag{II.13}$$

Where:

$$\Omega_{g,ref} = \frac{V\lambda_{opt}}{R}.G \tag{II.14}$$

The schematic illustrating this control method is shown in the following figure:

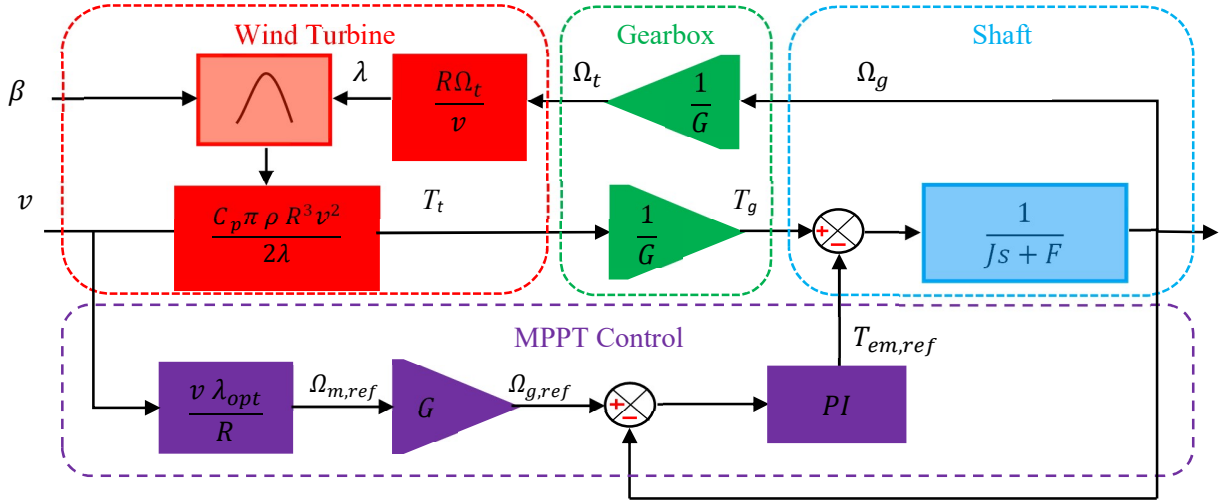

Figure II.7 Block diagram of power maximization through speed control.

II.5.3 Maximization of power without speed control

Inaccurate wind speed measurements introduce errors into the control process, adversely affecting the quality of the generated power. Therefore, it is preferable to avoid wind turbine control based on direct speed regulation. Instead, controlling the electromagnetic torque becomes a more effective approach, with wind speed being estimated using Equation II.13.

$$v_{est} = \Omega_t \frac{R}{\lambda_{opt}} \tag{II.15}$$

By utilizing Equation II.12 and Equation II.15, the reference electromagnetic torque is determined as follows:

$$T_{em\_ref} = \frac{C_{p\_max}}{2}.\frac{\rho.\pi.R^2}{\Omega_t}{v_{est}}^2 \tag{II.16}$$

Figure II.8 represents a detailed explanation of maximizing power without speed control

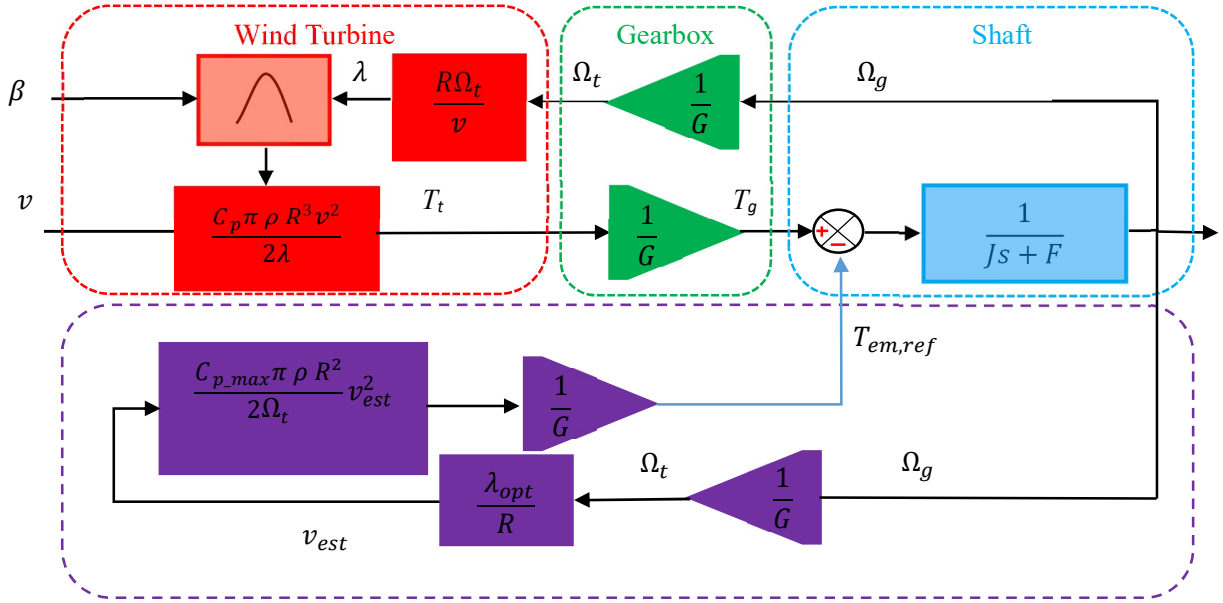

Figure II.8 Block diagram of power maximization without speed control.

II.6 Modeling of the Doubly Fed Induction Generator (DFIG)

The asynchronous generator model, utilizing rotating field theory diagrams, effectively manages the complexity of stator-rotor electromagnetic interactions despite its design simplicity. Matrix methods facilitate modeling, simulation, and control, particularly for the DFIG, which operates at a constant speed akin to a synchronous machine but with asynchronous characteristics due to the speed differential between the stator field and rotor. Equipped with three-phase windings, the DFIG enables magnetization through AC sources, presenting challenges due to its unique winding distribution and geometry. In wind power systems, the DFIG is crucial for converting mechanical to electrical energy, necessitating a mathematical model for control strategy design. This section introduces DFIG models in both three phase (abc) and rotating reference (dq) frames [1,22,23,35-37].

II.6.1 Three-Phase Model (a, b, c)

The doubly-fed induction generator (DFIG) is modeled by six electrical equations and one mechanical equation describing the rotor dynamics. The stator and rotor phases, designated respectively by a, b, c and A, B, C, are connected by an electrical angle defining their instantaneous relative position. By applying Faraday's and Ohm's laws to the windings, the stator and rotor voltages are expressed in a three phase framework. The stator consists of three fixed windings

spaced 120° apart in space, through which variable currents flow, while the rotor is modeled by three identical windings also spaced 120° apart [1,22,23,34-37].

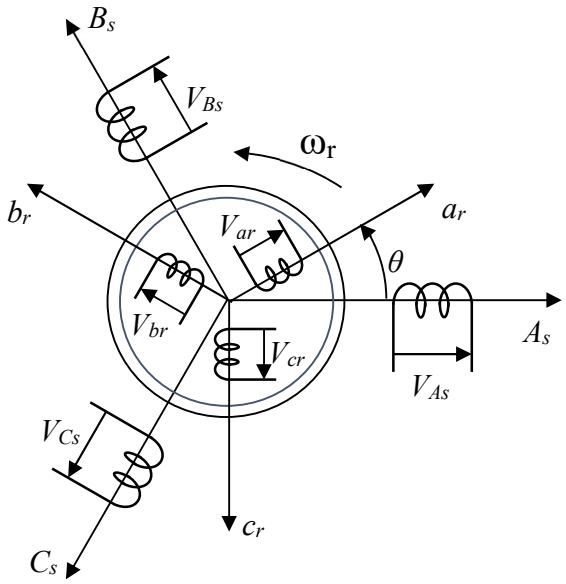

Figure II.9 Schematic representation of a doubly-fed induction generator in the three-phase reference frame.

Such that the electrical and magnetic equations for both the rotor and stator are as follows [1,22, 23,35-37]:

Electrical equations:

- **In the stator:**

$$\begin{cases} V_{sa} = R_s I_{sa} + \frac{d\varphi_{sa}}{dt} \\ V_{sb} = R_s I_{sb} + \frac{d\varphi_{sb}}{dt} \\ V_{sc} = R_s I_{sc} + \frac{d\varphi_{sc}}{dt} \end{cases} \quad \text{(II.17)}$$

- **In the rotor:**

$$\begin{cases} V_{ra} = R_r I_{ra} + \frac{d\varphi_{ra}}{dt} \\ V_{rb} = R_r I_{rb} + \frac{d\varphi_{rb}}{dt} \\ V_{rc} = R_r I_{rc} + \frac{d\varphi_{rc}}{dt} \end{cases} \quad \text{(II.18)}$$

Magnetic equations:

- **In the stator:**

$$\begin{cases} \varphi_{sa} = L_s I_{sa} + M I_{ra} \\ \varphi_{sb} = L_s I_{sb} + M I_{rb} \\ \varphi_{sc} = L_s I_{sc} + M I_{rc} \end{cases} \quad \text{(II.19)}$$

- **In the rotor**

$$\begin{cases} \varphi_{ra} = L_r I_{ra} + M I_{sa} \\ \varphi_{rb} = L_r I_{rb} + M I_{sb} \\ \varphi_{rc} = L_r I_{rc} + M I_{sc} \end{cases} \quad \text{(II.20)}$$

II.6.2 Simplifying assumptions

The modeling of the Doubly-Fed Induction Generator (DFIG) takes into account several simplifications due to the complex winding distribution and unique geometry. To address these challenges, conventional assumptions are applied, which are usually used for modeling electrical machines for general control purposes. These assumptions include simplifying the inherent complexities in the machine's structure, ensuring that the model is more manageable for analysis and application. Therefore, the following elements represent the assumptions that would simplify the modeling of the Doubly-Fed Induction Generator (DFIG) [1,22,23,35-37]:

- Non-Saturated Magnetic Circuit: It is assumed that the magnetic circuits of the stator and rotor are not saturated, allowing the relationships between the magnetic flux and currents to be considered linear. The magnetic permeability is therefore constant throughout the analysis;
- Negligible Losses: Losses due to hysteresis and eddy currents are neglected. This simplifies the model by eliminating the need to consider energy dissipation phenomena;
- Sinusoidal Magnetomotive Force: The magnetomotive force (MMF) is distributed sinusoidally along the periphery of both armatures, resulting in a sinusoidal spatial distribution of forces in the air gap. This is permitted by a symmetrical construction of the machine;
- Negligible Slot Effect: The slotting effect is considered negligible, allowing for the assumption that mutual inductances vary sinusoidally based on the angle between the rotor and stator axes, while self-inductances remain constant;
- Absence of Homopolar Mode: Since the neutral is not connected, there is no homopolar mode to consider in the model;

- Ignored Temperature and Skin Effects: The resistances of the windings are considered constant, regardless of temperature. Additionally, the skin effect is ignored, simplifying the electrical analysis of the machine;
- Symmetrical Construction of the Machine: The machine is considered to have perfect construction symmetry, implying an identical number of phases between the stator and rotor.

These assumptions allow for the development of a mathematical model of the DFIG that is both simple and sufficiently accurate for performance analysis and dynamic behavior studies in the context of wind energy conversion systems.

II.7 The Transition from Three-Phase to the Two-Phase (d, q) Model for the DFIG using Park Transformation

II.7.1 Park transformation

The Park transformation is an essential technique for simplifying the analysis of electrical machines, particularly in the context of doubly fed induction generators (DFIG). This transformation allows converting the variables of a three phase system (abc) into a two phase system using equivalent orthogonal windings. It is also reversible, allowing the conversion from the two phase system back to the three phase system (abc). This transformation relies on converting the stator and rotor windings into two orthogonal axes, typically referred to as the dq axes. This conversion facilitates obtaining a simplified mathematical model compared to the complex physical model of the original three phase system. where Park transformation is given like following [37,38-41]:

$$[X_{dq}] = [P(\theta)][X_{abc}] \tag{II.21}$$

The inverse Park transformation is given:

$$[X_{abc}] = [P(\theta)]^{-1}[X_{dq}] \tag{II.22}$$

Where:

$$[P(\theta)] = \sqrt{\frac{2}{3}}\begin{bmatrix} cos(\theta) & cos(\theta - \frac{2\pi}{3}) & cos(\theta + \frac{2\pi}{3}) \\ -sin(\theta) & -sin\left(\theta - \frac{2\pi}{3}\right) & -sin(\theta + \frac{2\pi}{3}) \\ \frac{1}{\sqrt{2}} & \frac{1}{\sqrt{2}} & \frac{1}{\sqrt{2}} \end{bmatrix} \tag{II.23}$$

$$[P(\theta)]^{-1} = \sqrt{\frac{2}{3}}\begin{bmatrix} cos(\theta) & -sin(\theta) & \frac{1}{\sqrt{2}} \\ cos(\theta - \frac{2\pi}{3}) & -sin\left(\theta - \frac{2\pi}{3}\right) & \frac{1}{\sqrt{2}} \\ cos(\theta + \frac{2\pi}{3}) & -sin(\theta + \frac{2\pi}{3}) & \frac{1}{\sqrt{2}} \end{bmatrix} \quad \text{(II.24)}$$

X: is voltage, current, or flux for the stator or rotor quantities.

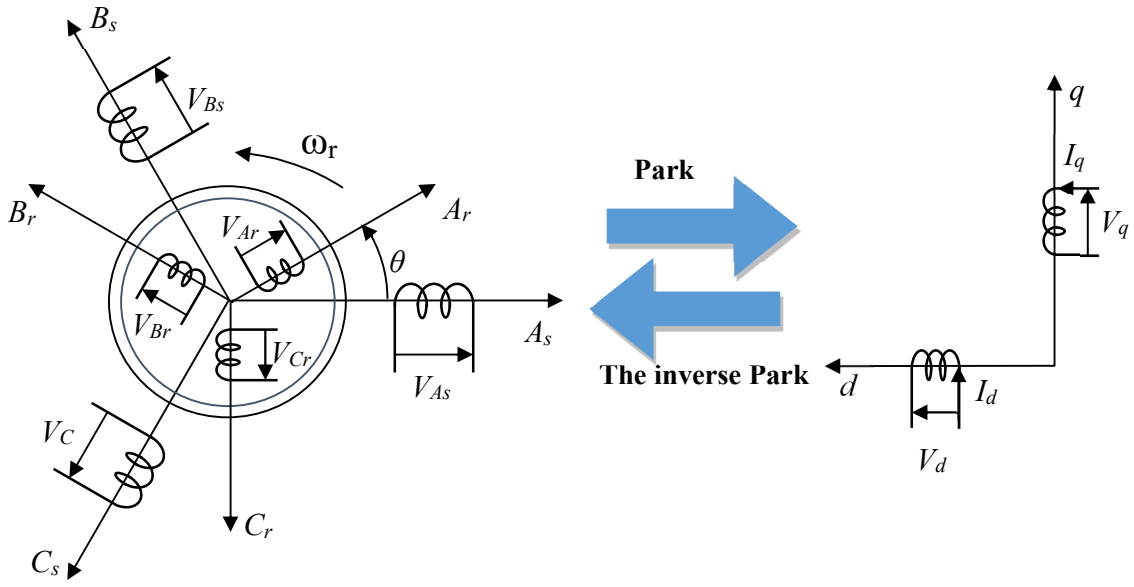

Figure II.10 Park transformation principle applied on DFIG.

II.7.2 Two-phase model of the DFIG in the (d, q) reference frame

The reference frame that coincides with the rotating field was chosen as the standard reference. After applying the Park transformation, the electrical, magnetic, and mechanical equations of the Doubly Fed Induction Generator (DFIG) were obtained as follows [33-36,39,40,42-47]:

- **Electrical equations:**

$$\begin{cases} V_{ds} = R_s I_{ds} + \frac{d\varphi_{ds}}{dt} - \omega_s \varphi_{qs} \\ V_{qs} = R_s I_{qs} + \frac{d\varphi_{qs}}{dt} + \omega_s \varphi_{ds} \\ V_{dr} = R_r I_{dr} + \frac{d\varphi_{dr}}{dt} - (\omega_s - \omega_r)\varphi_{qr} \\ V_{qr} = R_r I_{qr} + \frac{d\varphi_{qr}}{dt} + (\omega_s - \omega_r)\varphi_{qr} \end{cases} \quad \text{(II.25)}$$

- **Magnetic equations:**

$$\begin{cases} \varphi_{ds} = L_s I_{ds} + M I_{dr} \\ \varphi_{qs} = L_s I_{qs} + M I_{qr} \\ \varphi_{dr} = L_r I_{dr} + M I_{ds} \\ \varphi_{qr} = L_s I_{qr} + M I_{qs} \end{cases} \quad \text{(II.26)}$$

The active and reactive powers in the stator and rotor of the Doubly Fed Induction Generator (DFIG) are given as follows:

$$P_s = V_{ds} I_{ds} + V_{qs} I_{qs} \quad \text{(II.27)}$$

$$Q_s = V_{qs} I_{ds} - V_{ds} I_{qs} \quad \text{(II.28)}$$

$$P_r = V_{dr} I_{dr} + V_{qr} I_{qr} \quad \text{(II.29)}$$

$$Q_r = V_{qr} I_{dr} - V_{dr} I_{qr} \quad \text{(II.30)}$$

- **Expression of the electromagnetic torque:**

The electromagnetic torque can be expressed in terms of the fluxes and currents in the stator using the following relationship [33,35,36,39,40, 42-47]:

$$T_{em} = p \frac{M}{L_s} (\varphi_{ds} I_{qr} - \varphi_{qs} I_{dr}) \quad \text{(II.31)}$$

II.8 Conclusion

In summary, the Doubly-Fed Induction Generator (DFIG) emerges as a sophisticated and efficient solution for enhancing wind energy utilization. Its adaptability to variable wind conditions and high energy conversion efficiency make it a preferred choice in modern wind power applications. This chapter has provided a comprehensive overview of the fundamental components of a wind energy conversion system, including turbine modeling, mechanical shaft dynamics, and the role of speed multipliers. Furthermore, control strategies such as Maximum Power Point Tracking (MPPT) have been highlighted for their vital role in maximizing energy capture and maintaining operational stability. A detailed mathematical model of the DFIG was also introduced in both the three-phase (abc) and two-phase rotating reference (dq) frames, facilitated by the Park transformation. This model forms the analytical basis for subsequent chapters, serving as a foundational element for the design and development of advanced control techniques in wind energy systems, with the ultimate aim of supporting the transition toward long term sustainable energy solutions.

REFERENCES BIBLIOGRAPHIQUES

[1] Azzouz, T. (2015). *Modélisation et commande d'un système de conversion d'énergie éolienne à base d'une MADA* (Doctoral dissertation, Université Mohamed Khider-Biskra).

[2] TOUAM, M. (2012). *MODÉLISATION ET COMMANDE DE LA GÉNÉRATRICE ASYNCHRONE A DOUBLE ALIMENTATION MONTÉE DANS UN SYSTÈME ÉOLIEN* (Doctoral dissertation, Ecole nationale polytechnique d'Oran-Maurice Audin).

[3] BENMEZIANE, M. (2014). Contribution à la Commande Robuste de la Machine Asynchrone à Double Alimentation MADA (Doctoral dissertation, Ecole nationale polytechnique d'Oran-Maurice Audin).

[4] Echiheb, F., Ihedrane, Y., Bossoufi, B., Bouderbala, M., Motahhir, S., Masud, M., ... & ElGhamrasni, M. (2022). Robust sliding-backstepping mode control of a wind system based on the DFIG generator. *Scientific reports*, *12*(1), 11782.

[5] Idrissi, I., Chafouk, H., El Bachtiri, R., & Khanfara, M. (2019). Modeling and simulation of the variable speed wind turbine based on a doubly fed induction generator. IntechOpen.

[6] Ansari, A. A., & Dyanamina, G. (2022). Fault ride-through operation analysis of doubly fed induction generator-based wind energy conversion systems: a comparative review. *Energies*, *15*(21), 8026.

[7] Asghar, M. (2018). Performance comparison of wind turbine based doubly fed induction generator system using fault tolerant fractional and integer order controllers. *Renewable Energy*, *116*, 244-264.

[8] Yahdou, A. ‘‘*Commande hybride par mode glissant d’ordre 2 d’un systéme éolien à double rotor’’,* Doctoral dissertation, Alger, Ecole Nationale Polytechnique, 2017.

[9] ZOUGGAR, E. O. (2021). *Contribution à la modélisation et à la commande robuste d’un système éolien basé sur les génératrices asynchrones* (Doctoral dissertation, Université de Batna 2).

[10] CHEBEL AHLEM Contribution à l'amélioration de l'efficacité d'une chaine de conversion éolienne couplée à un réseau électrique, Doctoral dissertation, UNIVERSITE BADJI MOKHTAR-ANNABA 2022.

[11] Fateh, L. (2016). Modélisation et simulation d’une chaine de conversion d’énergie éolienne à base d’une machine synchrone à aimant permanent. *Mémoire Doctorat*.

[12] SLIMANE, W. (2021). : Modélisation et Commande d’une GADA Destinée à la Production de l’Energie Electrique dans une Chaine Eolienne (Doctoral dissertation, Université Mohamed Khider–Biskra).

[13] BENAICHA, S. (2014). *Étude Théorique et Expérimentale d'une Génératrice Synchrone utilisée dans une Chaine Eolienne à Axe Verticale* (Doctoral dissertation, Université de Batna 2).

[14] Douara, B.o.; Kouzou, A.; Hafaifa, A.; Rodriguez, J.; Abdelrahem, M. An Enhanced Second-Order Terminal Sliding Mode Control Based on the Super-Twisting Algorithm Applied to a Five-Phase Permanent Magnet Synchronous Generator for a Grid-Connected Wind Energy Conversion System. *Energies* 2025, *18*, 355. https://doi.org/10.3390/en18020355

[15] T. Mebkhouta, A. Golea, R. Boumaraf, T. M. Benchouia, and D. Karboua, “A High Robust Optimal Nonlinear Control with MPPT Speed for Wind Energy Conversion System (WECS) Based on Doubly Fed Induction Generator (DFIG)”, *Period. Polytech. Elec. Eng. Comp. Sci.*, vol. 68, no. 1, pp. 1–11, Jan. 2024.

[16] Yadav, Pankaj Kumar, Ankit Kumar, and Satyanand Jaiswal. "A critical review of technologies for harnessing the power from flowing water using a hydrokinetic turbine to fulfill the energy need." Energy Reports 9 (2023): 2102-2117.

[17] Messaoud, m. (2017). Etude comparative des architectures et strategies de controle d'un aerogenerateur synchrone a aimants permanents. Doctorat thesis (2014), université de batna 2.

[18] MAZOUZ, F. (2013). Commande d'un système éolien à base d'un générateur synchrone à aimants permanents (Doctoral dissertation, Université de Batna 2).

[19] Abderrahim, I. (2015). Amelioration de la qualite d'energie d'un systeme de conversion d'energie eolienne a base de machine asynchrone a double alimentation et connecte au reseau electrique=. Ph. D. Thesis.

[20] KHETTACHE, L. (2019). Contribution à l'Amélioration des Performances Des Systèmes Eoliens (Doctoral dissertation, UNIVERSITE MOHAMED KHIDER BISKRA).

[21] Poitiers, F. (2003). *Etude et commande de génératrices asynchrones pour l'utilisation de l'énergie éolienne-machine asynchrone a cage autonome-machine asynchrone a double alimentation reliée au réseau* (Doctoral dissertation, Université de Nantes).

[22] Boulaam, K. (2020). *Commande d'une machine à courant alternatif avec système hybride de stockage pour la production éolienne* (Doctoral dissertation).

[23] DJERIRI, Y. (2015). *Commande directe du couple et des puissances d'une MADA associée à un système éolien par les techniques de l'intelligence artificielle* (Doctoral dissertation).

[24] Gaillard, A. (2010). *Système éolien basé sur une MADA: contribution à l'étude de la qualité de l'énergie électrique et de la continuité de service* (Doctoral dissertation, Université Henri Poincaré-Nancy 1).

[25] Mourad, L. (2016). Synthèse de lois de commande non-linéaires pour le contrôle d'une machine asynchrone à double alimentation dédiée à un système aérogénérateur (Doctoral dissertation, Ph. D. Thesis, Université Aboubakr Belkaid–Tlemcen–Faculté de Technologie).

[26] Mensou, S., Essadki, A., Nasser, T., Idrissi, B. B., & Tarla, L. B. (2020). Dspace DS1104 implementation of a robust nonlinear controller applied for DFIG driven by wind turbine. *Renewable Energy*, *147*, 1759-1771.

[27] Guenoune, I. (2018). Commandes non linéaires robustes de systèmes éoliens (Doctoral dissertation, École centrale de Nantes; Université Abou Bekr Belkaid (Tlemcen, Algérie)).

[28] Gergaud, O. (2002). *Modélisation énergétique et optimisation économique d'un système de production éolien et photovoltaïque couplé au réseau et associé à un accumulateur* (Doctoral dissertation, École normale supérieure de Cachan-ENS Cachan).

[29] Aubrée, R. (2014). *Thèse de Doctorat Stratégies de commande sans capteur et de gestion de l'énergie pour les aérogénérateurs de petite puissance* (Doctoral dissertation, Université de Nantes).

[30] Rouabhi, R. (2016). Contrôle des puissances générées par un système éolien à vitesse variable basé sur une machine asynchrone double alimentée (Doctoral dissertation, Université de Batna 2).

[31] Rogez, V. (2004). Modélisation simplifiée de sources de production décentralisée pour des études de dynamique des réseaux. Application à l'intégration d'une production éolienne dans un réseau de distribution insulaire. Th: Génie Electrique: Université d'Artois, Béthune.

[32] Azzouz, S., Messalti, S., & Harrag, A. (2019). Innovative PID-GA MPPT controller for extraction of maximum power from variable wind turbine. Przegląd Elektrotechniczny, 1(8), 117-122.

[33] Mebkhouta, T., Golea, A., Boumaraf, R., Benchouia, T. M., & Karboua, D. (2024). A High Robust Optimal Nonlinear Control with MPPT Speed for Wind Energy Conversion System (WECS) Based on Doubly Fed Induction Generator (DFIG). Periodica Polytechnica Electrical Engineering and Computer Science, 68(1), 1-11.

[34] Ghoudelbourk, S., Dib, D., Omeiri, A., & Azar, A. T. (2016). MPPT control in wind energy conversion systems and the application of fractional control (PIα) in pitch wind turbine. *International Journal of Modelling, Identification and Control*, *26*(2), 140-151.

[35] TOUAL, B. (2019). *Contribution à la Commande et la Gestion des Sources Hybrides d'Energie Electrique* (Doctoral dissertation, Université de Batna 2).

[36] Yamina, T. (2011). *Detection de Défauts de la génératrice asynchrone à double alimentation (DFIG)* (Doctoral dissertation, Université Mohamed Boudiaf des sciences et de la technologi).

[37] Hamane, B. (2018). *Commande robuste d'un aérogénérateur à base de machine asynchrone à double alimentation pilotée par un convertisseur matriciel* (Doctoral dissertation, Université du Québec à Trois-Rivières).

[38] BOUSSEKRA, F. (2022). *Commande sans Capteur de Vitesse de la Machine Synchrone* (Doctoral dissertation, Université de Batna 2).

[39] Abdennour, D. (2010). *Contrôle direct du couple du moteur à induction sans capteur de vitesse associée à un observateur non linéaire* (Doctoral dissertation, Batna, Université El Hadj Lakhdar. Faculté des Sciences de l'Ingénieur).

[40] Abdelhak, M. B. (2016). *Ministère de l'Enseignement Supérieur et de la Recherche Scientifique* (Doctoral dissertation, UNIVERSITE BADJI MOKHTAR-ANNABA).

[41] Mazouz, F. (2020). CONTROLE DES PUISSANCE ACTIVE ET REACTIVE DANS LES AEROGENERATEURS DOUBLES ALIMENTES. *Thesis doctorat*.

[42] Chojaa, H., Derouich, A., Chehaidia, S. E., Zamzoum, O., Taoussi, M., Elouatouat, H. "Integral sliding mode control for DFIG based WECS with MPPT based on artificial neural network under a real wind profile", Energy Reports, 7, pp. 4809–4824, 2021.

[43] Radaideh, A., Bodoor, M., Al-Quraan, A. "Active and Reactive Power Control for Wind Turbines Based DFIG Using LQR Controller with Optimal Gain-Scheduling", Journal of Electrical and Computer Engineering, 2021, 1218236, 2021

[44] Kelkoul, B., Boumediene, A. "Stability analysis and study between classical sliding mode control (SMC) and super twisting algorithm (STA) for doubly fed induction generator (DFIG) under wind tur-bine", Energy, 214, 118871. 2021.

[45] Mazouz, F. Contrôle Des Puissances Actives et Réactives Dans Les Aérogénérateurs Doubles Alimentés. Thèse Doctorat. Université de Batna, Batna, Algeria, 2020.

[46] Yaichi, I. Contribution à l'amélioration de la qualité d'énergie électrique d'un système éolien basé sur la MADA. Thèse Doctorat. Université djillali liabes de sidi-bel-abbes, Algeria, 2019.

[47] BEN AMAR, A. S. M. A. (2016). ETUDE DE LA COMMANDE D'UN SYSTEME ÉOLIEN BASE SUR UNE GADA (Doctoral dissertation, Université de Batna 2).

CHAPTRE III

ADVANCED CONTROL STRATEGIES FOR DFIG-BASED WIND ENERGY SYSTEMS

III.1 Introduction

Nowadays, many commercial models of wind turbines are DFIG based, these generators are widely recommended for their ability to operate effectively under variable wind speeds, delivering high energy conversion efficiency. However, their complex structure and nonlinear dynamics which pose the need for develop advanced control strategies to ensure optimal performance, stability, and reliability in diverse operational scenarios.

This chapter is dedicated to constructing and analyzing control techniques to specify requirements of DFIGs, the primary objective is designing the control of active and reactive stator powers. To achieve this, advanced control techniques are employed and evaluated systematically for their effectiveness. The chapter begins by defining the operational loops that responsible for the DFIG performance, providing a clear framework for understanding its control architecture. Then the control strategies are classified, offering a typical overview of the techniques employed to address the unique challenges posed by DFIG operations.

The foundational concept of vector control is also revisited to characterized its role in modern DFIG control systems.

Following this groundwork, the chapter transits into the design of nonlinear control strategies with a particular focus on Backstepping Control (BSC). Nonlinear control methodologies, such as BSC are highly effective in managing the complex and dynamic behaviors of DFIGs, offering enhanced stability and robustness. This section explores the development of BSC, outlining its historical evolution, defining its principles, and presenting a structured approach to its application in DFIG systems.

Complementing the nonlinear control strategies, the chapter also examines optimal control design through the Linear Quadratic Regulator (LQR). Optimal control provides a powerful framework for achieving superior system performance by minimizing predefined cost functions. The discussion on LQR highlights its theoretical foundations and application steps, emphasizing its suitability for controlling the dynamics of DFIGs.

A significant contribution of this chapter lies in the integration of BSC and LQR to develop a hybrid control design. By leveraging the advantages of both methodologies, the hybrid control approach addresses the limitations of individual strategies while enhancing overall system performance. The hybrid design is detailed, encompassing the power and current loops of the DFIG, the active and reactive stator powers are controlled and regulated through these techniques,

ensuring precise and efficient operation of the DFIG under varying conditions. LQR is implemented in the current loop, further enhancing the flexibility and adaptability of the control system. A comprehensive description of the combined control design is provided, underscoring its potential for achieving optimal performance in various operational conditions.

The effectiveness of the proposed control strategies is demonstrated through MATLAB/Simulink. These simulations validate the ability of the designed control techniques to achieve stable and efficient regulation of the active and reactive stator power. Furthermore, the comparative study between BSC and the hybrid control design highlights their performance to DFIG systems.

III.2 Constructing the Control for DFIG Model

After modeling the DFIG, the next crucial step is the application of control strategies. This stage begins with the identification of the operational loops that need to be regulated for efficient performance. Once these loops are identified, the control techniques are presented, classified, and explained in details, with their application design to each individual loop or the overall system. In this section, we will focus on identifying the key loops of the DFIG, classifying the various control strategies, and providing an in-depth explanation of the primary objective of the vector control design.

III.2.1 Defining the operational loops of DFIG

A key feature of the DFIG system which is multi-input and multi-output (MIMO), combined with the nonlinearity inherent in its electromagnetic torque and external disturbances that arise in the *dq* axes, commonly known as back EMF. The closed-loop control system of the DFIG can be organized into three primary loops, based on its operational principles and model. These loops are current loop, power loop, and speed loop. While the current loop is essential for all control strategies, the decision to implement either the speed or power loop depends on the specific control goals and application requirements. Various modeling techniques, such as state-space models or transfer functions, can categorize the control strategies for the DFIG into decoupling-based, linearization-based, or nonlinear methods, each designed to manage the challenges introduced by the generator's configuration [1,2].

III.2.2 Classification of Control Strategies for DFIG

Control strategies for the DFIG can be divided into i three main categories: Scalar based controllers, Direct Torque Control (DTC), and Vector based controllers. Scalar control is simple and easy to implement but is limited by slower responses and less accuracy during changes in operating conditions. Direct Torque Control (DTC) represents a distinct and widely used strategy that enables fast dynamic response by directly controlling torque and flux without requiring coordinate transformation. It uses hysteresis regulators and lookup tables but may suffer from torque ripple and sensitivity to parameter variations. In contrast, vector control provides more advanced and precise regulation, making it ideal for controlling performance in both steady and dynamic states. This approach includes traditional techniques like Field-Oriented Control (FOC), which use basic controllers like PID and hysteresis regulators. While this method works well for simpler applications, they may struggle with complex scenarios.

To address the DFIG's nonlinearity, advanced strategies have been employed. These include nonlinear methods such as Sliding Mode Control (SMC) and Backstepping Control (BSC), which are effective in handling the generator's dynamic behavior without linearization. Optimal techniques, such as Model Predictive Control (MPC) and Linear Quadratic Regulator (LQR), focus on achieving performance targets under defined conditions. Adaptive methods, like Model Reference Adaptive Control (MRAC), adjust to changes in real time, offering flexibility in various operational settings. Intelligent control approaches, including Fuzzy Logic and Artificial Neural Networks (ANNs), are designed to improve or replace traditional control strategies using data-driven solutions.

These diverse control techniques are essential for managing the complex behavior of the DFIG, ensuring efficient operation across different applications and scenarios. Figure III.1 outlines these strategies and their classifications for control strategies [1,3,4].

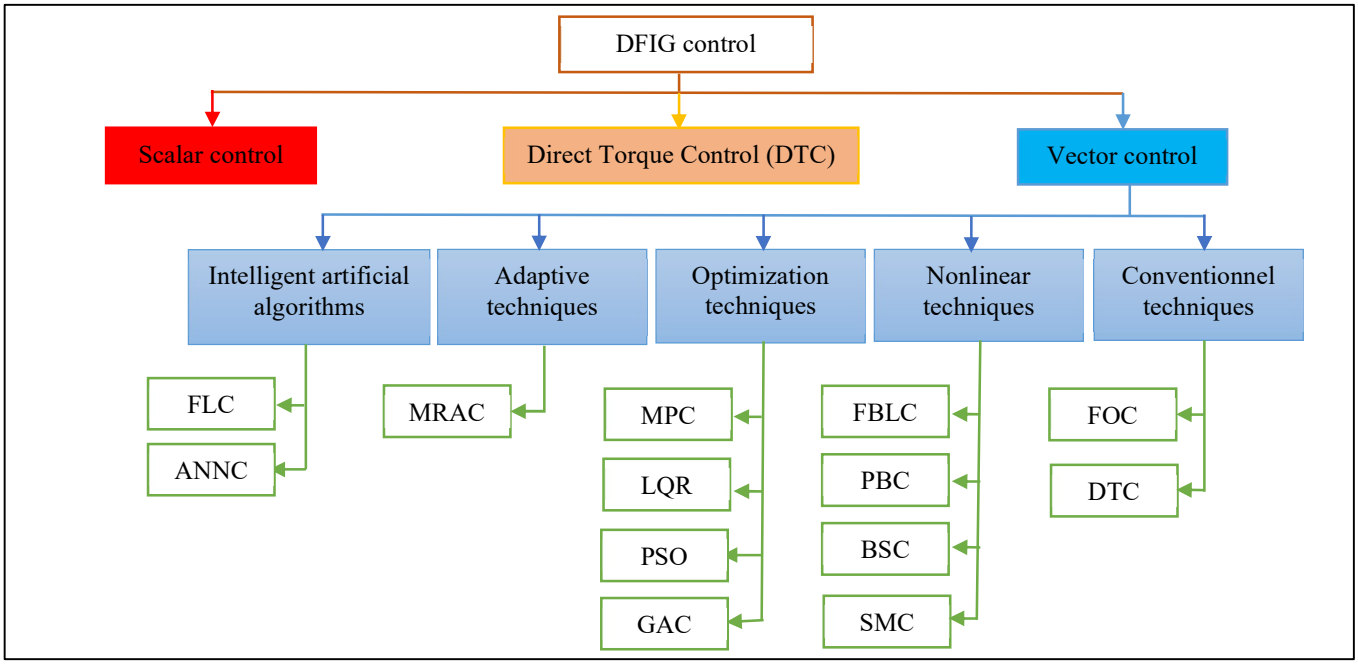

Figure III.1 Classification of control strategies for the DFIG.

III.2.3 Explanation of the main basic of the vector control

Vector control for the DFIG involves the decoupled control of active and reactive power by aligning the stator flux vector in a rotating reference frame. This approach treats the DFIG as a DC machine (DCM) by independently controlling the d-axis and q-axis components of the rotor currents (seen Figure III.2). The d-axis typically manages the reactive power or voltage control, while the q-axis manages the active power or torque. Using a mathematical model of the DFIG in the synchronously rotating reference frame, the control strategy ensures precise regulation of power exchange between the stator and the grid. In this method, the rotor current is decomposed into two perpendicular components: I_{dr} , which is responsible for controlling the stator flux, and I_{qr} , which directly influences torque generation. The control of speed or power (torque) is achieved exclusively by adjusting the d-axis flux, φ_{ds}, while the q-axis flux, φ_{qs}, is maintained at zero. This separation allows the torque to be directly managed by the value of I_{qr} , ensuring efficient and precise control, as defined in Equation III.1 [5-7].

$$T_{em} = \frac{pM}{L_s}(I_{qr}\varphi_{ds}) \quad \text{(III.1)}$$

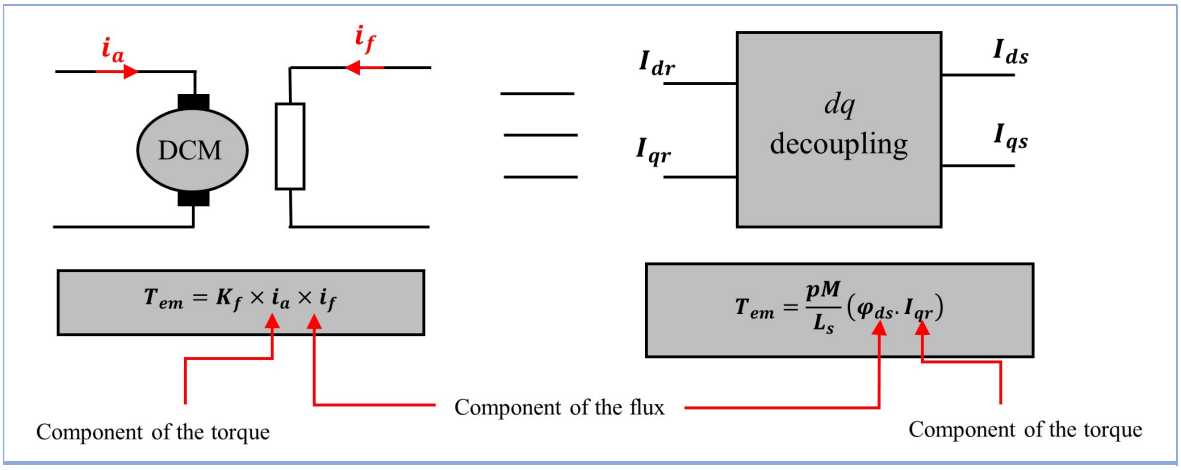

Figure III.2 Establishing the equivalence between the decoupled DCM and the DFIG.

As a consequence, the stator flux expressions become:

$$\begin{cases} \varphi_s = L_s I_{ds} + M I_{dr} \\ 0 = L_s I_{qs} + M I_{qr} \end{cases} \quad \text{(III.2)}$$

By neglecting the resistances of the stator phases, the expressions for the system can be simplified as follows:

$$\begin{cases} V_{ds} = 0 \\ V_{qs} = V_s = w_s \varphi_s \end{cases} \quad \text{(III.3)}$$

Then, rotor currents are used to express stator currents as follows:

$$\begin{cases} I_{ds} = \frac{\varphi_s}{L_s} - \frac{1}{L_s} M I_{dr} \\ I_{qs} = -\frac{M}{L_s} I_{qr} \end{cases} \quad \text{(III.4)}$$

By using Equations (II.27), (II.28), and the previously mentioned vector control principle, we obtain the active and reactive powers at the stator as follows:

$$\begin{cases} P_s = \frac{-V_s M}{L_s} I_{qr} \\ Q_s = \frac{-V_s M}{L_s} I_{dr} + \frac{V_s \varphi_s}{L_s} \end{cases} \quad \text{(III.5)}$$

As a result, the voltage equations of the rotor in the d-q axis are determined as follows [8, 9]:

$$\begin{cases} V_{dr} = R_r I_{dr} + a\dot{I}_{dr} - g w_s a I_{qr} \\ V_{qr} = R_r I_{qr} + a\dot{I}_{qr} + g w_s a I_{dr} + g \frac{M V_s}{L_s} \end{cases} \quad \text{(III.6)}$$

With: $a = L_r - \frac{M^2}{L_s} = L_r(1 - \sigma)$

III.3 Nonlinear control design with Backstepping control (BSC)

Based on a previous knowledge and works like Bouguerra Z and Benamor, Afaf, FOC and SMC suffer from chattering phenomena [8, 10], which led us to look for alternative control, to achieve enhanced performance and robustness in controlling the DFIG, the advanced nonlinear techniques is often presented. These methods address the limitations of linear control strategies by offering improved dynamic response and stability. One of these approaches is Backstepping Control (BSC), which is a nonlinear control strategy that is designed based on the Lyapunov function to ensure system stability with minimal chattering produced. In the following subsections, we will dive into the foundational principles of nonlinear control, define the BSC framework, and outline its primary objectives in optimizing DFIG performance.

III.3.1 Overall description of the nonlinear control

Since the 1970s, significant progress has been achieved in the theory and application of nonlinear control systems, driven largely by the adoption of advanced mathematical tools such as differential algebraic theory and modern differential geometry. Researchers like Slotine, Khalil, and Isidori pioneered the state feedback methodology to control the input-output behavior of nonlinear systems, leveraging Lie algebra for precise linearization [1,10]. Nonlinear control engineering focuses on systems exhibiting nonlinear behavior, where the input-output relations defy the principles of superposition and homogeneity that define linear systems. Its primary objective is to design controllers capable of stabilizing and managing such systems effectively. Among the advanced control strategies, nonlinear methods are regarded as highly developed and frequently applied in the control of electrical machines [11].

III.3.2 Conception History of the BSC

Backstepping control is a widely used nonlinear control strategy that effectively stabilizes systems by utilizing a Lyapunov function candidate. This method, which originated from the pioneering work of Kanellakopoulos et al. in 1991, is based on a step-by-step design approach. Each step introduces a virtual control law, ensuring the system's convergence to its equilibrium state. The concept of backstepping draws inspiration from earlier works, including those by T. Sinias (1989), Kokotivic & Sussmann (1989), and Feurer & Morse (1978). By breaking down the control problem into smaller, more manageable components, backstepping allows for the recursive

design of controllers, making it particularly effective in addressing the complexities and nonlinearities commonly found in control systems [12,13].

III.3.3 Definition of the BSC

Backstepping control is an advanced technique used to stabilize nonlinear systems, particularly when conventional linear control methods are ineffective. The key idea behind backstepping is to decompose the control task into a series of simpler tasks, more manageable subproblems, and then design a controller for each of these smaller problems. This method is often applied to systems described by ordinary differential equations (ODEs). The process involves constructing a sequence of controllers that target different aspects of the system's dynamics, with each step ensuring the stability of the closed-loop system. A Lyapunov function is used at every stage to validate that the system remains stable, and the process progresses with the addition of more controllers, the Lyapunov function provides the necessary assurance that the entire system's stability is maintained [1].

III.3.4 Analyze the main objectives and the application steps of the BSC

Designing controllers for nonlinear systems can be systematically approached using the BSC technique. The primary objective is to formulate a control law that guarantees the derivative of a selected Lyapunov function remains negative and the function itself stays positive definite. This is achieved by decomposing the system into a series of nested subsystems. The core of this method lies in constructing an algorithm that, for each subsystem, simultaneously determines the control law, adaptation dynamics, and a Lyapunov function to ensure system stability. As the process progresses, a new virtual order and a corresponding second Lyapunov function are calculated for each subsequent subsystem. Ultimately, this process leads to the formulation of a control expression that ensures the system's overall stability and performance. The applicability of the backstepping approach, similar to other control strategies, is generally limited to specific types of systems [12,14]. To express the system in "strict feedback" form, a variable transformation is performed, which modifies the system described by Equation III.6 into:

$$\begin{cases} \dot{\varphi}_1 = \varphi_2 \\ \dot{\varphi}_2 = \varphi_3 \\ \quad \vdots \\ \dot{\varphi}_{i-1} = \varphi_i \\ \quad \vdots \\ \dot{\varphi}_{n-1} = \varphi_n \\ \dot{\varphi}_n = u \\ y = \varphi_1 \end{cases} \tag{III.7}$$

Where the vector $\varphi = [\varphi_1 \quad \varphi_2 \quad \cdots \quad \varphi_n]^T$ is introduced. This transformation allows us to define the virtual control law for the first subsystem in terms of the state φ_2, which is driven by φ_3, with the final equation managed by the control law u, which controls the entire system.

Step 1: Trajectory Following and Error Definition

To ensure the system follows a specified trajectory, a tracking controller must be designed. The error between the output y and its reference y^* is defined as:

$$\varepsilon_1 = y^* - y = y^* - \varphi_1 \tag{III.8}$$

The time derivative of this error is:

$$\dot{\varepsilon}_1 = \dot{y}^* - \dot{\varphi}_1 = \dot{y}^* - \varphi_2 \tag{III.9}$$

The first Lyapunov function is chosen as:

$$V_1 = \frac{1}{2}{\varepsilon_1}^2 \tag{III.10}$$

And its derivative is:

$$\dot{V}_1 = \varepsilon_1 . \dot{\varepsilon}_1 = \varepsilon_1(\dot{y}^* - \dot{\varphi}_1) = \varepsilon_1(\dot{y}^* - \varphi_2) \tag{III.11}$$

To ensure the error converges to zero, the derivative of the Lyapunov function must be negative. Therefore, we choose:

$$\dot{y}^* - \varphi_2 = -k_1\varepsilon_1 \tag{III.12}$$

With $k_1 > 0$, leading to:

$$\varphi_2 = \dot{y}^* + k_1\varepsilon_1 \tag{III.13}$$

Step 2: Error Dynamics for φ_2

Since φ_2 cannot be directly controlled, a new error term is introduced:

$$\varepsilon_2 = {\varphi_2}^* - \varphi_2 = \dot{y}^* + k_1\varepsilon_1 - \varphi_2 \tag{III.14}$$

Its derivative is:

$$\dot{\varepsilon}_2 = \ddot{y}^* + k_1\dot{\varepsilon}_1 - \dot{\varphi}_2 \tag{III.15}$$

Substituting the expressions for $\dot{\varepsilon}_1$ and ε_2, we can write:

$$\dot{\varepsilon}_2 = \ddot{y}^* + k_1(\varepsilon_2 - k_1\varepsilon_1) - \dot{\varphi}_2 \tag{III.16}$$

A new candidate Lyapunov function is introduced:

$$V_2 = \frac{1}{2}({\varepsilon_1}^2 + {\varepsilon_2}^2) \tag{III.17}$$

and its derivative is:

$$\dot{V}_2 = \varepsilon_1.\dot{\varepsilon}_1 + \varepsilon_2.\dot{\varepsilon}_2 = -k_1{\varepsilon_1}^2 + \varepsilon_2(\varepsilon_1 - \dot{\varphi}_2 + \dot{\varphi}_2{}^*) \tag{III.18}$$

To satisfy the Lyapunov stability criterion, the term inside the brackets must be equal to $-k_1\varepsilon_2$, which leads to the following expression for the second virtual order$\varphi_3{}^*$:

$$\varphi_3{}^* = \varepsilon_1\left(1 - {k_1}^2\right) + \varepsilon_2(k_1 + k_2) + \ddot{y}^* \tag{III.19}$$

The Lyapunov function satisfies the stability condition when:

$$\dot{V}_2 = -k_1{\varepsilon_1}^2 - k_2{\varepsilon_2}^2 \tag{III.20}$$

Thus, the error terms converge to zero, and the system stability is guaranteed.

Steps for Subsequent

The process proceeds similarly for subsequent steps, introducing new error terms and Lyapunov functions for each subsystem. For each step, the error is defined as:

$$\varepsilon_i = \varphi_i{}^* - \varphi_i \tag{III.21}$$

And the corresponding Lyapunov function is:

$$V_i = \frac{1}{2}\sum_{j=1}^{i}\varepsilon_j^2 \tag{III.22}$$

The virtual control law is then determined as:

$$\varphi_{i+1}^* = k_i\varepsilon_i + \varepsilon_{i-1} + \dot{\varphi}_i{}^* \tag{III.23}$$

Finally, at the n-th step, the actual control law u is expressed as:

$$u = \dot{\varphi}_n^* \tag{III.24}$$

And the complete backstepping control law is:

$$u = k_n\varepsilon_n - \varepsilon_{n-1} + \dot{\varphi}_n^* \tag{III.25}$$

This procedure provides a systematic approach for controlling nonlinear systems using the backstepping technique, ensuring stability and performance across all subsystems. The control strategy based on the backstepping technique can be illustrated in a diagram (seen Figure III.3), where each subsystem and its corresponding control law are depicted, reflecting the step-by-step process for ensuring the system's stability.

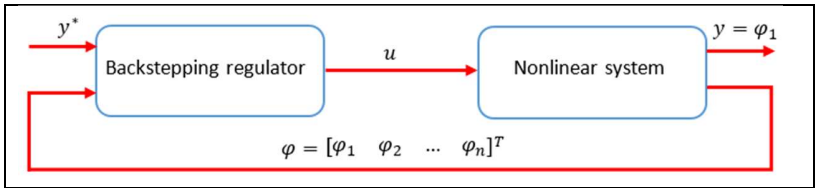

Figure III.3 Diagram illustrating the principle of backstepping control.

III.4 Optimal control design with Linear Quadratic Control

The backstepping control theory isn't handling well against the sudden external disturbance. therefore, its recommended to combine this previous strategy with another control strategy to get benefit of both strategies, to reach an optimized performance. Among these strategies, optimal control has emerged as a powerful and widely adopted approach for resolving classical vector control challenges. By formulating control problems within the framework of performance criteria, optimal control enables the design of controllers that ensure the best possible system behavior according to predefined objectives.

The following section explores the key aspects of LQR, starting with a general overview of optimal control theory, followed by a formal definition of LQR and a detailed description of its primary objectives. This foundation sets the stage for understanding how LQR contributes to addressing dynamic challenges in vector control systems

III.4.1 General overview of the optimal control

Optimal control is a branch of control theory that focuses on determining the most effective control strategy for a dynamic system while adhering to specific objectives and constraints. The primary aim is to identify control inputs that guide a system, referred to as the plant, from its initial state to a desired final state while meeting physical restrictions and optimizing a given performance metric, also known as the cost function or performance index.

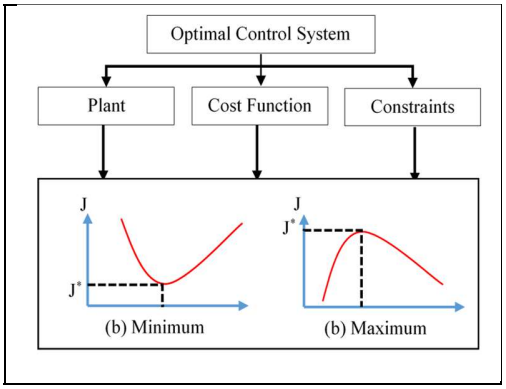

Figure III.4 Statement of the Optimal Control Problem.

As illustrated in Figure III.4, the optimal control u*(t) (* denotes optimal condition) ensures the system's trajectory is both constrained and performance-optimized. This methodology operates on several foundational principles [1,15-17]:

- **Dynamic Systems:** Optimal control applies to systems that evolve over time, where the relationships between state variables and control inputs are modeled using differential or difference equations.
- **Control Inputs:** These are parameters that influence system behavior. The optimal control problem involves determining the time-dependent values of these inputs to achieve a specific objective.
- **Cost Function:** This is a mathematical representation of the system's performance, which serves as the metric to be minimized or maximized. The choice of cost function depends on the control problem's objectives, such as minimizing energy consumption, enhancing stability, or improving other performance indicators.
- **Constraints:** Practical applications often impose limitations on state variables and control inputs. These constraints may arise from operational limits, safety considerations, or physical boundaries, all of which must be accounted for in the optimization process.
- **Feedback Mechanisms:** Real-time feedback is often incorporated to adjust control inputs based on the system's current state, enabling adaptability to disturbances and changes in operating conditions.

Optimal control plays a pivotal role in various engineering and scientific fields such as aerospace, robotics, economics, finance, and chemical engineering. In these domains, optimizing the performance of dynamic systems under constraints is a key objective. The selection of an appropriate optimal control strategy is influenced by the system's dynamics, the structure of the cost function, and the nature of the constraints involved. Depending on the specific problem characteristics, optimization techniques are generally classified into two main categories: local and global optimization methods, each offering distinct advantages, each suited to specific types of challenges. The choice of technique is tailored to the problem's specific requirements, ensuring effective solutions for dynamic system optimization.

Table III.1: Optimization solution techniques

Technique	Optimization category
Dynamic Programming	Global
Pontryagin's Minimum Principle	Local
Linear Quadratic Regulator (LQR)	Local
Model Predictive Control (MPC)	Global
Gradient-Based Methods	Local
Genetic Algorithms	Global
Simulated Annealing	Global
Interior-Point Methods	Local
Sequential Quadratic Programming (SQP)	Local
Particle Swarm Optimization (PSO)	Global
Mixed-Integer Linear Programming (MILP)	Global

III.4.2 Definition of the LQR

The Linear Quadratic Regulator (LQR) is a fundamental optimal control method designed to achieve closed-loop stability and high performance in dynamic systems. It minimizes a quadratic cost function that balances system performance and control effort, ensuring precision, stability, and energy efficiency. By solving the algebraic Riccati equation, LQR computes optimal state feedback gains, making it particularly effective for linear systems with quadratic performance criteria. Its widespread use in various engineering fields highlights its computational efficiency and practical applicability.

III.4.3 Description of the main objectives of the LQR

LQR is a control design methodology aimed at achieving optimal system performance by minimizing a quadratic cost function while ensuring system stability. This approach frames the control problem as an optimization task, where the objective is to determine the optimal control input that minimizes the sum of penalties associated with both the system states and the control inputs. The quadratic cost function serves as a tool to balance the trade-off between reducing control effort and achieving the desired system behavior. The solution to the LQR problem is derived using principles from the calculus of variations and dynamic programming, resulting in a control law that is expressed as a linear feedback function of the system's state. To compute the

optimal state feedback gains, the algebraic Riccati equation is solved, providing an efficient and analytical solution. LQR is particularly well-suited for systems with linear dynamics and finds applications in diverse fields such as robotics, aerospace, and industrial process control. Its popularity in real-time systems arises from its computational simplicity and reliability. Moreover, LQR ensures stability and optimality under specific conditions, making it a robust choice for control design. For multi-input, multi-output (MIMO) systems, LQR employs feedback control to compute the correction matrix k that regulates the system inputs. This process aims to minimize the cost function, which is typically defined by two key components: the first, managed by the Q matrix, focuses on performance and stability, while the second, defined by the R matrix, emphasizes minimizing energy usage. The mathematical formulation of this cost function, as described in Equation III.26 [11,18,19], underscores LQR's ability to deliver precise and efficient control.

$$J = \int_0^{\infty}((x^T.Q.x) + (u^T.R.u))dt \quad \text{(III.26)}$$

Where R and Q are positive definite matrices.

The feedback control law for state space is given by:

$$u(t) = -k.x(t) = (-R^{-1}.B^T.P).x(t) \quad \text{(III.27)}$$

Where P is positive definite matrix. Its solution for satisfies the Algebraic Riccati Equation (ARE) as follows:

$$\mathrm{A^T.P + P.A - P.B.R^{-1}.B^T.P + Q = 0} \quad \text{(III.28)}$$

Using the state-space model, the control design based on the LQR technique can be structured as follows:

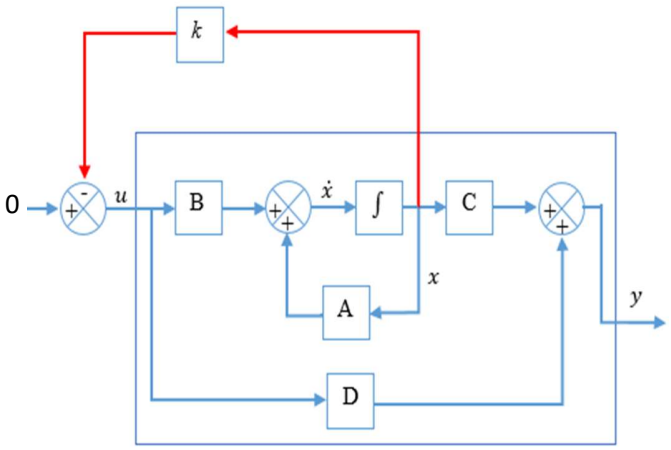

Figure III.5 Design of an LQR controller for systems based on SSM.

III.5 Hybrid control design using BSC and LQR

The nonlinear dynamics and multi-loop control requirements of the DFIG present significant challenges for conventional control methods. To address these complexities, this section explores a hybrid control design approach that combines Backstepping Control (BSC) and Linear Quadratic Regulator (LQR).

The backstepping Control method is chosen for its capability to systematically handle nonlinearities, ensuring robust stability and precise tracking in the power and current loops of the DFIG. On the other hand, the Linear Quadratic Regulator offers an optimal control solution by minimizing a predefined performance cost, enabling enhanced current regulation and efficient energy conversion.

In this section, we will first design the power and current loops of the DFIG using BSC, followed by the application of BSC on the power loop and LQR on the current loop design. Finally, the combination of these two control strategies will be described, demonstrating how their integration can yield improved system performance in terms of stability, robustness, and energy efficiency.

III.5.1 Design of the power loop of the DFIG using BSC

The power loop of the DFIG plays an important role in ensuring efficient energy conversion. In this subsection, the power loop will be designed using the BSC technique. Known for its ability to handle the nonlinear dynamics of DFIG, BSC enables systematic control law, while ensuring stability through Lyapunov functions. This design process will involve establishing the mathematical model of the power loop and applying BSC to regulate active and reactive power effectively under varying operating conditions. In order to apply the BSC, we should define the active and reactive power tracking errors, which are essential for formulating the control laws [3]. These errors can be defined as:

$$\begin{cases} \varepsilon_p = P_{s\_ref} - P_s \\ \varepsilon_q = Q_{s\_ref} - Q_s \end{cases} \tag{III.29}$$

Next, select a Lyapunov candidate function for both active and reactive power tracking errors. The functions are defined as:

$$\begin{cases} V_p = \frac{1}{2}.\varepsilon_p^2 \\ V_q = \frac{1}{2}.\varepsilon_q^2 \end{cases} \tag{III.30}$$

The time derivatives of these Lyapunov functions are:

$$\begin{cases}\dot{V}_p = \varepsilon_p . \dot{\varepsilon}_p \\ \dot{V}_q = \varepsilon_q . \dot{\varepsilon}_q \end{cases} \quad \text{(III.31)}$$

For system stability, we need to ensure that the time derivatives of these functions are negative. This condition is met if the derivatives of the tracking errors are negative:

$$\begin{cases}\dot{\varepsilon}_p = -k_p . \varepsilon_p \\ \dot{\varepsilon}_q = -k_q . \varepsilon_q \end{cases} \quad \text{(III.32)}$$

Here, k_p and k_q are positive constants. The negative sign ensures the stability of the system, and this results in the system being stable, as indicated by the negative time derivatives of the Lyapunov functions:

$$\begin{cases}\dot{V}_p = -k_p . \varepsilon_p^2 < 0 \\ \dot{V}_q = -k_q . \varepsilon_q^2 < 0 \end{cases} \quad \text{(III.33)}$$

Now, the reference rotor currents can be derived from the errors in active and reactive power tracking:

$$\begin{cases} I_{qr\_ref} = (k_p \varepsilon_p + \dot{P}_{s\_ref}) \frac{aL_s}{V_s M R_r} + (V_{qr} - g w_s a I_{dr} - g \frac{M V_s}{L_s}) / R_r \\ I_{dr\_ref} = \left(k_q \varepsilon_q + \dot{Q}_{s\_ref}\right) \frac{aL_s}{V_s M R_r} + \frac{V_{dr} + g w_s a I_{qr}}{R_r} \end{cases} \quad \text{(III.34)}$$

III.5.2 Design of the current loop of the DFIG using BSC

The current loop is fundamental for regulating the rotor currents in the DFIG, ensuring robust performance with minimal distortions. This subsection is dedicated to applicate Backstepping Control (BSC) in designing the current loop, leveraging its recursive structure to manage the inherent nonlinear behavior of the DFIG system. The control strategy aims to achieve precise current tracking and stability while effectively handling the external disturbances and uncertainties in the DFIG model. In this subsection, we focus on the second step of computing the rotor voltage control law, which addresses tracking errors associated with rotor currents. These errors can be defined as follows:

$$\begin{cases}\varepsilon_{I_{dr}} = I_{dr\_ref} - I_{dr} \\ \varepsilon_{I_{qr}} = I_{qr\_ref} - I_{qr} \end{cases} \quad \text{(III.35)}$$

Their time derivatives can be written as:

$$\begin{cases}\dot{\varepsilon_{I_{dr}}} = \dot{I_{dr\_ref}} - \dot{I_{dr}} \\ \dot{\varepsilon_{I_{qr}}} = \dot{I_{qr\_ref}} - \dot{I_{qr}} \end{cases} \quad \text{(III.36)}$$

Using Equation (III.6) in Equation (III.36), we obtain:

$$\begin{cases} \dot{\varepsilon_{I_{dr}}} = \dot{I_{dr\_ref}} - (V_{dr} - R_r I_{dr} + g w_s a I_{qr})/a \\ \dot{\varepsilon_{I_{qr}}} = \dot{I_{qr\_ref}} - (V_{qr} - R_r I_{qr} - g w_s a I_{dr} - g\frac{MV_s}{L_s})/a \end{cases} \quad \text{(III.37)}$$

To ensure system stability, the time derivatives of these tracking errors must also be negative:

$$\begin{cases} \dot{V}_{I_{qr}} = -k_{I_{qr}} . \varepsilon_{I_{qr}}^2 < 0 \\ \dot{V}_{I_{dr}} = -k_{dr} . \varepsilon_{I_{dr1}}^2 < 0 \end{cases} \quad \text{(III.38)}$$

Where $k_{I_{qr}}$ and k_{dr} are positive constants.

Finally, the rotor voltage references V_{dr} and V_{qr} are computed from the following global control law:

$$\begin{cases} V_{qr\_ref} = a\left(k_{I_{qr}}\varepsilon_{I_{qr}} + \dot{I_{qr_{ref}}}\right) + R_r I_{qr} + g w_s a I_{dr} + g\frac{MV_s}{L_s} \\ V_{dr\_ref} = a\left(k_{I_{dr}}\varepsilon_{I_{dr}} + \dot{I_{dr_{ref}}}\right) + R_r I_{dr} - g w_s a I_{qr} \end{cases} \quad \text{(III.39)}$$

The figure below illustrates the block diagram of a DFIG controlled by the BSC:

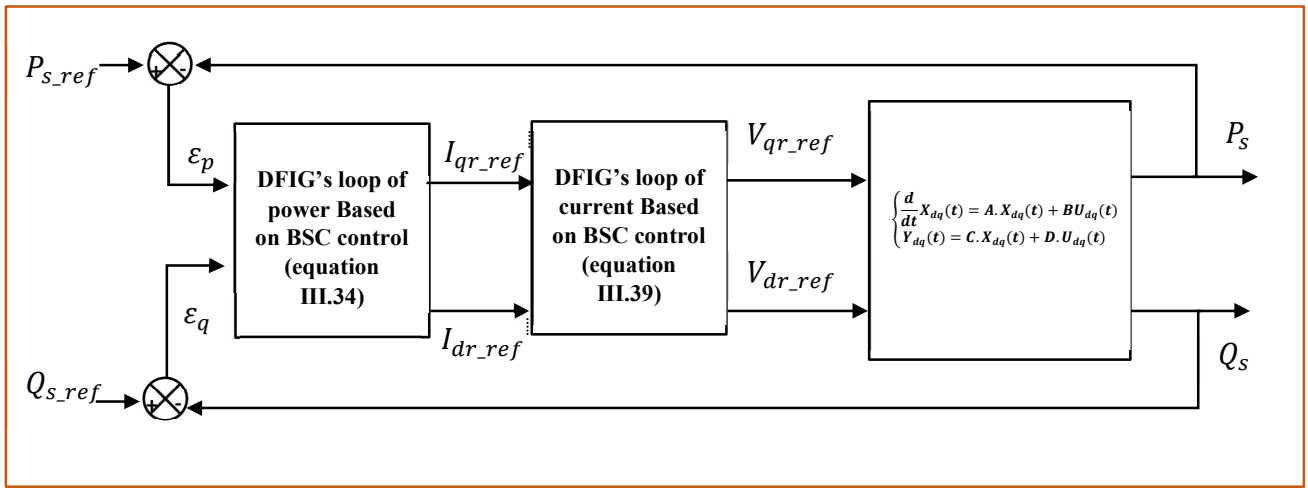

Figure III.6 Block diagram of BSC applied on DFIG system.

III.5.3 Design of the current loop of the DFIG using LQR

The LQR is widely recognized for its effectiveness in optimizing system performance by minimizing a quadratic cost function, which balances performance and control effort. In this section, the LQR technique have been applied to regulate the current loop. By formulating a quadratic cost function based on the DFIG's system dynamics and utilizing the linear state equations, LQR offers an optimal control solution that ensures both stability and efficiency in the current loop. LQR stands out in modern control theory for its robustness to uncertainties and disturbances, as well as its high efficiency in achieving optimal system performance. This makes it an excellent choice for controlling DFIGs, particularly when facing system disturbances and

uncertainties. The system will be constructed using the state-space model (SSM) method presented to facilitate the application of the LQR control strategy. In this framework, two distinct LQR-based designs will be developed for managing the current loop of the DFIG, leveraging the strengths of both LQR and the BSC [19-21].

A. Design of the current loop based on the 2nd order using the LQR

In this approach, the current loop model of the DFIG is developed by combining the linear system model with the disturbance components. The DFIG model, as represented in Equation III.6, can subsequently be reformulated as follows:

$$\begin{cases} V_{dr} = V_{dr}{}' + E_{dr} \\ V_{qr} = V_{qr}{}' + E_{qr} \end{cases} \quad \text{(III.40)}$$

Based on the decoupling method, the internal linear model of the DFIG can be represented as shown in Equation III.41, while the Back-EMF affecting the system are described in Equation III.42.

$$\begin{cases} V_{dr}{}' = R_r I_{dr} + a\dot{I}_{dr} \\ V_{qr}{}' = R_r I_{qr} + a\dot{I}_{qr} \end{cases} \quad \text{(III.41)}$$

$$\begin{cases} E_{dr} = -gw_s a I_{qr} \\ E_{qr} = gw_s a I_{dr} + g\frac{MV_s}{L_s} \end{cases} \quad \text{(III.42)}$$

To manage this, a decoupling compensation technique is incorporated, facilitating the implementation of the closed-loop control based on an innovative design. The Back-EMF are defined in Equation III.42, while the linear model of the system relies on two state variables: the direct and quadrature components of the current. As a result, the system model is structured as follows:

$$\begin{cases} \frac{d}{dt}X_{dq}(t) = A.X_{dq}(t) + BU_{dq}(t) \\ y_{dq}(t) = C.X_{dq}(t) + D.U_{dq}(t) \end{cases} \quad \text{(III.43)}$$

Based on Equation III.43, the internal model of the DFIG is described as follows:

$$\begin{cases} \frac{d}{dt}[\mathrm{I_{dr}} \quad \mathrm{I_{qr}}]^{\mathrm{T}} = \begin{bmatrix} -\frac{\mathrm{R_r}}{\alpha} & 0 \\ 0 & -\frac{\mathrm{R_r}}{\alpha} \end{bmatrix}.[\mathrm{I_{dr}} \quad \mathrm{I_{qr}}]^{\mathrm{T}} + \begin{bmatrix} \frac{1}{\alpha} & 0 \\ 0 & \frac{1}{\alpha} \end{bmatrix}.[\mathrm{V_{dr}}' \quad \mathrm{V_{qr}}']^{\mathrm{T}} \\ [y_1 \quad y_2]^T = \begin{bmatrix} 1 & 0 \\ 0 & 1 \end{bmatrix}.[I_{dr} \quad I_{qr}]^T + \begin{bmatrix} 0 & 0 \\ 0 & 0 \end{bmatrix}.[V_{dr}{}' \quad V_{qr}{}']^T \end{cases} \quad \text{(III.44)}$$

To implement the LQR control, it is necessary to define the state variable vector $X_{dq}(t)$, the input vector $U_{dq}(t)$, and the system matrices: the state matrix A and the input matrix B. These are formulated as follows:

$$\begin{cases} A = \begin{bmatrix} -\frac{R_r}{\alpha} & 0 \\ 0 & -\frac{R_r}{\alpha} \end{bmatrix} \\ B = \begin{bmatrix} \frac{1}{\alpha} & 0 \\ 0 & \frac{1}{\alpha} \end{bmatrix} \\ X_{dq}(t) = [I_{dr} \quad I_{qr}]^T \\ U_{dq}(t) = [V_{dr}' \quad V_{qr}']^T \end{cases} \quad \text{(III.45)}$$

By performing this identification, the cost function derived from the current loop model (Equation III.44) is expressed as follows in Equation III.46:

$$J = \int_0^\infty (([I_{dr} \quad I_{qr}].Q.[I_{dr} \quad I_{qr}]^T) + ([V_{dr}' \quad V_{qr}'].R.[V_{dr}' \quad V_{qr}']^T))dt \quad \text{(III.46)}$$

Where R and Q are both positive definite matrices of size 2×2.

The feedback control law based on this control design become as follows:

$$U_{dq}(t) = -k.[I_{dr} \quad I_{qr}]^T = (-R^{-1}.B^T.P).[I_{dr} \quad I_{qr}]^T \quad \text{(III.47)}$$

Here, P is specified in Equation III.28.

B. Design of the current loop based on the 4th order using the LQR

Through this design, a new state variable, referred to as the steady-state error, will be introduced, improving the performance characteristics of the internal linear model. As a result, the new state-space model is defined by the following equation:

$$\begin{cases} \dot{X}_{dq}(t) = A.X_{dq}(t) + B.U_{dq}(t) \\ y_{dq} = C.X_{dq}(t) \\ \dot{\varepsilon}_{Idqr}(t) = X_{dq}^*(t) - C.X_{dq}(t) \end{cases} \quad \text{(III.48)}$$

The feedback control law for this design is expressed as follows:

$$U_{dq}(t) = -k.X_{dq}(t) + k_r.\varepsilon_{Idqr}(t) \quad \text{(III.49)}$$

The new state-space model is given by Equation III.50:

$$\begin{bmatrix} \dot{X}_{dq}(t) \\ \dot{\varepsilon}_{Idqr}(t) \end{bmatrix} = \begin{bmatrix} A & 0 \\ -C & 0 \end{bmatrix}.\begin{bmatrix} X_{dq}(t) \\ \varepsilon_{Idqr}(t) \end{bmatrix} + \begin{bmatrix} B \\ 0 \end{bmatrix}.\begin{bmatrix} V_{dr}'(t) \\ V_{qr}'(t) \end{bmatrix} + \begin{bmatrix} 0 \\ I \end{bmatrix}.\begin{bmatrix} I_{dr-ref}(t) \\ I_{qr-re}\ (t) \end{bmatrix} \quad \text{(III.50)}$$

Where I represent the identity matrix.

The objective of the updated design for the internal linear model, utilizing the state feedback law, is to eliminate steady-state errors and ensure the system achieves asymptotic stability. This results in the variables mean $X_{dq}(\infty)$, $\varepsilon_{Idqr}(\infty)$ and $U_{dq}(\infty)$ converging to constant values.

Additionally, the steady-state behavior of Equation III.48 is represented by Equation III.51, as shown below:

$$\begin{bmatrix} \dot{X}_{dq}(\infty) \\ \dot{\varepsilon}_{Idqr}(\infty) \end{bmatrix} = \begin{bmatrix} A & 0 \\ -C & 0 \end{bmatrix} . \begin{bmatrix} X_{dq}(\infty) \\ \varepsilon_{Idqr}(\infty) \end{bmatrix} + \begin{bmatrix} B \\ 0 \end{bmatrix} . \begin{bmatrix} V_{dr}'(\infty) \\ V_{qr}'(\infty) \end{bmatrix} + \begin{bmatrix} 0 \\ I \end{bmatrix} . \begin{bmatrix} I_{dr-r} \ (\infty) \\ I_{qr-ref}(\infty) \end{bmatrix} \quad \text{(III.51)}$$

The reference vector corresponds to the step vector, which implies that:

$$\begin{bmatrix} 0 \\ I \end{bmatrix} . \begin{bmatrix} I_{dr-re} \ (\infty) \\ I_{qr-ref}(\infty) \end{bmatrix} = \begin{bmatrix} 0 \\ I \end{bmatrix} . \begin{bmatrix} I_{dr-ref}(\mathrm{t}) \\ I_{qr-ref}(\mathrm{t}) \end{bmatrix} = constant \ \text{ For } t > 0 \quad \text{(III.52)}$$

Next, the error dynamics are calculated by subtracting the values at time t from those at (∞):

$$\begin{bmatrix} \dot{X}_{dq}(t) - \dot{X}_{dq}(\infty) \\ \dot{\varepsilon}_{Idqr}(t) - \dot{\varepsilon}_{Idqr}(\infty) \end{bmatrix} = \begin{bmatrix} A & 0 \\ -C & 0 \end{bmatrix} . \begin{bmatrix} X_{dq}(t) - X_{dq}(\infty) \\ \varepsilon_{Idqr}(t) - \varepsilon_{Idqr}(\infty) \end{bmatrix} + \begin{bmatrix} B \\ 0 \end{bmatrix} . \begin{bmatrix} V_{dr}'(t) - V_{dr}'(\infty) \\ V_{qr}'(t) - V_{qr}'(\infty) \end{bmatrix} \quad \text{(III.53)}$$

We define:

$$\begin{cases} \bar{X}_{dq}(t) = X_{dq}(t) - X_{dq}(\infty) \\ \bar{\varepsilon}_{Idqr}(t) = \varepsilon_{Idqr}(t) - \varepsilon_{Idqr}(\infty) \\ \bar{U}_{dq}(t) = V_{dqr}'(t) - V_{dqr}'(\infty) \end{cases} \quad \text{(III.54)}$$

To follow a constant reference:

$$\begin{cases} y_{dq} = C.X_{dq}(\infty) + D.U_{dq}(\infty) \rightarrow X_{dq}^{*}(t) \\ \dot{X}_{dq}(\mathrm{t}) = A.X_{dq}(\infty) + B.U_{dq}(\infty) \rightarrow 0 \end{cases} \quad \text{(III.55)}$$

From Equation III.54 and Equation III.55, the following results:

$$\frac{d}{dt} \begin{bmatrix} \bar{X}_{dq}(t) \\ \bar{\varepsilon}_{Idqr}(t) \end{bmatrix} = \begin{bmatrix} \mathrm{A} & 0 \\ -C & 0 \end{bmatrix} . \begin{bmatrix} \bar{X}_{dq}(t) \\ \bar{\varepsilon}_{Idqr}(t) \end{bmatrix} + \begin{bmatrix} \mathrm{B} \\ 0 \end{bmatrix} . [\bar{U}_{dq}(t)]^{\mathrm{T}} \quad \text{(III.56)}$$

Subsequently, the error vector is expressed in Equation III.57:

$$e_{dq}(t) = [\bar{X}_{dq}(t) \quad \bar{\varepsilon}_{Idqr}(t)]^{\mathrm{T}} \quad \text{(III.57)}$$

From Equation III.56 and Equation III.57, the error dynamics are given by:

$$\dot{e}_{dq}(t) = \bar{A}.e_{dq}(t) + \bar{B}.\bar{U}_{dq}(t) \quad \text{(III.58)}$$

Where: $\bar{A} = \begin{bmatrix} \mathrm{A} & 0 \\ -\mathrm{C} & 0 \end{bmatrix}$, and $\bar{B} = \begin{bmatrix} \mathrm{B} \\ 0 \end{bmatrix}$

It is apparent that the control law governing the dynamic error, outlined in Equation III.58, can be formulated as:

$$\bar{U}_{dq} = -\bar{K}.e_{dq}(t) \quad \text{(III.59)}$$

Where $\bar{K} = [\bar{k} \quad -\bar{k}_r]$

Nonetheless, based on Equation III.58 and Equation III.59, the closed-loop dynamic error is formulated as follows:

$$\dot{e}_{dq}(t) = (\bar{A} - \bar{B}\bar{K}).e_{dq}(t) \quad \text{(III.60)}$$

In Equation III.44 and Equation III.50, the direct and quadratic currents are decoupled from one another. Therefore, Equation III.43 highlights this decoupling through the application of optimal LQR control, with the linear state feedback law being formulated as follows:

$$\begin{bmatrix} V_{dr-r} \\ V_{qr-ref} \end{bmatrix}^{T} = -[\bar{k} \quad -\bar{k}_r]. \begin{bmatrix} I_{dr} \\ I_{qr} \\ \bar{\varepsilon}_{Idr} \\ \bar{\varepsilon}_{Iqr} \end{bmatrix}^{T} \tag{III.60}$$

Where:

$$[\bar{k} \quad -\bar{k}_r] = \bar{R}^{-1}.\bar{B}^{T}.\bar{P} \tag{III.61}$$

Where $\bar{P}$ is a positive definite matrix. Its solution is given in the Algebra Riccati Equation (ARE) which represents the Equation III.62 with the new condition of steady state error.

$$\bar{A}^{T}.\bar{P} + \bar{P}.\bar{A} - \bar{P}.\bar{B}.\bar{R}^{-1}.\bar{B}^{T}.\bar{P} + \bar{Q} = 0 \tag{III.62}$$

The current loop of the DFIG based on the SSE-LQR is designed as follows:

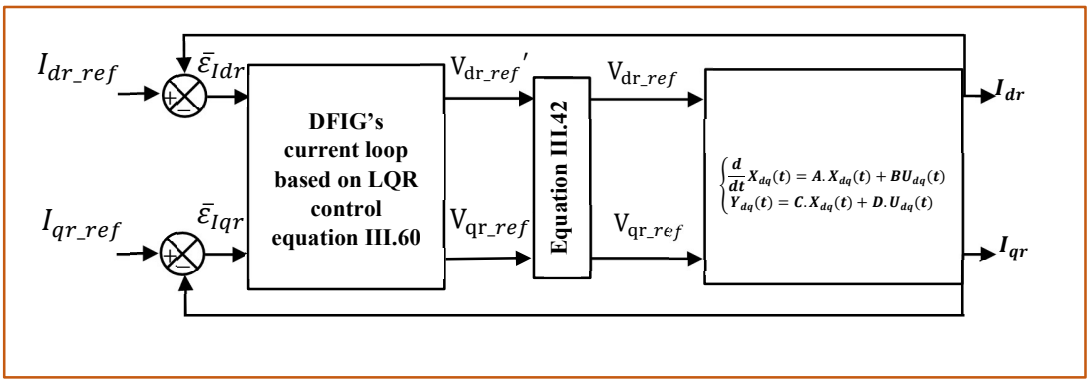

Figure III.7 Decoupling the DFIG current model using the LQR technique.

III.5.4 Description of the combined control design between BSC and LQR

In this section, A hybrid control design approach using BSC and LQR is proposed for controlling the DFIG. In this scheme, BSC is applied to regulate the power loops, where the inputs are power signals, and the outputs are the reference rotor currents, meaning that power regulation is achieved through BSC. For the current loops, LQR is implemented to regulate the rotor currents, ensuring precise control to achieve the desired control law. The overall framework of this hybrid control design is formulated based on the control laws of both techniques, as presented in Equations (III.34) and (III.60). This combination of control strategies enhances system stability, robustness, and energy efficiency by effectively addressing the challenges associated with nonlinear dynamics and

multi-loop control in the DFIG. The comprehensive control scheme based on this hybrid control design for the DFIG can be expressed as follows:

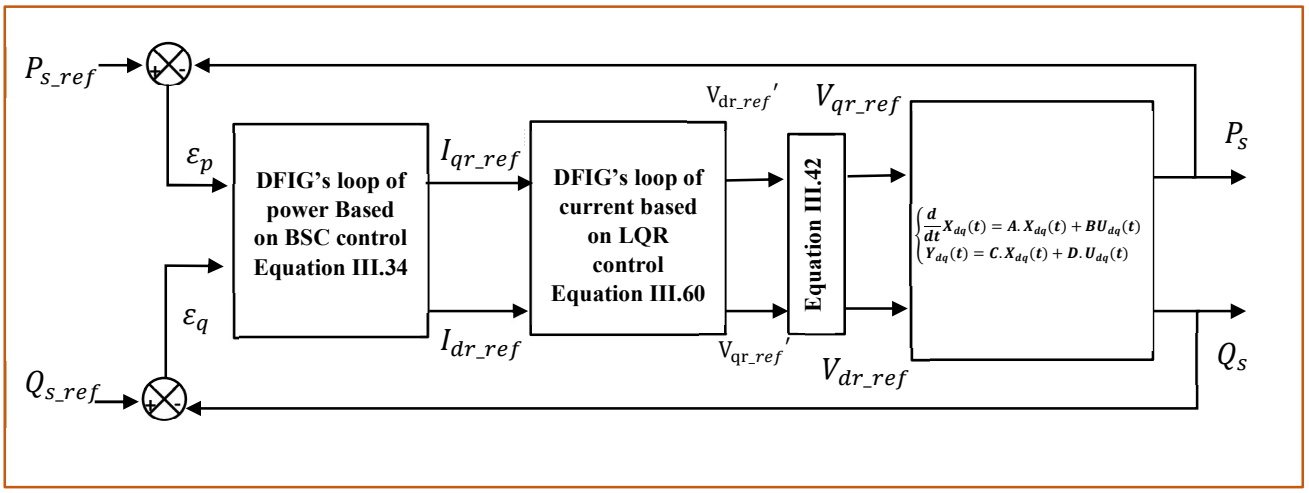

Figure III.8 Block diagram of the hybrid BSC-LQR applied on DFIG system.

III.6 Simulation Results and Comparative Study of BSC and hybrid control design for the DFIG

To demonstrate the effectiveness of the studied and applied control techniques presented in this chapter, the results have been validated using MATLAB/Simulink. This section presents these findings, with Figure III.9 illustrating the overall scheme of the applied control technique within the WECS. The results are analyzed and discussed in this section, evaluating the performance of the applied control strategy (BSC) under two wind speed scenarios. The first scenario considers a randomly varying wind speed, as shown in Figure III.10, while the second scenario involves step changes in wind speed with sudden variations, as depicted in Figure III.11. Subsequently, this same wind speed scenario is applied to the hybrid BSC-LQR control, demonstrating the observed improvements and advantages of the proposed hybrid control strategy.

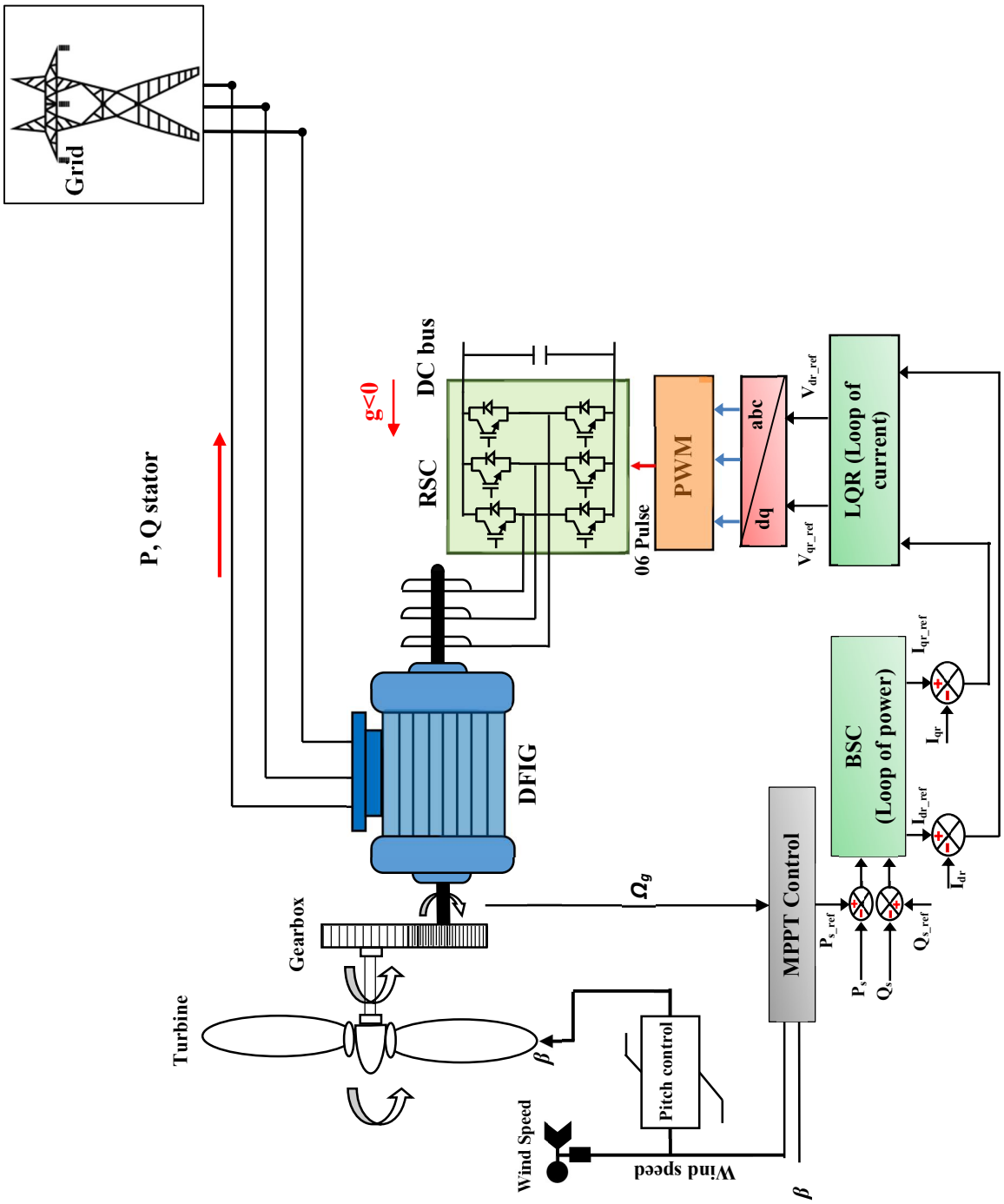

Figure III.9 Global scheme control of WECS based on DFIG control.

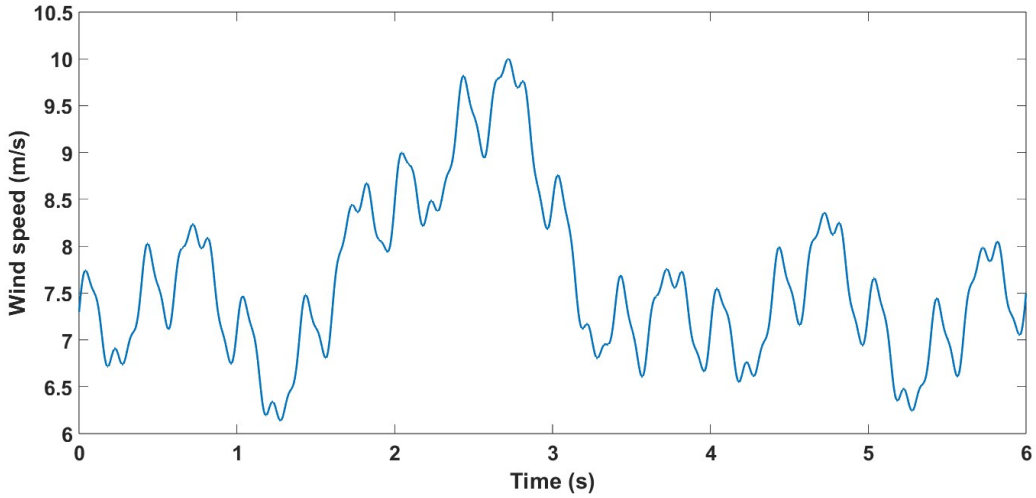

Figure III.10 Randomly varying wind speed.

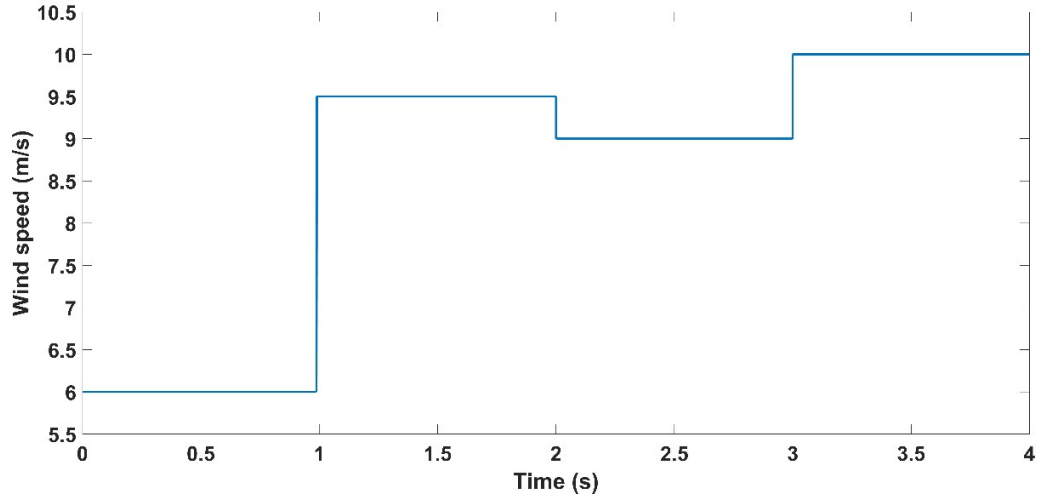

Figure III.11 Wind speed with sudden variations.

The evaluation and analysis of the stator active and reactive power performance under the implementation of the BSC technique for both the power and current control loops formulated by their control laws in Equation III.34 and Equation III.39 respectively and depicted in the closed-loop control scheme in Figure III.6 have been conducted for the first scenario, characterized by a randomly varying wind speed profile. The simulation results, illustrated in Figure III.12, demonstrate the effectiveness of the BSC strategy in regulating power flow under fluctuating wind conditions. The active power (seen Figure III.12(a)) closely follows the turbine's reference power output, dynamically adapting to wind variations and achieving a maximum power around 2170 W. This tracking accuracy highlights the capability of the BSC controller to optimize power extraction.

Simultaneously, the reactive power (seen Figure III.12(b)) precisely tracks its reference of zero, with only minor chattering oscillations within ±10 var, which remain an acceptable tolerance band. This indicates the ability of the BSC technique to suppress undesirable reactive power fluctuations effectively. These findings substantiate the relative robustness of the BSC control strategy in the presence of stochastic wind speed variations, ensuring stable and efficient power regulation despite external disturbances. The minimized chattering in reactive power and the precise tracking of active power validates the effectiveness of the applied control approach in enhancing the system's overall performance and reliability.

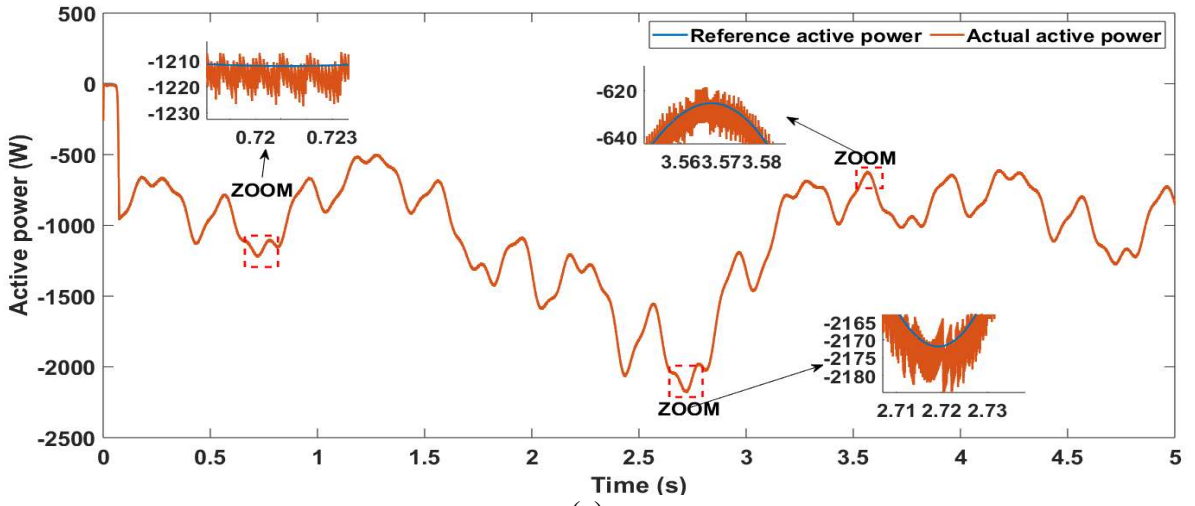

(a)

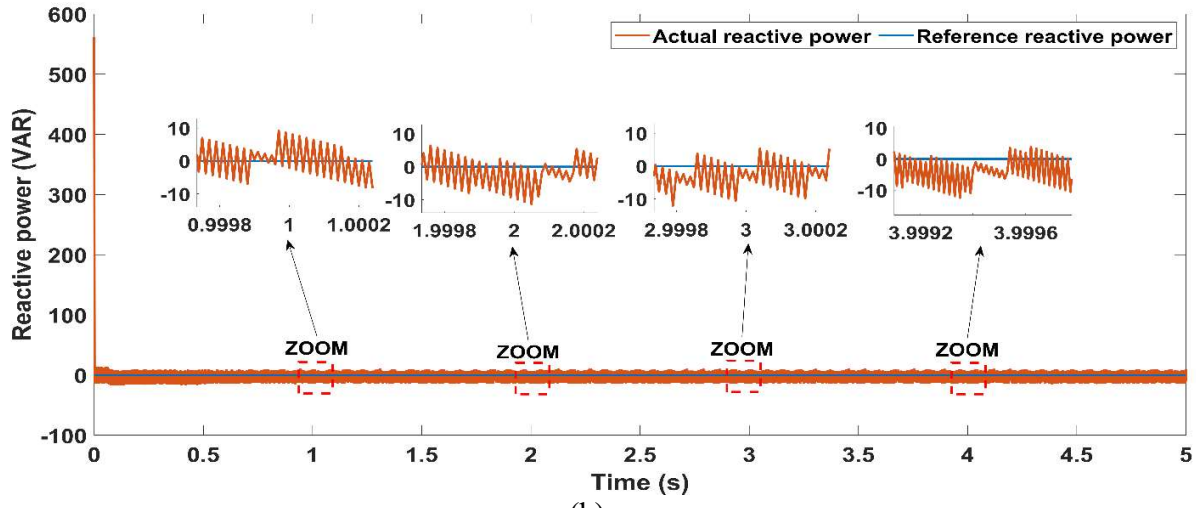

(b)

Figure III.12 Dynamic response of powers under the BSC technique for a randomly varying wind speed profile; (a) Active power tracking performance, (b) Reactive power regulation performance.

The simulation results, presented in Figure III.13, reveal the transient response of the BSC technique when exposed to sudden wind speed changes. The active power (seen Figure III.13(a)) exhibits significant overshoots and undershoots upon each abrupt wind speed transition, deviating from its reference trajectory before settling into a steady-state condition. These transient power fluctuations indicate the system's inability to instantaneously compensate for the rapid variations in mechanical input, leading to a temporary mismatch between the generated and the reference power. Such deviations not only degrade power quality but also impose excessive electrical and thermal stress on the generator components, potentially affecting long-term reliability.

Similarly, the reactive power (as shown in Figure III.13(b)), which is expected to maintain a reference value of zero to ensure a good power factor operation, experiences a clear overshoots and downshoots during each wind sudden change. This temporary deviation indicates that the controller temporarily loses its ability to regulate reactive power under extreme conditions, resulting in fluctuations that may cause additional losses and affect the stability of the electrical system.

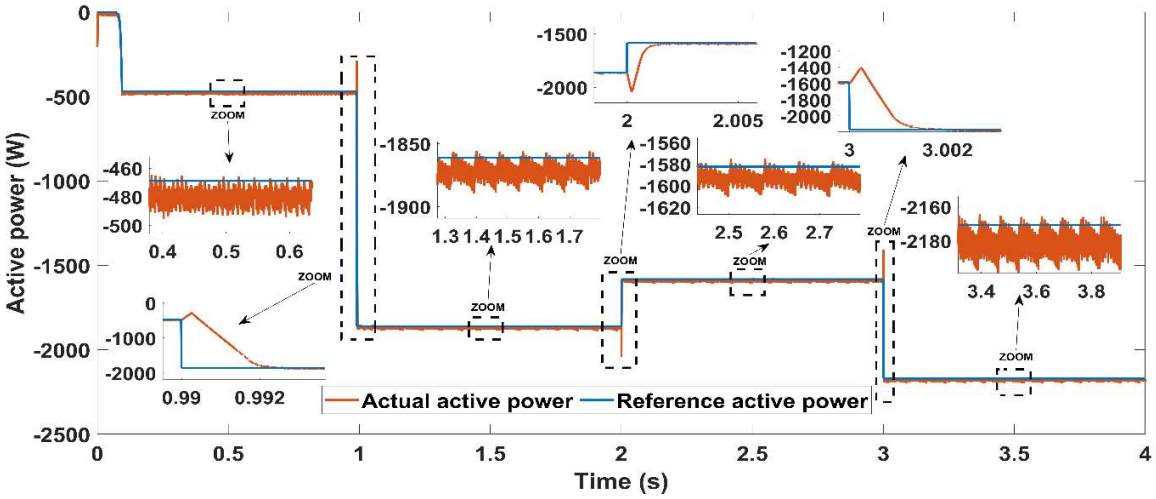

(a)

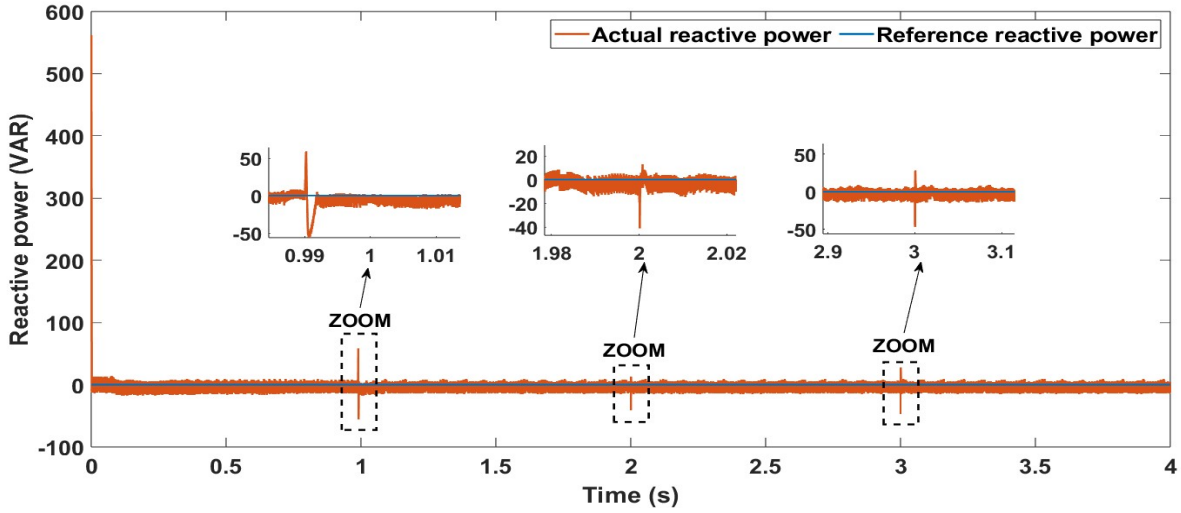

(b)

Figure III.13 Dynamic response of powers under the BSC technique for step changes in wind speed with abrupt variations; (a) Active power tracking performance, (b) Reactive power regulation performance.

These findings highlight a critical limitation of the BSC approach in handling aggressive wind speed variations, where the transient instability significantly impacts the quality of the generated power. The presence of overshoots/undershoots and oscillatory behavior in active and reactive powers underscores the need for an enhanced control strategy capable of mitigating these transient effects and ensuring smoother power regulation.

To address these limitations, the hybrid BSC-LQR control strategy has been introduced and analyzed under the same abrupt wind speed scenario. As shown in Figure III.14, the simulation results demonstrate the superior performance of the hybrid controller in mitigating power fluctuations. The active power exhibits highly accurate reference tracking, effectively eliminating the transient peaks observed in the BSC implementation. This smooth tracking behavior indicates that the hybrid control is dealing optimally to overcome the peaks in case of abrupt changes in wind speed, ensuring continuous and stable power delivery without excessive overshoots or undershoots. Similarly, the reactive power maintains a strict adherence to reach its reference of zero, without observable oscillations nor big chattering effects, confirming the hybrid controller's ability to sustain near-unity power factor operation under severe wind variations.

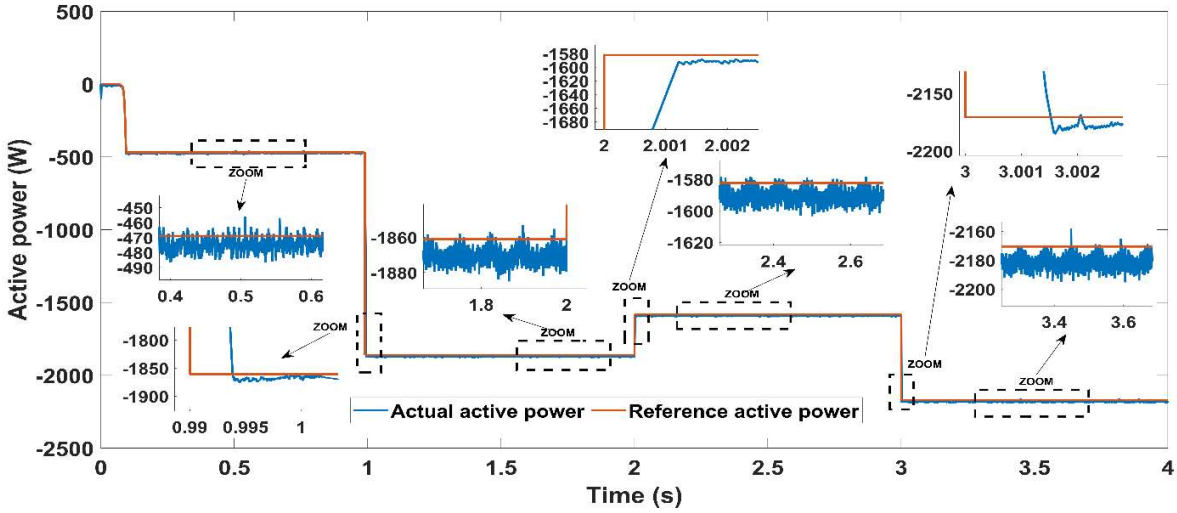

(a)

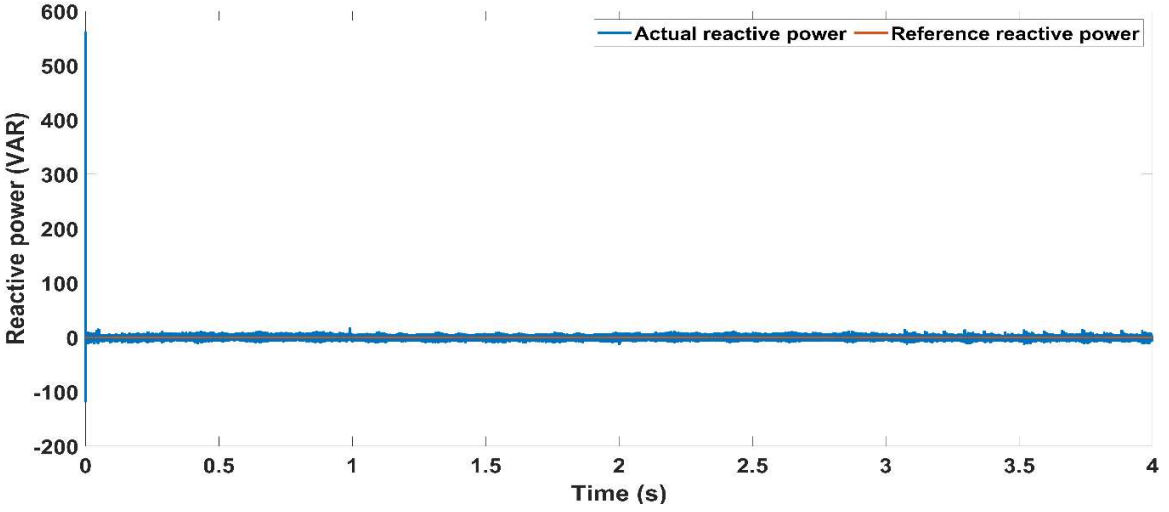

(b)

Figure III.14 Dynamic response of powers under the hybrid control design (LQR-BSC) technique for step changes in wind speed with abrupt variations; (a) Active power tracking performance, (b) Reactive power regulation performance.

The evaluation of the generator's performance under the hybrid BSC-LQR technique has been conducted, focusing on key operational parameters that reflect the system's stability and dynamic response. The corresponding simulation results, presented in Figure III.15, provide a comprehensive assessment of the generator's behavior under step changes in wind speed with sudden variations, demonstrating the effectiveness of the proposed control scheme in ensuring smooth and stable operation. Figures III.15(a) and III.15(b) illustrate the stator and rotor current waveforms, respectively, both exhibiting sinusoidal profiles with minimal distortion. The

magnitudes of both stator and rotor currents dynamically adjust in proportion to step changes in wind speed with sudden variations, indicating an adaptive response of the control system to changing power generation demands. The absence of abrupt transients or oscillatory instabilities further confirms the robustness of the hybrid BSC-LQR strategy in maintaining optimal current regulation across different operating conditions.

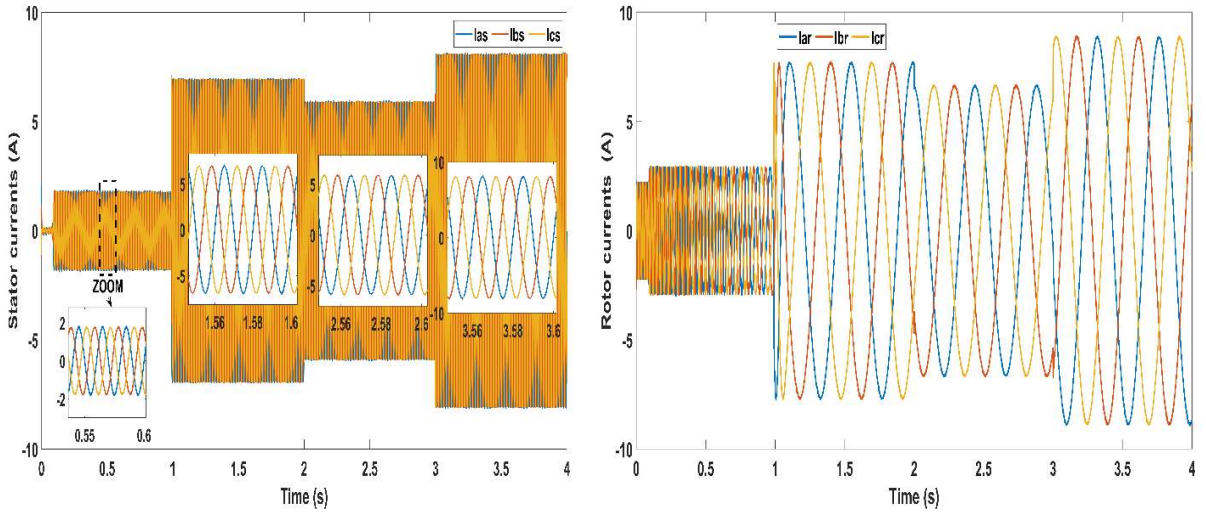

(a) (b)

Figure III.15 Parameter Response of DFIG under the Hybrid BSC-LQR Controller: (a) stator current (I_{sabc}), (b) rotor current (I_{sabc}).

The effectiveness of the hybrid control design has also been further demonstrated through the calculation of the Total Harmonic Distortion (THD) of the stator currents. The THD values for the four zoomed regions identified in Figure III.15(a) were calculated, with results ranging from 0.32% to 1.66% (seen Figure III.16). These low THD values indicate that the hybrid BSC-LQR technique scheme effectively minimizes harmonic distortion in the stator currents. Moreover, the smoothness of these waveforms highlights the hybrid controller's ability to suppress harmonic content and mitigate current ripples, thereby reducing electromagnetic losses and enhancing the overall efficiency of the DFIG.

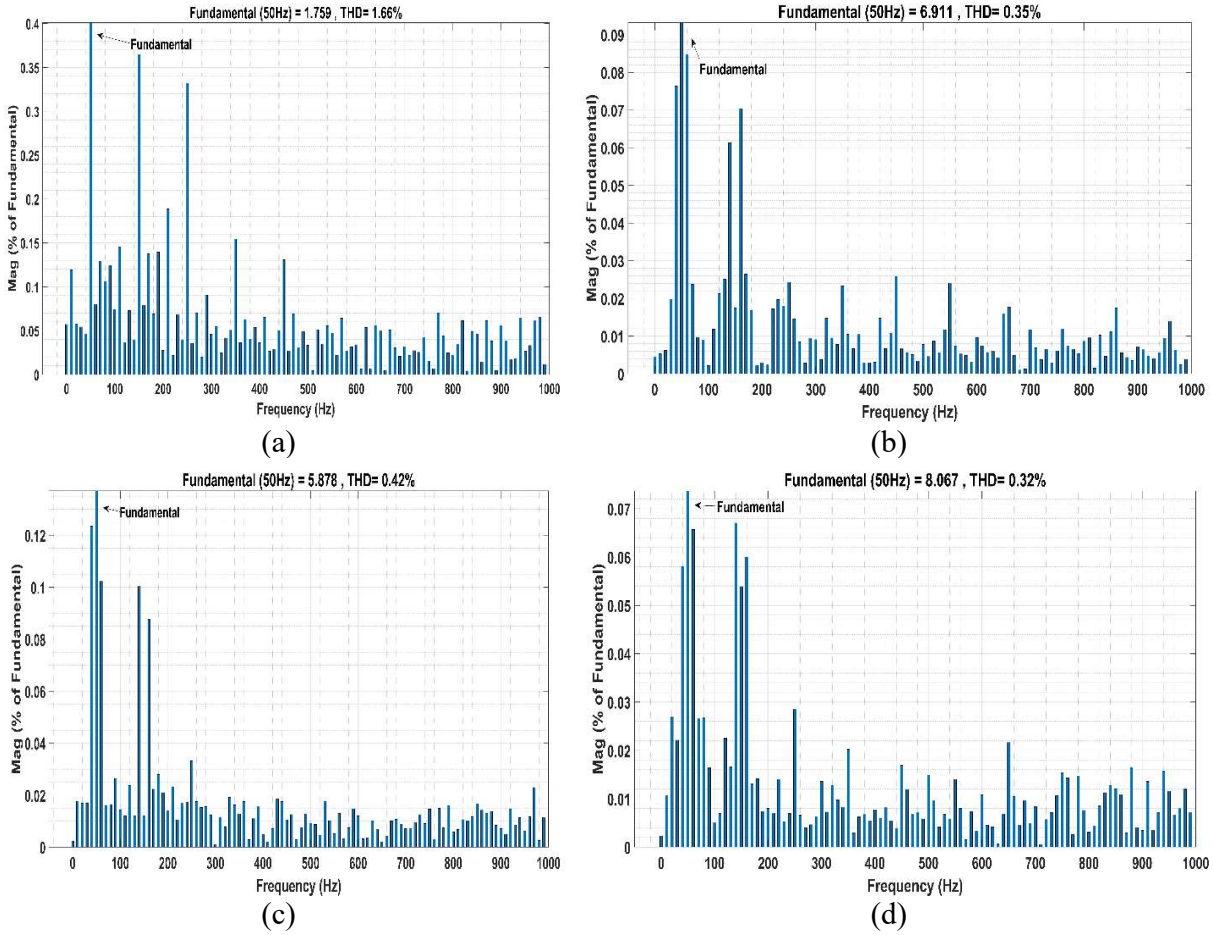

Figure III.16 The THD of the stator currents; (a): THD of Zone 1, (b): THD of Zone 2, (c): THD of Zone 3 and (a): THD of Zone 4.

Figure III.17(a) presents a good matching between the rotor currents and their reference values in the *dq* reference frame, where the decoupled control structure of the applied strategy is evident. The direct-axis current component I_{dr} remains precisely regulated constant at 2.72 A, demonstrating that reactive power is effectively controlled to maintain a near-unity power factor at the stator terminals. This confirms the controller's ability to eliminate unnecessary reactive power exchange, minimizing losses and optimizing grid integration performance. Conversely, the quadrature-axis current component I_{qr} exhibits a dynamic variation directly correlated with wind speed fluctuations, reflecting its role in active power regulation. The consistent and stable response of I_{qr} without excessive oscillations highlights the effectiveness of the hybrid control approach in achieving precise power tracking while maintaining current stability. Additionally, the electromagnetic torque (T_{em}), shown in Figure III.17(b), follows the step changes in wind speed with sudden variations, demonstrating the generator's capacity to adapt to fluctuating mechanical

inputs. The controlled torque response confirms that the hybrid BSC-LQR technique ensures smooth torque transitions without inducing excessive oscillations or sudden peaks, which could otherwise introduce lower mechanical stress on the drive system.

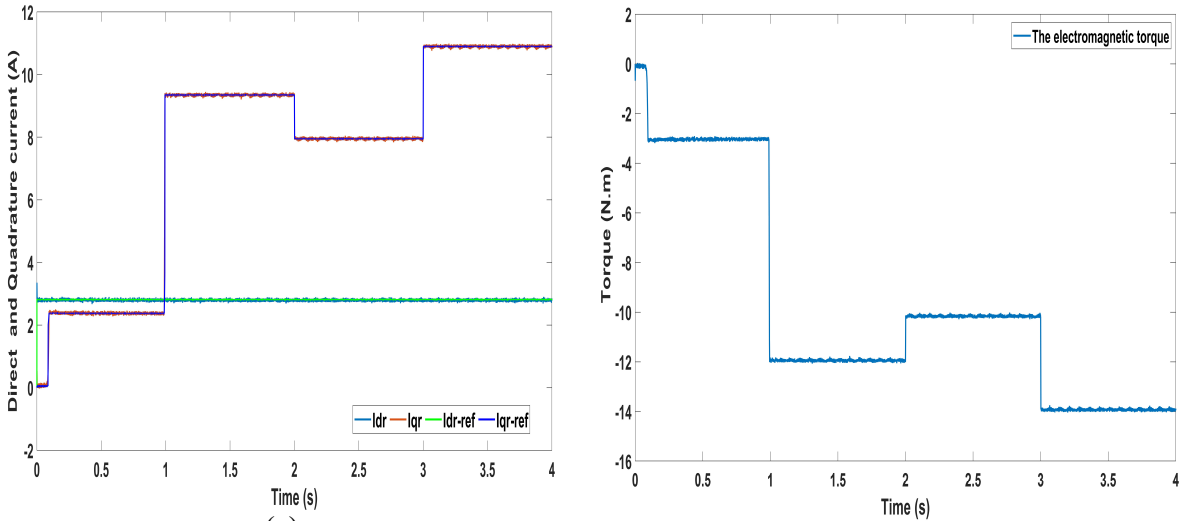

(a) (b)

Figure III.17 Parameter Response of DFIG under the Hybrid BSC-LQR Controller: (a): the rotor currents in the *dq* reference frame (I_{dqr}), (b): the electromagnetic torque (T_{em}).

To evaluate the robustness of the proposed hybrid BSC-LQR control strategy under parameter uncertainties, two distinct scenarios were considered, where the rotor resistance (R_r) and mutual inductance (M) were intentionally varied. The simulation results, depicted in Figures III.18 and III.19, provide a comprehensive assessment of the controller's performance under these perturbations.

Figure III.18 illustrates the behavior of active and reactive power when the rotor resistance R_r is subjected to variations. Despite this perturbation, the proposed BSC-LQR control strategy demonstrates a high degree of robustness, effectively against the resistance fluctuation. The controller maintains a well-regulated stator active and reactive power profile, ensuring minimal deviations from the desired reference values. Additionally, the control scheme exhibits excellent disturbance rejection capabilities, as evidenced by the rapid stabilization of power dynamics without noticeable overshoot or undershoot transients. This result confirms that the proposed approach can reliably handle variations in R_r while preserving system stability and performance.

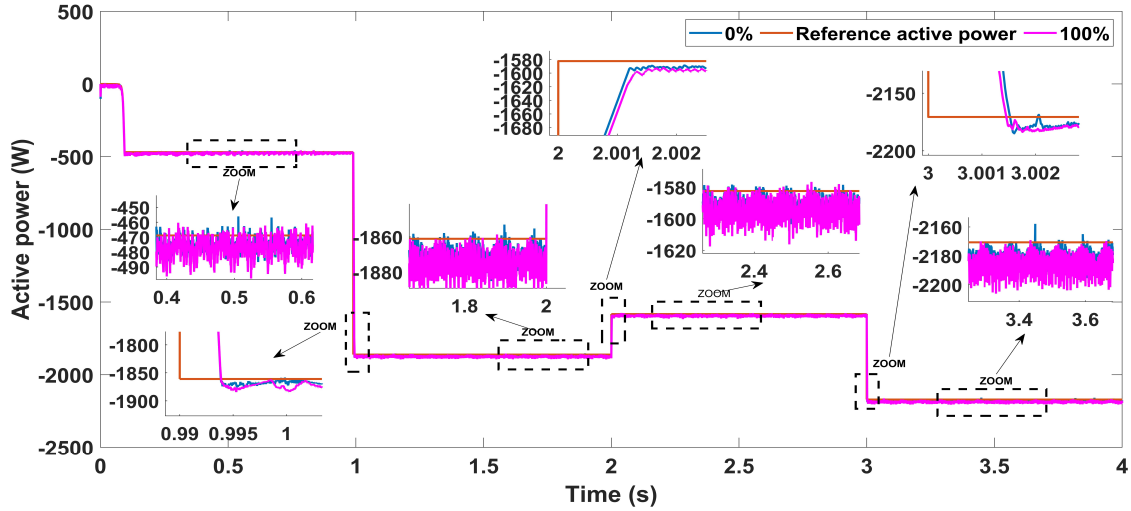

(a)

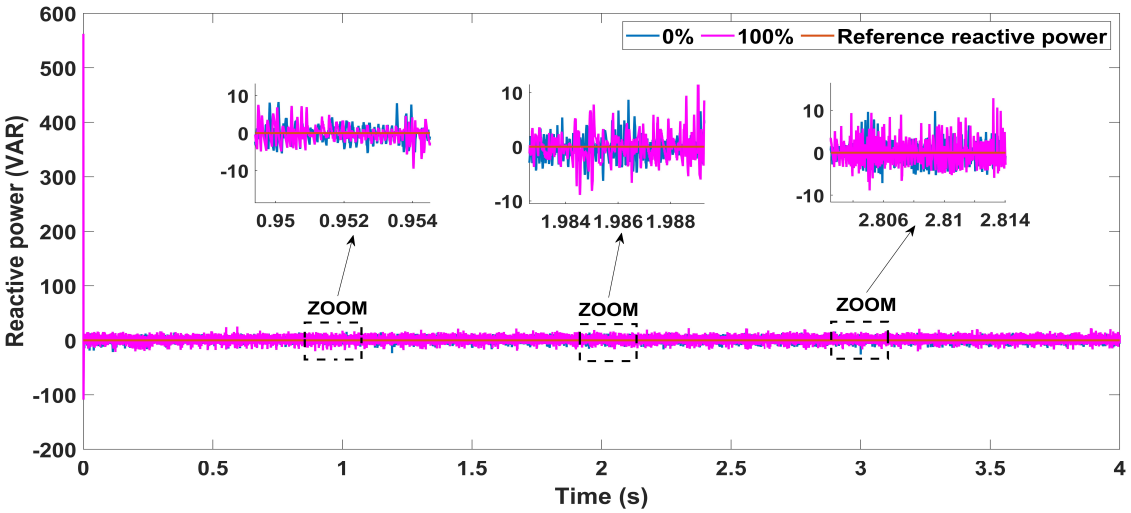

(b)

Figure III.18 Powers behavior under the BSC-LQR technique with R_r variation; (a) Active power tracking performance, (b) Reactive power regulation performance.

Similarly, Figure III.19 presents the stator active and reactive power response under variations in the mutual inductance *M*. The results reaffirm the robustness of the control strategy, as the power trajectories remain highly stable despite the imposed uncertainty. The controller effectively mitigates any adverse effects introduced by changes in *M*, maintaining precise power tracking with minimal steady-state error and reduced fluctuations.

Collectively, these results validate the superior performance of the hybrid BSC-LQR control strategy in regulating both electrical variables of the DFIG system. The ability to maintain smooth

sinusoidal current waveforms, effectively decouple active and reactive power components, ensure stable electromagnetic torque dynamics, and minimize harmonic distortion underscores the controller's robustness in managing wind energy conversion efficiently. These findings demonstrate that the proposed hybrid control methodology successfully addresses the inherent limitations of conventional approaches, enhancing the reliability, efficiency, and stability of the wind energy generation system under fluctuating in wind conditions.

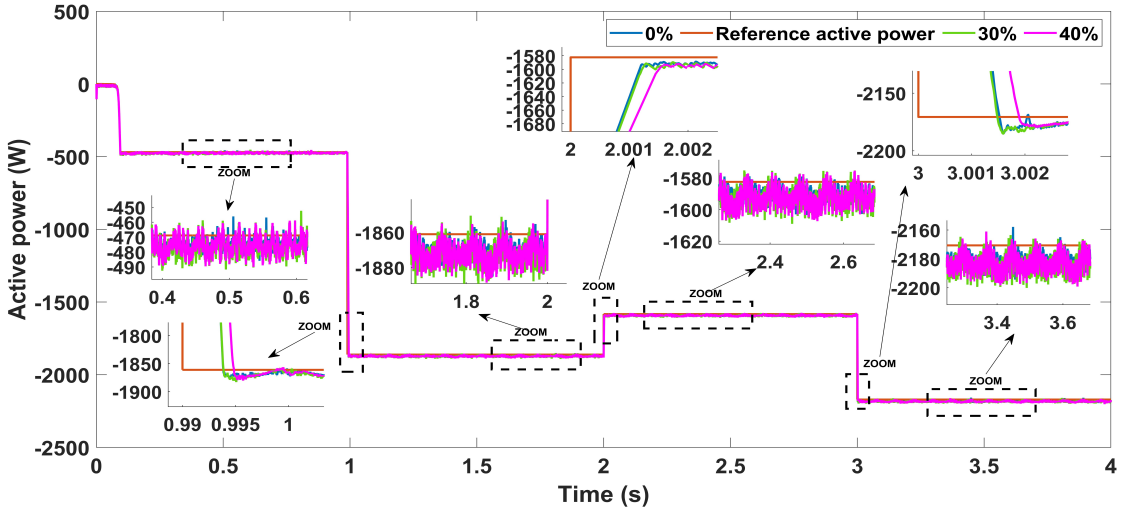

(a)

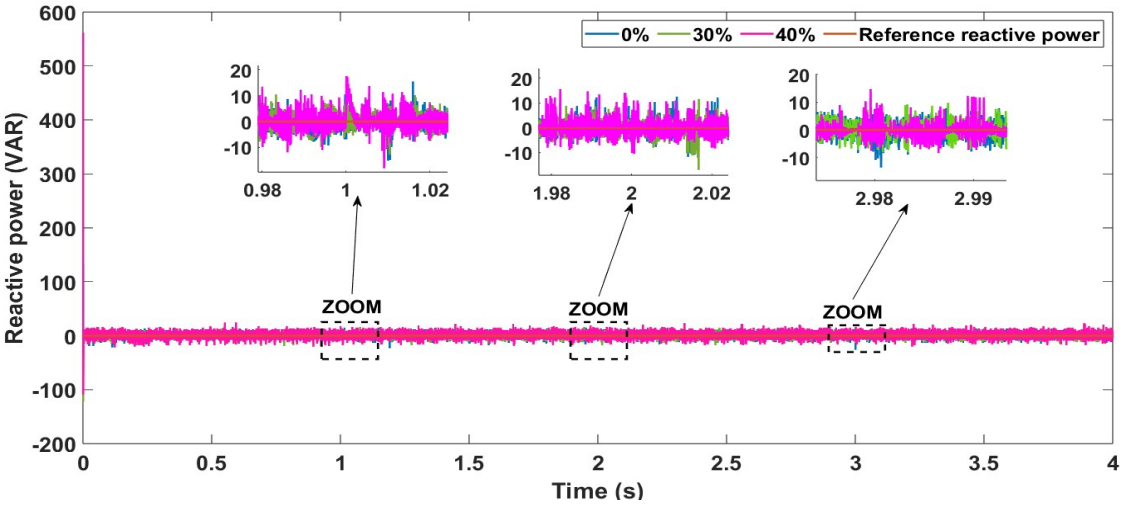

(b)

Figure III.19 Powers behavior under the BSC-LQR technique with *M* variation; (a) Active power tracking performance, (b) Reactive power regulation performance.

III.7 Conclusion

In this chapter, the control design for DFIGs has been systematically developed and analyzed. The chapter began with the construction of the control model, including the definition of the operational loops and classification of control strategies, laying the foundation for understanding the DFIG's control architecture. Advanced methodologies such as nonlinear control using BSC and optimal control through the LQR were explored in detail. The integration of these approaches in a hybrid control design was proposed to leverage their individual advantages and address the challenges of DFIG operation. The active and reactive stator powers were effectively controlled using the proposed control strategies, ensuring precise and efficient performance. The hybrid design, which combines BSC and LQR, demonstrated its ability to optimize the power and current loops of the DFIG, offering robust control under various operating conditions benefiting from both controls where BSC handling the system nonlinearity and robust against parameter uncertainties while LQR handling against sudden external disturbance underscore balancing performance and control effort.

The effectiveness of the proposed control designs was validated through comprehensive simulations in MATLAB/Simulink. The simulation results highlighted the capability of these control strategies to achieve stable, efficient, and reliable operation of the DFIG, even under dynamic conditions. The comparative study between BSC and the hybrid control approach underscored the significant performance improvements achieved through the hybrid design, making it a promising solution for advanced DFIG control systems.

REFERENCES BIBLIOGRAPHIQUES

[1] D. KARBOUA, B. TOUAL, and A. KOUZOU, "Contribution to the control of three-phase permanent magnet synchronous based on advanced technique." Ph.D. dissertation, Ziane Achour University of Djelfa,, 2024.

[2] Khalil HK. Nonlinear control. New York, NY: Pearson, 2015.

[3] Karboua D, Belgacem T, Khan ZH, et al. Robust performance comparison of PMSM for flight control applications in more electric aircraft. PLoS One 2023; 18: e0283541.

[4] Abu-Rub H, Iqbal A, Guzinski J. High Performance Control of AC Drives with Matlab/Simulink. John Wiley & Sons; 2021.

[5] Mousa, H. H., Youssef, A. R., & Mohamed, E. E. (2020). Optimal power extraction control schemes for five-phase PMSG based wind generation systems. Engineering science and technology, an international journal, 23(1), 144-155.

[6] Rhaili, S. E., Abbou, A., El Hichami, N., & Marhraoui, S. (2023). Sensorless optimal power tracking through enhanced hybrid strategies for five-phase PMSG-based variable-speed wind turbine. In *Power Electronics Converters and their Control for Renewable Energy Applications* (pp. 93-113). Academic Press.

[7] Faisal Amin, Erwan Sulaiman, and Hassan Soomro. Field oriented control principles for synchronous motor. International Journal of Mechanical Engineering and Robotics Research, 8:284–288, 01 2019. doi: 10.18178/ijmerr. 8.2.284-288.

[8] Bouguerra, Z. (2023). Comparative study between PI, FLC, SMC and Fuzzy sliding mode controllers of DFIG wind turbine. Journal of Renewable Energies, 26(2), 209-223.

[9] Ilyes, H. M. (2011). Commande sans capteur de vitesse d'un moteur synchrone à aimants permanents (MSAP) par l'utilisation de la commande directe du couple et d'un observateur de vitesse à mode glissant (Doctoral dissertation).

[10] Benamor, Afaf. *Contribution à la Modélisation, à la Commande et au Contrôle des Systèmes de Production de l'Energie Électrique Renouvelable*. Diss. Université Mohamed Khider-Biskra, 2019.

[11] Karboua D, Belgacem T, Khan ZH, Labiod C, Ibraheem IK. Toward an optimal twisting-sliding mode control of a three-phase PMSM for electric vehicles. *Advances in Mechanical Engineering*. 2023;15(9). doi:10.1177/16878132231198664

[12] A. R. Benaskeur, "Aspects de l'application du backstepping adaptatif à la commande décentralisée des systèmes non linéaires", Thèse de Doctorat, Université Laval, Québec, 2000

[13] Lin CH. Permanent-magnet synchronous motor drive system using backstepping control with three adaptive rules and revised recurring sieved pollaczek polynomials neural network with reformed grey wolf optimization and recouped controller. Energies. 2020; 13(22):5870. https://doi.org/10.3390/ en13225870

[14] Belabbes, B., Fellah, M. K., Lousdad, A., Meroufel, A., & Massoum, A. (2006). Speed control by backstepping with nonlinear observer of a permanent magnet synchronous motor. *Acta Electrotechnica et Informatica No*, *6*(1), 4.

[15] Janga Reddy, M., & Nagesh Kumar, D. (2020). Evolutionary algorithms, swarm intelligence methods, and their applications in water resources engineering: a state-of-the-art review. h2oj, 3(1), 135-188.

[16] Doma, M. I. (2013). Particle swarm optimization in comparison with classical optimization for GPS network design. Journal of Geodetic Science, 3(4), 250-257.

[17] Hollweg, G. V., Singh Chawda, G., Chaturvedi, S., Bui, V. H., & Su, W. (2025). Optimization Techniques for Low-Level Control of DC–AC Converters in Renewable-Integrated Microgrids: A Brief Review. Energies, 18(6), 1429.

[18] M. A. M. Cheema and J. E. Fletcher, “Optimal, Combined Speed and Direct Thrust Force Control of a Linear Permanent Magnet Synchronous Motors,” Power Syst., vol. 31, no. 3, pp. 135–153, 2020, doi: 10.1007/978-3-030-40325-6_5.

[19] Mebkhouta, T., Golea, A., Boumaraf, R., Benchouia, T. M., Karboua, D. “A High Robust Optimal Nonlinear Control with MPPT Speed for Wind Energy Conversion System (WECS) Based on Doubly Fed Induction Generator (DFIG)”, Periodica Polytechnica Electrical Engineering and Computer Science, 68(1), pp. 1–11, 2024. https://doi.org/10.3311/PPee.22595

[20] Ha, V. T., & Giang, P. T. (2023). A study on PMSM drive systems fed by multi-level inverter using linear quadratic regulator control for electric vehicle applications. TELKOMNIKA (Telecommunication Computing Electronics and Control), 21(4), 917-925.

[21] M. A. M. J. E. D. M. F. Cheema, "A Linear Quadratic Regulator-Based Optimal Direct Thrust Force Control of Linear Permanent-Magnet Synchronous Motor," IEEE Transactions on Industrial Electronics, vol. 63, no. 5, pp. 2722-2733, 2016.

CHAPTRE IV

STANDALONE DFIG CONTROL AND FAULT DETECTION USING ADVANCED ESTIMATION TECHNIQUES

IV.1 Introduction

This chapter presents a comprehensive study on the compensation of current sensor faults in a standalone Doubly-Fed Induction Generator (DFIG) system using the Extended Kalman Filter (EKF) observer. Current sensors play a crucial role in ensuring accurate and reliable control of renewable energy systems. However, their failure can significantly impact the stability and performance of the system. Therefore, this chapter aims to analyze the effects of sensor faults and evaluate the effectiveness of the EKF observer in estimating unmeasured currents and maintaining system performance.

To achieve this, a series of simulation scenarios have been designed to assess the impact of current sensor loss and the ability of the EKF observer to compensate for missing measurements. The study begins by investigating the system's response in the absence of sensor compensation, where the removal of a single current sensor during operation is examined to highlight its effect on voltage and current tracking. Subsequently, the EKF observer is introduced to estimate the missing stator and rotor currents, demonstrating its capability to restore accurate current measurements. In more advanced scenarios, multiple sensor failures are considered simultaneously to assess the robustness of the proposed observer under more challenging fault conditions. The simulations analyze key performance indicators, including voltage tracking, generated current waveforms, residual analysis, and fault detection accuracy.

Through this structured investigation, the chapter provides valuable insights into the importance of sensor redundancy and observer-based estimation techniques for improving the reliability of DFIG-based wind energy systems. The findings contribute to the development of more resilient control strategies capable of maintaining optimal performance even in the presence of sensor malfunctions.

IV.2 Direct stator voltage control (DSVC) approach for a standalone DFIG based wind energy conversion system

IV.2.1 System Overview

The direct stator voltage control (DSVC) strategy is essential for regulating the stator voltage of a stand-alone Doubly-Fed Induction Generator (DFIG) in wind energy systems, particularly under fluctuating wind speeds and load conditions. This approach ensures stable and balanced voltage output, which is critical for the reliability of isolated power systems. The following sections detail the key aspects of DSVC in this context [1-2].

IV.2.2 Control Objectives: The primary objectives of DSVC include:

- Maintaining a constant stator voltage amplitude despite variations in wind speed.;
- Ensuring a balanced and sinusoidal stator and rotor current;
- Regulating the rotor-side converter (RSC) to compensate for disturbances and unbalanced loads.

IV.2.3 Implementation of DSVC Strategy

The direct stator voltage control (DSVC) strategy relies on regulating the rotor-side converter (RSC) to maintain a stable stator voltage. This section details the step by step implementation of the DSVC technique, ensuring precise control over the DFIG system in standalone mode.

Step 1: Stator Voltage Reference Generation and Regulation

The actual stator voltage magnitude is calculated using [3]:

$$|V_s| = \sqrt{(V_{ds})^2 + \left(V_{qs}\right)^2} \tag{IV.1}$$

The actual stator voltage $V_s$is measured and compared to V_{s_ref} where the difference between them is processed through a PI regulator. This results in obtaining the reference rotor current I_{dr_ref}

$$I_{dr\_ref} = PI(V_{s\_ref} - V_s) \tag{IV.2}$$

Step 2: Quadrature Rotor Current Calculation

The quadrature axis rotor current reference I_{qr_ref} is determined based on the stator current using:

$$I_{qr\_ref} = \frac{M}{L_s} I_{qs} \tag{IV.3}$$

Step 3: Transformation of Rotor Current References

The computed rotor current references I_{dr_ref} and I_{qr_ref} are transformed into the rotor's stationary reference frame to obtain the rotor current reference in *abc* coordinates I_{rabc_ref}. Where the transformation from the *dq* rotating reference frame to the *abc* stationary reference frame using inverse Park transformation as following:

$$\begin{bmatrix} I_{ar\_ref} \\ I_{br\_ref} \\ I_{cr\_ref} \end{bmatrix} = \sqrt{\frac{2}{3}} \begin{bmatrix} cos(\theta) & -sin(\theta) & \frac{1}{\sqrt{2}} \\ cos(\theta - \frac{2\pi}{3}) & -sin\left(\theta - \frac{2\pi}{3}\right) & \frac{1}{\sqrt{2}} \\ cos(\theta + \frac{2\pi}{3}) & -sin(\theta + \frac{2\pi}{3}) & \frac{1}{\sqrt{2}} \end{bmatrix} \begin{bmatrix} I_{dr\_ref} \\ I_{qr\_ref} \end{bmatrix} \quad \text{(IV.4)}$$

Step 4: Hysteresis Based Current Control for RSC

After transforming the rotor current references into three-phase currents I_{rabc_ref}, the next step is to regulate these currents using hysteresis-based current control in the rotor-side converter (RSC). This control technique ensures that the actual rotor currents accurately follow their reference values, thereby maintaining the desired stator voltage.

The process begins by measuring the actual rotor currents I_{rabc} and comparing them with their respective reference values. The differences between these currents, known as error signals, are then processed through a hysteresis controller. This controller operates by defining an upper and lower tolerance band around each reference current. Whenever the actual current deviates beyond this band, the converter switches are adjusted to bring it back within the desired range.

By continuously adjusting the rotor-side converter's switching states, the hysteresis controller ensures precise current regulation, allowing the direct stator voltage control (DSVC) strategy to effectively stabilize the stator voltage. This approach is particularly advantageous due to its fast dynamic response, simplicity of implementation. Figure IV.1 represents the block diagram of DSVC that is applied to standalone DFIG [3-6].

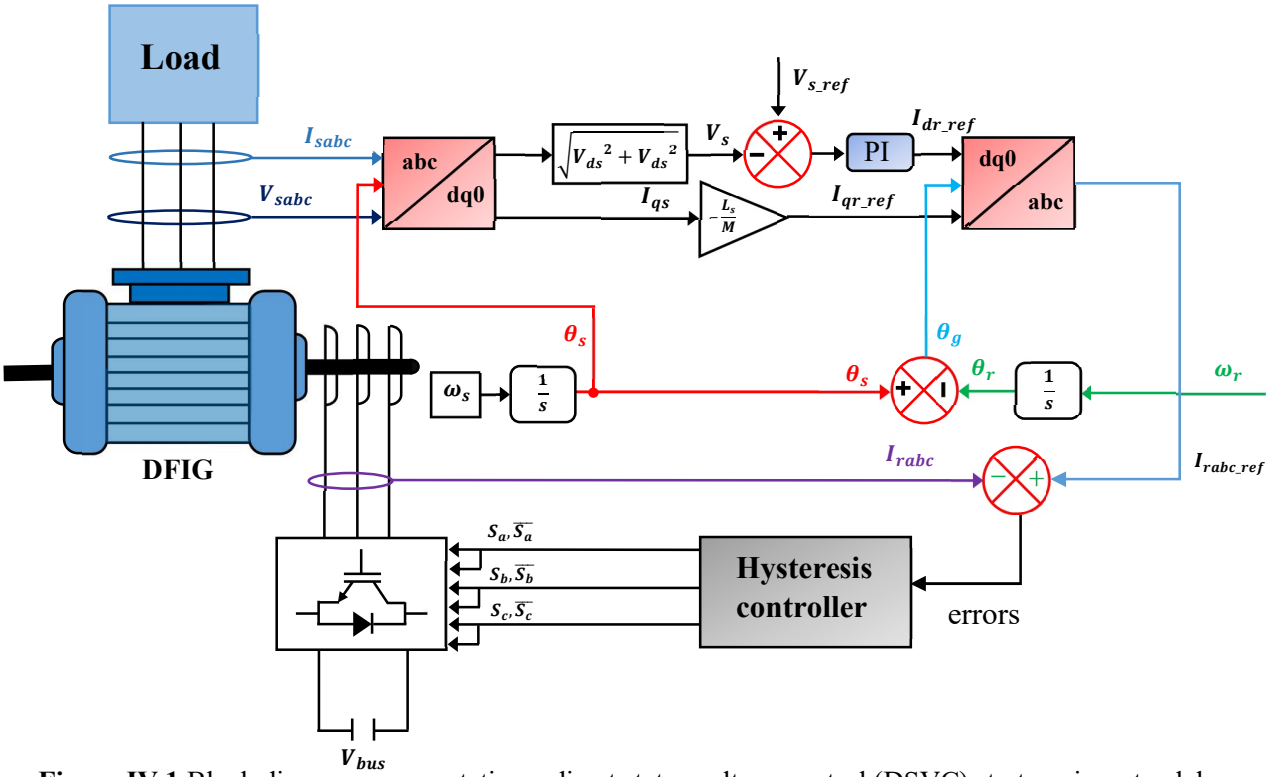

Figure IV.1 Block diagram representation a direct stator voltage control (DSVC) strategy in a standalone DFIG system.

After implementing DSVC, the following section will discuss the importance of current sensors, the principle of observation techniques, and their types for compensating for sensor absence or failure. Additionally, it will cover the application of the Extended Kalman Filter (EKF) to detect and estimate both rotor and stator currents, thereby enhancing system performance and fault diagnosis.

IV.3 EKF for detect the faults and estimate rotor and stator currents of standalone DFIG

IV.3.1 Importance of current sensors in DFIG systems

Current sensors are essential components in Doubly-Fed Induction Generator (DFIG) systems, where they enable real-time monitoring and control of power flow. By providing accurate current measurements, these sensors support advanced control strategies that optimize energy conversion efficiency and maintain system stability. Additionally, they play a crucial role in fault detection and protection mechanisms, preventing potential damage from overcurrent conditions or component failures. Their reliability and precision are fundamental to ensuring the efficient and secure operation of modern energy generation systems.

IV.3.2 Overview of Current Sensor Faults and Their Impact on DFIG Control

Faults in current sensors, such as drift, noise, or failure, can severely disrupt the control of DFIG systems by providing inaccurate or missing measurements. This leads to instability in power regulation, degraded dynamic response, and potential damage to system components due to unregulated currents. In standalone and grid-connected DFIG systems, sensor faults can mislead the controller, causing improper modulation of control parameters, which may result in power quality issues or loss of synchronization. To mitigate these effects, robust fault detection and observation strategies [7].

IV.3.3 Estimators

Estimators are computational methods that utilize the state model of the system. Operating in an open-loop configuration, they lack feedback, making them highly sensitive to modeling errors and system disturbances. These estimators rely on a replica of the system model, either in steady-state conditions (static estimator) or during transient operations (dynamic estimator). The dynamic behavior of an estimator is influenced by the intrinsic modes of the machine [8-9].

IV.3.4 Observers

Observers are designed to estimate parameters that are technically difficult to measure directly or those whose measurement is lost during operation. In such cases, observers are used to estimate these parameters by utilizing information that is more easily accessible through sensors. Essentially, "an observer is an estimator with feedback" This feedback involves comparing the estimated values to the measured values provided by the sensors, thereby reducing the observation error [8-9, 10-11].

IV.3.5 Principle of Observers

In many electrical systems, including Doubly-Fed Induction Generators (DFIGs), certain state variables cannot be directly measured due to sensor limitations or failures. Observers are employed to estimate these unmeasured or inaccessible states using available system inputs and outputs. The primary objective of an observer is to reconstruct the missing state variables through indirect estimation techniques, enabling improved monitoring and control of the system. This approach enhances operational reliability by compensating for sensor deficiencies and ensuring accurate state feedback for advanced control strategies. Figure IV.2 provides a schematic representation illustrating the principle of observer operation [8], [12].

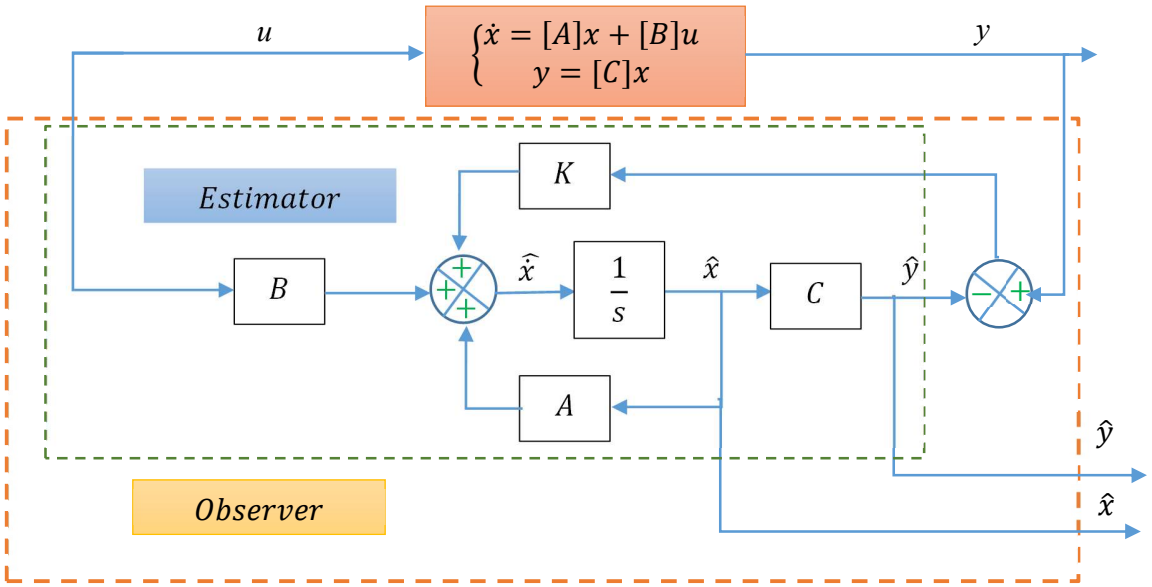

Figure IV.2 Schematic diagram of an observer.

IV.3.6 Classifications of Sensor Faults observation techniques

Observers play a critical role in electrical applications, as they contribute to the continuity of operation by estimating the values of parameters whose sensors may have failed. Furthermore, observers can help identify the location of faults, thereby ensuring the system's operational stability and maintaining the efficiency of control systems in generators. Various types of observers, such as the Luenberger Observer (LO), Sliding Mode Observer (SMO), Model Reference Adaptive System (MRAS), and Extended Kalman Filter (EKF), are commonly used to detect and estimate sensor faults in these systems [13-15].

IV.3.7 Design of the DFIG's for estimate and diagnostics currents using EKF

IV.3.7.1 Extended Kalman Filter (EKF)

The Extended Kalman Filter (EKF) is a state observer designed for use in nonlinear systems, operating effectively in stochastic environments by reducing the error variance between actual variables and their estimates. It is particularly useful in sensorless control applications, such as estimating the rotor position and speed, as well as current estimation in Doubly-Fed Induction Generators (DFIGs). By utilizing available voltage and current measurements from the machine, the EKF can reconstruct system states that are difficult to measure directly. In the case of DFIG systems, the EKF provides accurate estimates of both rotor and stator currents, enhancing fault detection capabilities and ensuring reliable performance during real-time operation [16-17].

IV.3.7.2 Principle of the EKF technique

The principle of the EKF lies in its ability to predict the system's state based on a dynamic model while accounting for measurement noise and process disturbances. In a DFIG system, the EKF operates by recursively updating estimates of system states such as the currents through iterative corrections based on measured data. This process involves a two-step operation: prediction and update. During the prediction phase, the EKF uses the system model to predict the next state, and in the update phase, it adjusts the prediction based on the difference between the predicted and measured outputs. The EKF's ability to handle non-linearity and its optimal performance in noisy environments make it an ideal choice for fault detection and state estimation in DFIG systems [16-17].

IV.3.7.3 EKF observer equations

The Extended Kalman Filter (EKF) is an estimation technique that uses a state-space model to predict and update system states based on voltage and current measurements. It assumes the noise in the system is Gaussian, with process noise uncorrelated to measurement noise. The EKF optimally adjusts estimates using a calculated gain to refine state predictions. In DFIG systems, the EKF observer equations are derived from a linearized state-space model, where the system states are iteratively updated based on measurements. This allows for real-time corrections, improving the accuracy of state estimation and ensuring reliable system performance even with sensor faults or uncertainties.

The EKF observer equations are derived from the following general state-space representation of the system [18]:

$$\begin{cases} \dot{x} = [A]x + [B]u \\ y = [C]x \end{cases} \tag{IV.5}$$

x is the state vector is expressed in the fixed (α-β) reference frame, where I_α and I_β represent the stator and rotor currents in the $\alpha\beta$ frame, respectively. The input vector u consists of the applied voltages, while the output vector y represents the measured currents. It should be noted that the matrices [A], [B], and [C] correspond to the state-space matrices of the DFIG machine model to the input and output measurements. These state-space equations are crucial for the proper estimation of the rotor and stator currents using the Extended Kalman Filter (EKF) in a DFIG-based system.

IV.3.7.4 Application of EKF for detect the faults and estimate rotor and stator currents of standalone DFIG

To apply the Extended Kalman Filter (EKF) for estimating the stator and rotor currents and identifying the faulty sensor location during operation, we model the Doubly Fed Induction Generator (DFIG) in the (α, β) reference frame, which is aligned with the rotating magnetic field. Under steady-state conditions, the system can be expressed as follows:

$$\begin{aligned} \dot{x_1} &= [A_1]x_1 + [B_1]u_1 \\ y_1 &= [C_1]x_1 \end{aligned} \tag{IV.6}$$

In this context, the state-space matrix is:

$$A_1 = \begin{bmatrix} -\frac{R_s}{\sigma L_s} & \frac{\omega_r M^2}{\sigma L_s L_r} & \frac{R_r M}{\sigma L_s L_r} & \frac{\omega_r M}{\sigma L_s} \\ -\frac{\omega_r M^2}{\sigma L_s L_r} & -\frac{R_s}{\sigma L_s} & -\frac{\omega_r M}{\sigma L_s} & \frac{R_r M^2}{\sigma L_s L_r} \\ \frac{R_s M}{\sigma L_s L_r} & -\frac{\omega_r M}{\sigma L_r} & -\frac{R_r}{\sigma L_r} & -\frac{\omega_r}{\sigma} \\ \frac{\omega_r M}{\sigma L_r} & \frac{R_s M}{\sigma L_s L_r} & -\frac{\omega_r}{\sigma} & -\frac{R_r}{\sigma L_r} \end{bmatrix}$$

The input matrix:

$$B_1 = \begin{bmatrix} \frac{1}{\sigma L_s} & 0 & -\frac{M}{\sigma L_s L_r} & 0 \\ 0 & \frac{1}{\sigma L_s} & 0 & -\frac{M}{\sigma L_s L_r} \\ -\frac{M}{\sigma L_s L_r} & 0 & \frac{1}{\sigma L_r} & 0 \\ 0 & -\frac{M}{\sigma L_s L_r} & 0 & -\frac{R_r}{\sigma L_r} \end{bmatrix}$$

And the output matrix is:

$$C_1 = \begin{bmatrix} 1 & 0 & 0 & 0 \\ 0 & 1 & 0 & 0 \\ 0 & 0 & 1 & 0 \\ 0 & 0 & 0 & 1 \end{bmatrix}$$

Where: $x_1 = [I_{\alpha s}, I_{\beta s}, I_{\alpha r}, I_{\beta s}]^t$ represents the stator vector compressing the stator and rotor currents in the $\alpha\beta$ reference frame; $u_1 = [V_{\alpha s}, V_{\beta s}, V_{\alpha r}, V_{\beta s}]^t$ are represents the input voltage vector; y_1 is the output vector.

The application of the Extended Kalman Filter (EKF) for fault diagnosis and the estimation of stator and rotor currents relies on identifying discrepancies between the sensor measurements and the values estimated by the EKF bank derived from the state-space model. These discrepancies are processed during the decision-making phase to accurately pinpoint the faulty sensor. This approach leverages the EKF's capability to analyze dynamic system states and deviations, thus ensuring precise fault detection and improving the system's operational reliability.

IV.3.7.4.1 Discretization Process

The discretization process is a critical step in adapting the continuous-time state-space model of the Doubly-Fed Induction Generator (DFIG) to a discrete-time framework, suitable for digital implementation. The state-space model is initially defined by the continuous-time matrices. To achieve discretization:

The discrete-time state matrix A_d is computed using the matrix exponential:

$$A_d = e^{A_1 T_s} \tag{IV.7}$$

Where T_s is the sampling time.

The discrete-time input matrix B_d is derived from the continuous-time model:

$$B_d = A_1^{-1}(A_d\text{-}I_{4*4})\, B_1 \tag{IV.8}$$

These matrices, A_d and B_d, form the backbone of the EKF's discrete-time implementation, enabling the prediction and update of system states based on sampled data.

IV.3.7.4.2 Prediction Step

The prediction step represents the initial phase of the Extended Kalman Filter (EKF) algorithm, where both the system's state and covariance are predicted based on the discretized model and control inputs. This step is essential for accounting for the system's dynamic behavior before integrating new measurements. The prediction step comprises two main components [17] [19]:

- State prediction: The process of forecasting the system's state based on the previous state estimate and control inputs:

$$y_{1pred} = A_d y_{1est} + B_d u_1 \tag{IV.9}$$

  Where $y_{1est}$is the previous state estimate, and u_1 is the control input vector.

- Covariance prediction: The estimation of the error covariance associated with the predicted state, which helps quantify the uncertainty in the prediction:

$$P_{pred} = A_d P_{est}\, A_d^t + Q \tag{IV.10}$$

Where P_{est} is the previous state estimate and Q is the process noise covariance matrix, modeling uncertainties in the system dynamics.

IV.3.7.4.3 Update Step

The update step refines the predicted state and covariance using the incoming measurements, ensuring accurate estimation of rotor and stator currents. This step involves three key components [17] [19]:

- Kalman Gain Calculation: The Kalman gain (K) determines the degree of influence assigned to the measurement relative to the prediction:

$$K = P_{pred}\ {C_1}^t (C_1\ P_{pred} {C_1}^t + R)^{-1} \quad \text{(IV.11)}$$

Where *R* represent the measurement noise covariance matrix.

- State Update: The updated state estimate incorporates the predicted state and the measurement residual:

$$y_{1est} = y_{1pre}\ + K\ (y_1 - C_1\ y_{1pre}\ ) \quad \text{(IV.12)}$$

In the context y_1 represents the measured output vector.

- Covariance update: The updated covariance matrix reflects the reduced uncertainty after incorporating the measurement:

$$P_{est} = (I - K\ C_1) P_{pred} \quad \text{(IV.13)}$$

To illustrate the operation of the Extended Kalman Filter (EKF) in estimating rotor and stator currents, the following figure outlines the key stages of the EKF process. This visualization highlights the steps of prediction and update, which are critical for achieving accurate state and covariance estimations in a DFIG system.

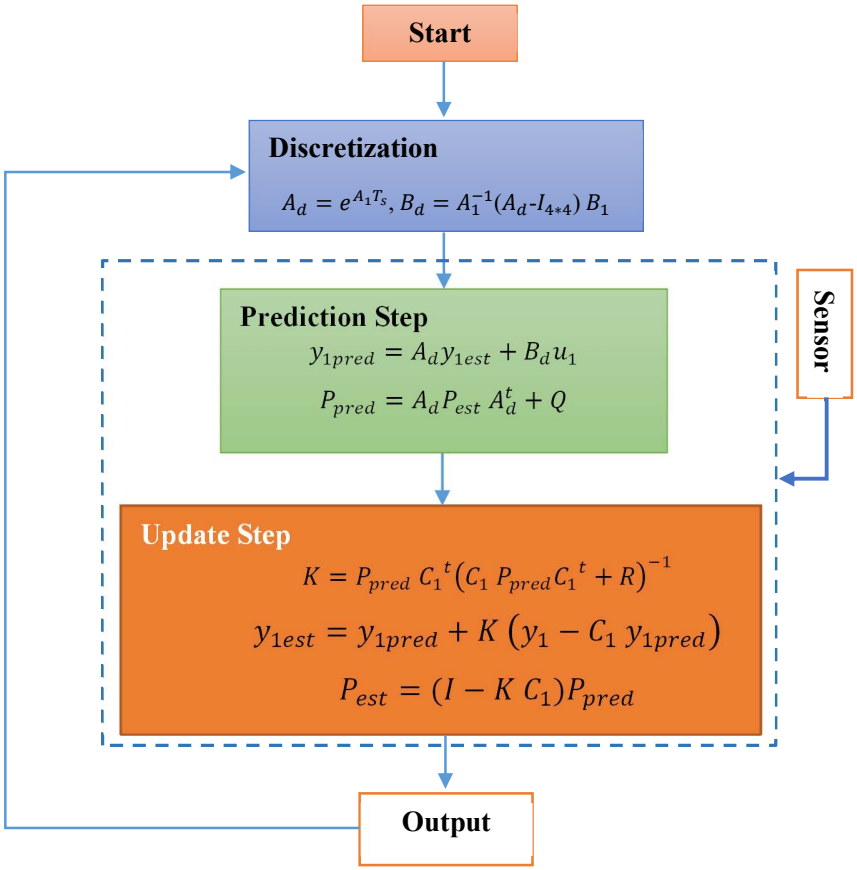

Figure IV.3 Diagram of the Extended Kalman Filter (EKF) Process in DFIG Current Estimation.

IV.3.7.5 Residual Calculation

The residual involves calculating the difference between the measured currents and the estimated currents, as expressed by the following equation:

$$Residual = y_1 - y_{1est} \tag{IV.14}$$

This difference serves as an indicator of sensor performance and is utilized for fault detection. By monitoring this discrepancy, it becomes possible to identify anomalies and ensure reliable operation of the system.

IV.3.7.6 Fault Detection Algorithm

A fault detection mechanism identifies faulty sensors based on the root mean square (RMS) of the residual and a predefined threshold. Where If the maximum RMS value exceeds the threshold, the corresponding sensor is flagged as faulty.

IV.4 Simulation Results and Analysis

Figure IV.4 provides a detailed representation of the overall system, illustrating the application of Direct Stator Voltage Control (DSVC) in conjunction with an Extended Kalman Filter (EKF) observer for rotor and stator current estimation and sensor fault detection in a standalone Doubly Fed Induction Generator (DFIG). The system consists of a DFIG driven by a wind energy source, where the stator is directly connected to a three-phase resistive load, while the rotor is controlled via an inverter. The DSVC strategy is employed to regulate the stator voltage, ensuring stable operation under varying conditions. Simultaneously, the EKF observer estimates the rotor and stator currents, compensating for potential sensor failures and contributing to fault detection and diagnosis.

To evaluate the performance of the proposed control strategy, a simulation study was conducted in MATLAB/Simulink. The implemented system integrates the DSVC technique with the EKF observer to estimate rotor and stator currents and diagnose sensor faults in a stand-alone DFIG. The simulation framework is designed to assess the effectiveness of the control approach under various operating conditions and fault scenarios. The analysis begins by demonstrating the performance of the DSVC and EKF observer under normal operating conditions. The estimated rotor and stator currents obtained through the EKF observer are compared with their actual values to validate the accuracy of the estimation process. Next, different fault scenarios are introduced by remove the current sensors to evaluate the system's ability to detect and locate sensor faults.

The simulation results provide a comprehensive evaluation of the DSVC strategy combined with EKF for sensor fault detection, highlighting its robustness in estimating missing current measurements and ensuring the continuity of operation in stand-alone DFIG-based systems.

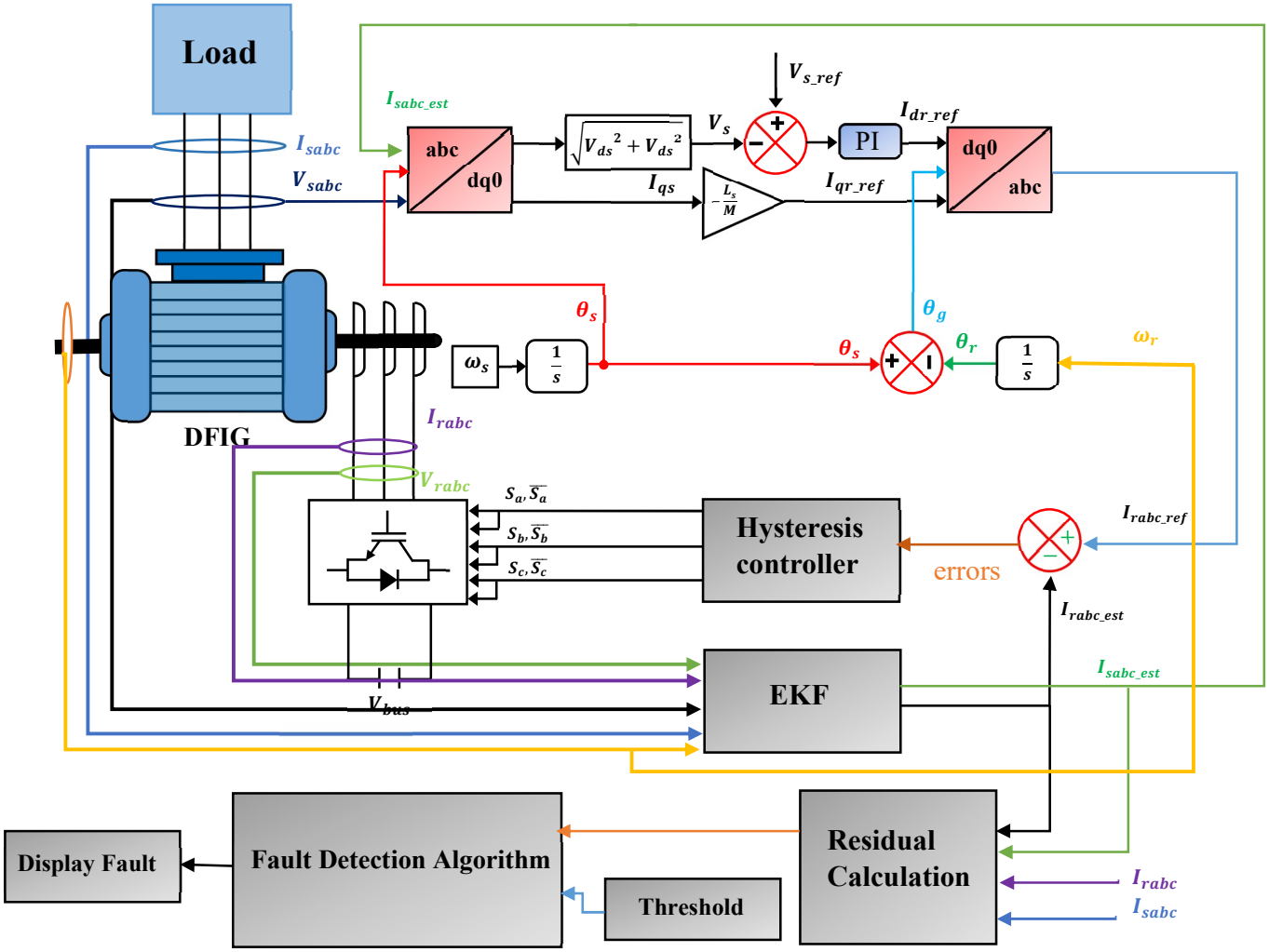

Figure IV.4 DSVC Applied to a DFIG System with EKF Observer for Rotor and Stator Current Estimation and Sensor Fault Detection.

The performance of the standalone Doubly-Fed Induction Generator (DFIG) under Direct Stator Voltage Control (DSVC) without an observer is illustrated in Figure IV.5. This scenario evaluates the impact of the absence of current sensors on the generator's performance under steady-state operating conditions. The system is tested with a stator voltage reference V_{s_ref}=150 V, a connected load of 2 kW, and an operating speed of 1200 rpm.

As depicted in Figure IV.5.a, during the initial time interval (0-1s), the stator voltage V_s accurately tracks the reference value of 150V, demonstrating the effectiveness of DSVC. However, from (1-2s), the stator current sensor is deliberately removed, leading to noticeable performance degradation, characterized by increased chattering in V_s. When the missing current sensor is reinstated at (2-3s), the system recovers, and the chattering effect is reduced.

Subsequently, from (3-4s), a rotor current sensor is removed, significantly increasing chattering in V_S, further impacting voltage tracking. Finally, from (4-5s), restoring the rotor current sensor reestablishes proper voltage tracking, confirming the crucial role of current sensors in maintaining system stability. Figures IV.5.b and IV.5.c illustrate the measured stator and rotor currents (I_{s_abc} and I_{r_abc}) in the *abc* reference frame. The disturbances observed during sensor removal highlight the critical role of current sensors in ensuring stable operation and maintaining the quality of generated electrical power. These findings emphasize the necessity of integrating observers to compensate for sensor failures, thereby preserving the accuracy of current estimation and ensuring the reliability of the control strategy.

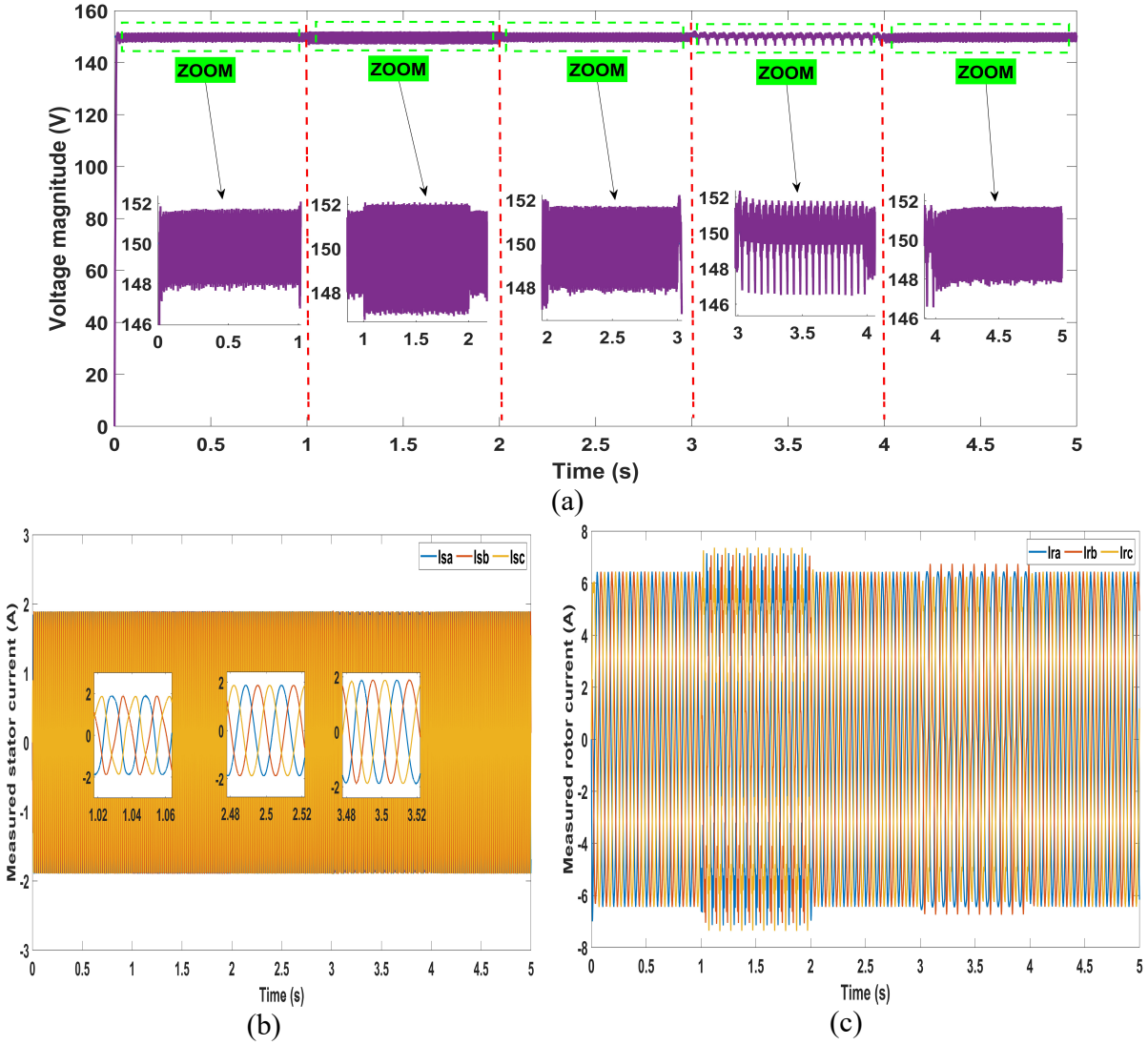

Figure IV.5 Performance of standalone DFIG under DSVC control without observer Impact of current sensor failures on system stability.

The EKF observer is introduced to estimate the rotor and stator currents, compensating for any missing current sensor measurements. Figure IV.6 presents the estimated currents obtained through the observer and compares them with the measured currents. Specifically, Figure IV.6.a illustrates the measured stator current I_{sa} alongside its estimated counterpart I_{sa_est}, while Figure IV 6.b displays the measured rotor current I_{ra} compared to the estimated I_{ra_est}. The results demonstrate the strong performance of the EKF observer in accurately estimating both stator and rotor currents, ensuring reliable system operation despite sensor failures.

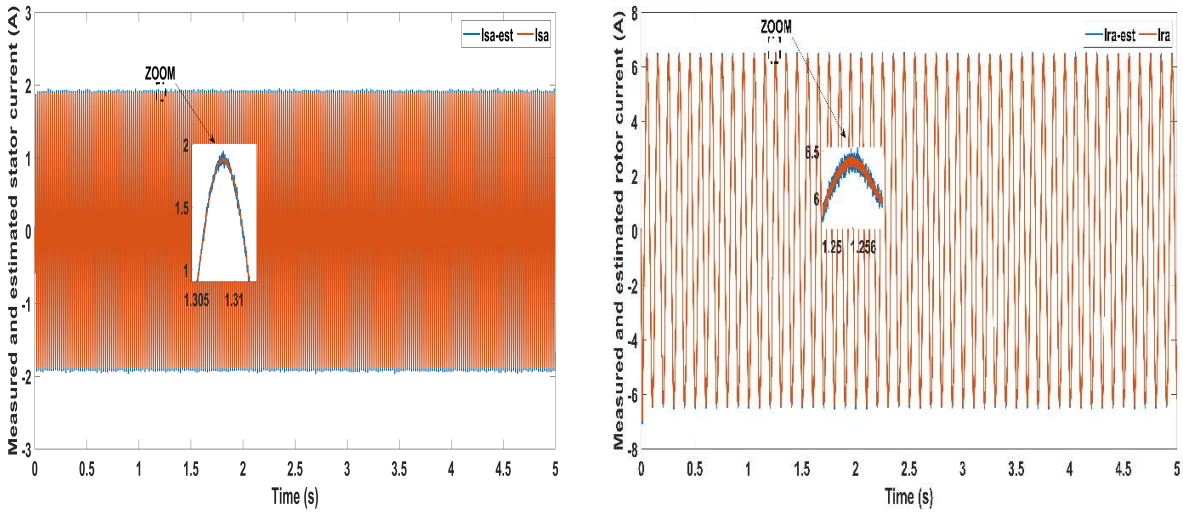

(a) (b)

Figure IV.6 Performance of the Standalone DFIG under EKF observer for rotor and stator current estimation.

To evaluate the performance of the system in the absence of EKF observation, a single current sensor fault was intentionally introduced during operation. Specifically, one of the stator current sensors was disconnected between (1-2s), followed by its reconnection. Subsequently, between (3-4s), a rotor current sensor was removed. Figure IV.7.a illustrates that during the first second (0-1s), the stator voltage V_s effectively tracks its reference V_{s_ref}, demonstrating stable operation. However, between (1-2s), the stator current sensor I_{sa} was deliberately removed, followed by the rotor current sensor I_{ra} between (3-4s). Despite these sensor losses, the tracking performance of V_s relative to V_{s_ref} remained unaffected. Furthermore, the output currents of the standalone DFIG, represented by I_{s_abc} and I_{r_abc}, retained their sinusoidal shape without distortion, as depicted in Figure IV.7.b and Figure IV.7.c. This highlights the robustness of the EKF observer, which successfully compensated for the missing current sensor signals by providing accurate estimations.

Figures IV.7.d and IV.7.e further validate this performance by showing the comparison between the measured and estimated stator current (I_{sa} and I_{sa_est}) and rotor current (I_{ra} and I_{ra_est}), respectively. The strong agreement between the measured and estimated currents confirms the effectiveness of the EKF in maintaining accurate current estimations even in the absence of sensors.

Additionally, Figure IV.7.f presents the residual signals, representing the difference between the measured and estimated currents. These residuals serve as indicators for fault detection, where significant deviations signal a sensor failure. Finally, Figure IV.7.g visualizes the faulty sensor identification mechanism. The fault detection system assigns each sensor a position from 1 to 6 (I_{sa}=1, I_{sb}=2, I_{sc}=3, I_{ra}=4, I_{rb}=5, I_{rc}=6). A threshold of 0.4 A is set, and if the residual exceeds this threshold, the faulty sensor is identified and flagged accordingly.

The results obtained in this scenario further demonstrate the efficiency of the EKF observer in maintaining the stability of the standalone DFIG by accurately estimating the missing current signals. This highlights its crucial role in ensuring system reliability, even in the presence of sensor faults.

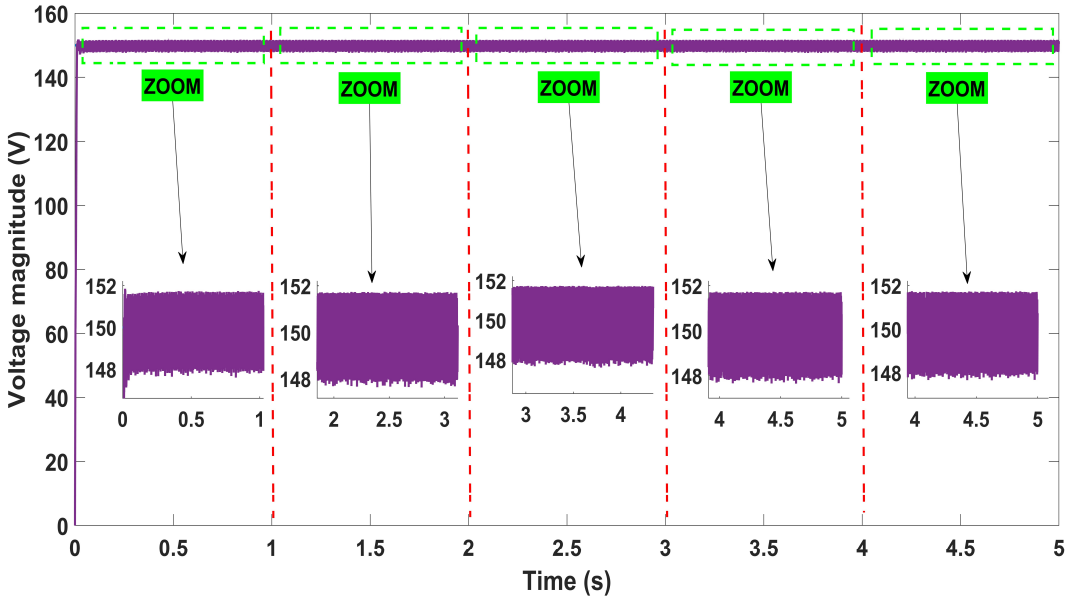

(a)

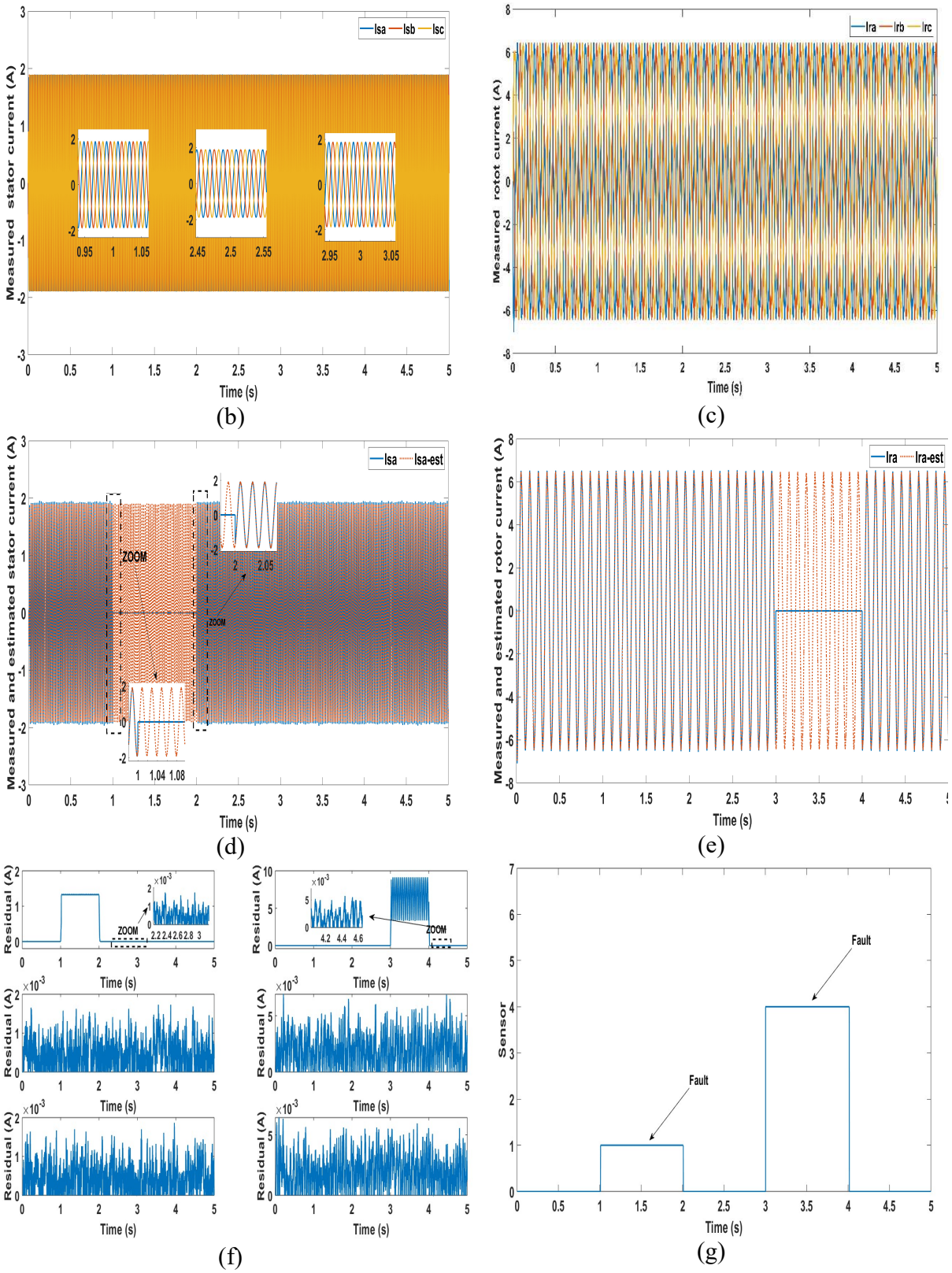

Figure IV.7 Performance of Standalone DFIG During the Applied DSVC with EKF Observation with a single fault.

In this scenario, the effectiveness of the EKF observer in compensating for missing current sensors and detecting faulty sensors is evaluated under multiple sensor fault conditions during operation. Unlike the previous cases, this scenario introduces simultaneous sensor failures to assess the robustness of the observer. The following sequence of sensor faults was applied:

- The stator current sensor I_{sa} was removed from 1 to 3s.
- The stator current sensor I_{sb} was removed from 2 to 4s.
- The rotor current sensor I_{ra} was removed from 3 to 5s.

Figure IV.8.a illustrates the stator voltage V_s tracking the reference voltage V_{s_ref}, showing stable tracking performance without any significant increase in chattering, despite the presence of multiple sensor faults.

Figures IV.8.b and IV.8.c present the generated stator and rotor currents, which maintain a well-sustained sinusoidal waveform, confirming that the EKF observer successfully compensates for missing current measurements.

Figure IV.8.d depicts the residuals, representing the difference between the measured and estimated currents, which indicate sensor malfunctions.

Figure IV.8.e provides the sensor fault detection results, where:

From 1 to 2s, the system identifies the absence of I_{sa}, marked as 1.

From 2 to 3s, both I_{sa} and I_{sb} are missing, with the indicator oscillating between 1 and 2.

From 3 to 4s, I_{sb} and Ira are simultaneously missing, causing the fault indicator to switch between 2 and 4.

From 4 to 5s, only I_{ra} remains missing, marked as 4.

In the time intervals 0 to 1 second and 5 to 6 seconds, no sensor faults occur, and the indicator remains at 0.

These results demonstrate the EKF observer's ability to maintain accurate current estimation and effectively detect multiple sensor failures, ensuring robust fault compensation and stable operation of the standalone DFIG system.

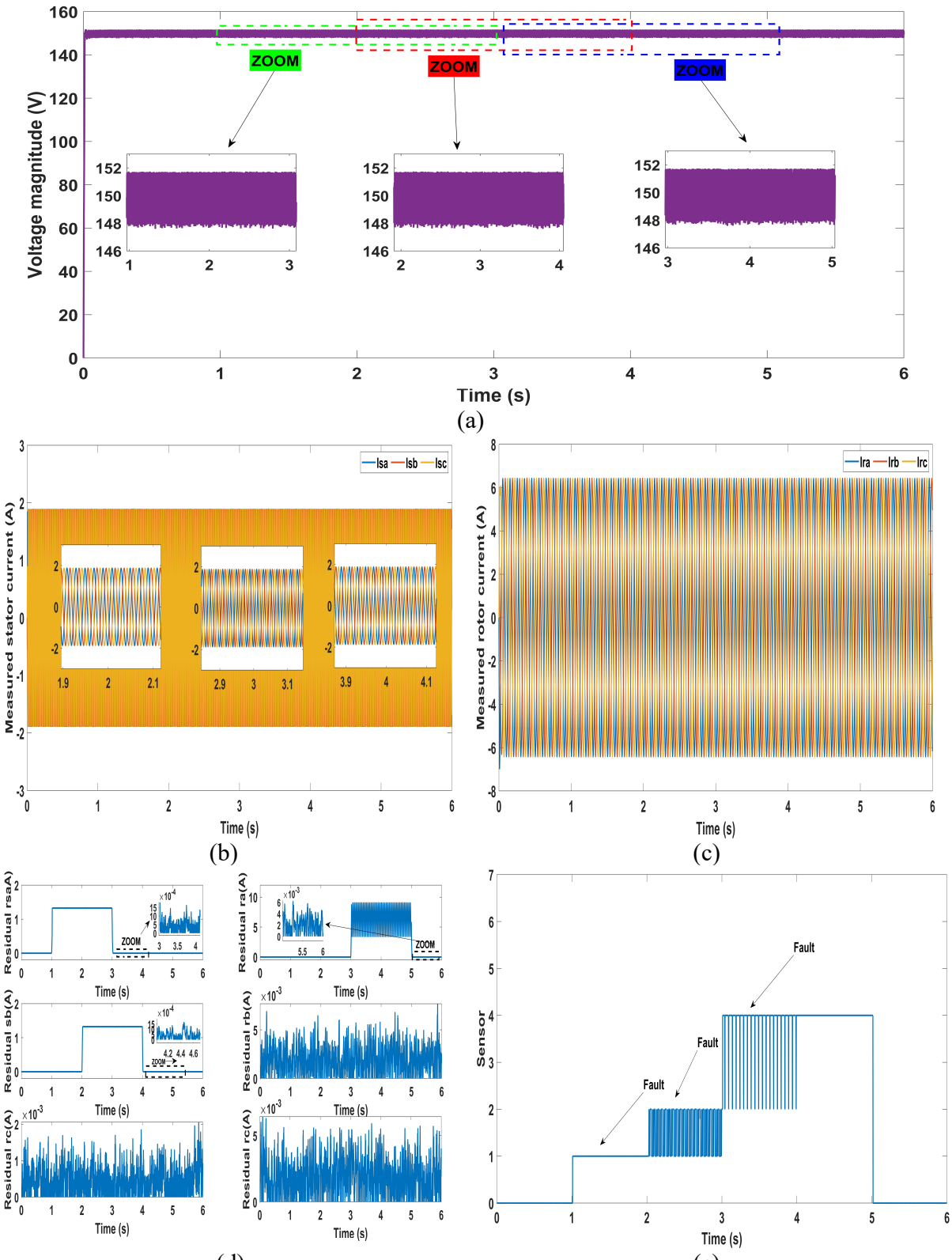

Figure IV.8 Performance of Standalone DFIG During the Applied DSVC with EKF Observation with Multiple Current Sensor Faults Compensation and Detection Using EKF.

Figure IV.9 presents the comparison between the measured currents and those estimated by the EKF observer, both before and during the absence of specific current sensors. The results demonstrate the effectiveness of the EKF observer in accurately estimating the missing currents, ensuring stable system operation despite sensor failures.

Figure IV.9.a illustrates the measured stator current I_{sa} alongside its estimated counterpart I_{sa_est}. The figure shows a perfect match between the two signals, confirming the high accuracy of the EKF observer. Even when the sensor for I_{sa} is removed between 1 to 3s, the estimated current closely follows the actual behavior, compensating for the missing measurement.

Figure IV.9.b depicts the measured stator current I_{sb} and its estimated value I_{sb_est}. Similarly, the EKF observer effectively tracks the current, maintaining a precise estimation even when the I_{sb} sensor is removed between 2 to 4s. This demonstrates the observer's capability to reconstruct missing data and ensure uninterrupted system performance.

Figure IV.9.c displays the measured rotor current I_{ra} and its estimated counterpart I_{ra_est}. The results indicate a perfect correlation between the two signals, confirming the EKF observer's reliability. Despite the absence of the I_{ra} sensor between 3 to 5s, the observer accurately reconstructs the missing current, maintaining system stability.

These findings validate the effectiveness of the EKF observer in compensating for current sensor failures, ensuring accurate current estimation even in cases of multiple simultaneous sensor losses. This capability is crucial for enhancing the reliability and fault tolerance of standalone DFIG-based wind energy systems.

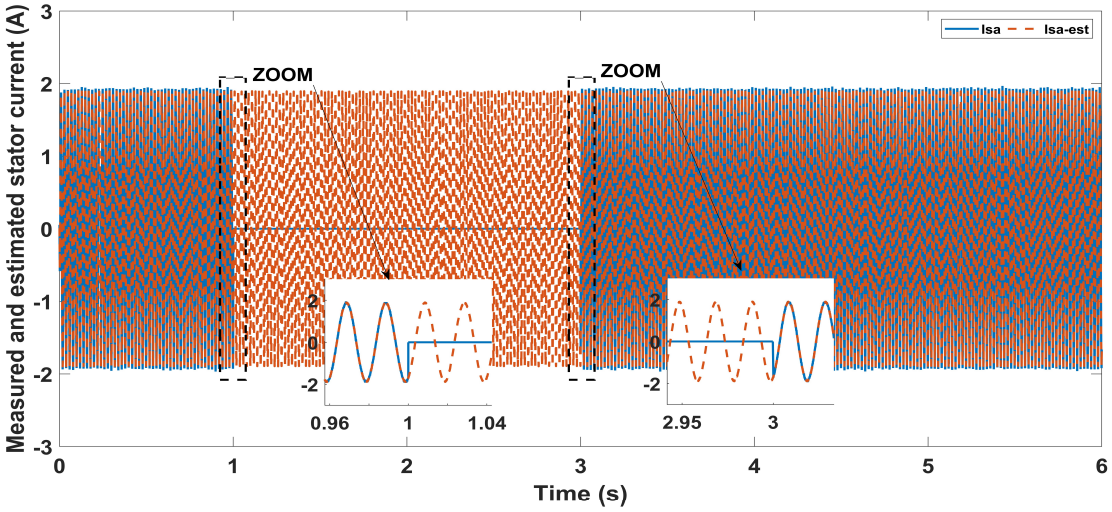

(a)

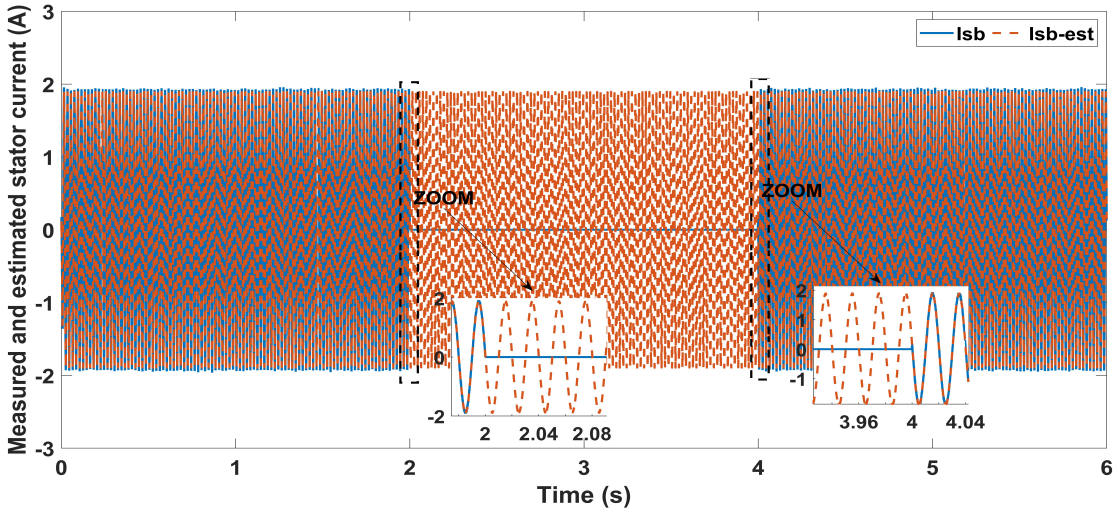

(b)

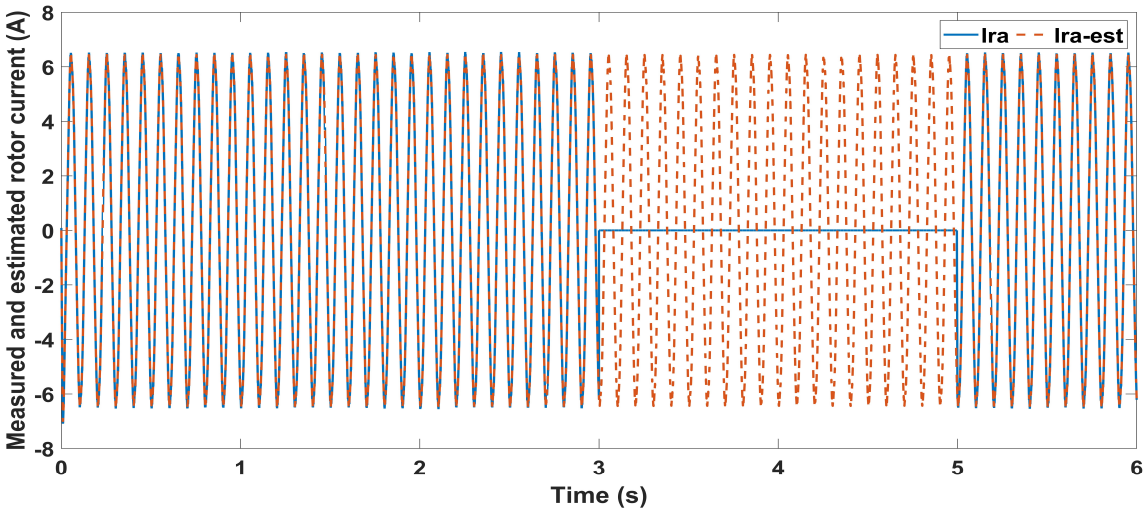

(c)

Figure IV.9 Estimated and Measured Currents Using EKF Observer Under Sensor Fault Conditions

IV.5 Conclusion

This chapter has provided an in-depth analysis of the impact of current sensor faults on the performance of a standalone DFIG system and the effectiveness of the EKF observer in compensating for such faults. The simulation results demonstrated that sensor failures significantly affect voltage and current tracking when no compensation mechanism is employed. However, the implementation of the EKF observer successfully estimated the missing currents, ensuring stable and accurate system operation.

Furthermore, a fault detection strategy based on residual analysis was evaluated, effectively identifying faulty sensors and distinguishing between different fault conditions. The results confirmed that the EKF observer is a powerful tool for maintaining system reliability by providing accurate current estimations and enabling prompt fault identification. The study also highlighted the observer's robustness in handling both single and multiple sensor faults without compromising the quality of the generated electrical signals.

These findings emphasize the importance of advanced observer-based fault compensation techniques in renewable energy systems. Future research could explore the integration of more sophisticated filtering methods or artificial intelligence-based approaches to further enhance fault detection accuracy and compensation efficiency. Additionally, experimental validation of the proposed approach could be conducted to confirm its applicability in real-time implementation DFIG-based wind energy systems.

REFERENCES BIBLIOGRAPHIQUES

[1] Hussien, M. G., Xu, W., & Liu, Y. (2018, October). Vector control schemes for direct voltage control of the stand-alone brushless doubly-fed induction generator. In 2018 21st International Conference on Electrical Machines and Systems (ICEMS) (pp. 1307-1312). IEEE.

[2] Liu, Y., Xu, W., Xiong, F., & Blaabjerg, F. (2017, August). Sensorless direct voltage control of the stand-alone brushless doubly-fed generator. In *2017 20th International Conference on Electrical Machines and Systems (ICEMS)* (pp. 1-6). IEEE.

[3] Chabani, M. S., Benchouia, M. T., Golea, A., & Boumaaraf, R. (2017, October). Implementation of direct stator voltage control of stand-alone DFIG-based wind energy conversion system. In *2017 5th International Conference on Electrical Engineering-Boumerdes (ICEE-B)* (pp. 1-6). IEEE.

[4] Mohammed, S. C. (2022). *Contribution to the Control of Doubly Fed Induction Machine DFIM* (Doctoral dissertation, Université Mohamed Khider-Biskra).

[5] Singh, H., & Singh, M. (2021, June). Investigations on the control strategy of rotor side converter in doubly fed induction generator. In *2021 International Conference on Communication, Control and Information Sciences (ICCISc)* (Vol. 1, pp. 1-6). IEEE.

[6] Tiwari, N., Nema, R. K., Kumar, R., Varathe, N. K., & Nema, S. (2024, June). Current Estimator Based Model Adaptive Sensorless Vector Control Using Hysteresis Controllers for Induction Motors. In *2024 IEEE 3rd International Conference on Electrical Power and Energy Systems (ICEPES)* (pp. 1-5). IEEE.

[7] Tran, C. D., Kuchar, M., Sotola, V., & Nguyen, P. D. (2024). Fault-Tolerant Control Based on Current Space Vectors against Total Sensor Failures. *Sensors*, *24*(11), 3558.

[8] Yildiz, T., Abur, A., Tripathy, S., Singhvi, V., & Patel, M. (2024, July). Implementation of a State Estimator Ensuring Visibility for the Largest Possible Set of Buses. In *2024 IEEE Power & Energy Society General Meeting (PESGM)* (pp. 1-5). IEEE.

[9] Course, K., & Nair, P. B. (2023). State estimation of a physical system with unknown governing equations. *Nature*, *622*(7982), 261-267.

[10] Zhao, R., Yang, G., Li, P., Parisini, T., & Chen, B. (2024, June). State Estimation Using a Network of Observers for a Class of Nonlinear Systems with Communication Delay. In *2024 European Control Conference (ECC)* (pp. 762-767). IEEE.

[11] Ibrahim, K. A., & Ding, F. (2024). Parameter estimation methods for time-invariant continuous-time systems from dynamical discrete output responses based on the Laplace transforms. *International Journal of Adaptive Control and Signal Processing*, *38*(9), 3213-3232.

[12] Janisch, G., Kugi, A., & Kemmetmüller, W. (2024, June). Implementation aspects for state and parameter observers for induction machines at low sample-to-fundamental frequency ratios. In *2024 European Control Conference (ECC)* (pp. 1851-1856). IEEE.

[13] Luo, R., Wang, Z., & Sun, Y. (2022). Optimized Luenberger Observer-Based PMSM Sensorless Control by PSO. *Modelling and Simulation in Engineering*, *2022*(1), 3328719.

[14] Ding, W. (2024). A review of sensorless permanent magnet synchronous motors with adaptive observer. In *MATEC Web of Conferences* (Vol. 404, p. 02011). EDP Sciences.

[15] Zhang, Y., Zhao, Z., Lu, T., Yuan, L., Xu, W., & Zhu, J. (2009, September). A comparative study of Luenberger observer, sliding mode observer and extended Kalman filter for sensorless vector control of induction motor drives. In *2009 IEEE Energy Conversion Congress and Exposition* (pp. 2466-2473). IEEE.

[16] Ruan, G., Su, Y., Yang, K., Cao, J., Su, Y., Gong, Z., & Hu, X. (2024). A sensorless control system of permanent magnet synchronous motor based on observation error threshold EKF. *Transactions of the Institute of Measurement and Control*, 01423312241273770.

[17] Chebaani, M., Mahmoud, M. M., Tazay, A. F., Mosaad, M. I., & Nouraldin, N. A. (2023). Extended Kalman Filter design for sensorless sliding mode predictive control of induction motors without weighting factor: An experimental investigation. *Plos one*, *18*(11), e0293278.

[18] Zahraoui, Y., & Akherraz, M. (2020). Kalman filtering applied to induction motor state estimation. *Dynamic Data Assimilation-Beating the Uncertainties*.

[19] Kaniewski, P. (2020). Extended Kalman filter with reduced computational demands for systems with non-linear measurement models. *Sensors*, *20*(6), 1584.

CHAPTRE V

ADVANCED CONTROL AND SENSORLESS ESTIMATION FOR STANDALONE DFIG SYSTEMS

V.1 Introduction

This chapter focuses on the development and analysis of a comprehensive control and observation for standalone Doubly-Fed Induction Generator (DFIG) systems. The first section emphasizes the design of a sensorless speed estimation technique based on the Model Reference Adaptive System (MRAS), tailored to the unique requirements of standalone systems. By eliminating the need for mechanical sensors, the MRAS enhances system reliability, reduces complexity, and significantly lowers operating costs, making it particularly suitable for standalone applications. The theoretical foundation and operational principles of the MRAS are discussed, highlighting its robustness and accuracy under standalone conditions. This section concludes by detailing the application of the MRAS observer to estimate the rotor speed of the DFIG, effectively replacing the speed sensor.

Building on this foundation, the second section introduces Model Predictive Control (MPC) as a primary control strategy for standalone DFIG systems. The discussion encompasses the definition, historical evolution, and key advantages of MPC, along with its limitations and various types. Specifically, the Finite-Set Model Predictive Current Control (FS-MPCC) is applied, demonstrating its capability to achieve effective current regulation and dynamic performance in standalone systems.

The third section highlights the seamless integration of FS-MPCC with the MRAS observer, forming a unified control-observation scheme optimized for standalone DFIG environments.

The final section provides a detailed configuration of this co-design, illustrating the interaction between the FS-PCC-based control strategy and the MRAS speed estimation approach. The proposed system's performance is evaluated through MATLAB simulations and experimental verification conducted in the Electrical Engineering Laboratory (LGEB) at the University of Biskra. Results are analyzed under a variety of dynamic scenarios, including sudden changes in speed, load, and reference voltage. Comparisons between simulation and experimental findings underline the consistency and reliability of the proposed approach, validating its effectiveness for real-time applications.

V.2 Design of sensorless speed using MRAS for standalone DFIG

This section outlines the study and application of a sensorless speed observation system for Doubly-Fed Induction Generators (DFIGs) based on the Model Reference Adaptive System (MRAS). By eliminating the need for speed sensors, this approach simplifies the system, reduces

associated costs, and enhances overall reliability. The applied observation system employs an adaptive mechanism that continuously evaluates and aligns the actual performance of the DFIG with a predefined reference model to achieve accurate and responsive speed regulation. As part of this work, a reference model reflecting the desired speed behavior of the DFIG has been constructed to ensure consistent and optimal performance across various operating scenarios.

V.2.1 Principle of the MRAS Method

A Model Reference Adaptive System (MRAS) is a technique used for state estimation in dynamic systems, such as electrical machines. It works by comparing the measured values (e.g., currents or speeds) with those estimated by an adjustable model based on the system's analytical equations. The adaptation mechanism then adjusts the model to reduce the error between the measured and estimated values. This process allows the MRAS to track the system's behavior accurately. While it offers benefits like simplicity and fast computation. So, the principle of MRAS technique can be detailed in the Figure V.1 as follows [1-5]:

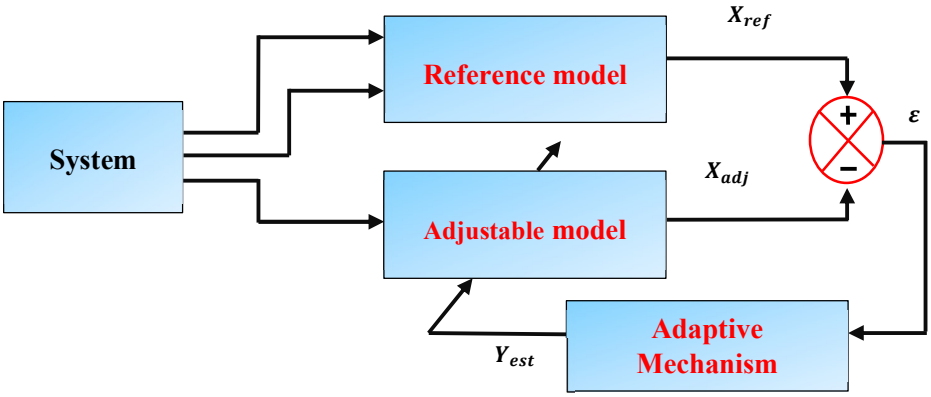

Figure V.1 Block diagram of principle MRAS estimator.

IV.2.2 Application of MRAS Observation for estimation DFIG speed

To apply the Model Reference Adaptive System (MRAS) for rotor speed estimation in a Doubly-Fed Induction Generator (DFIG), the following principal steps are generally involved [6-7]:

- **The reference model**

The first step is to establish a reference model based on the DFIG's dynamic equations in Park frame of reference. This model provides a theoretical estimate of the rotor currents. After Park transformation the mathematical model of a generator in the *dq* reference frame simplifies the stator

electrical equations under steady-state conditions, where the derivatives of the magnetic fluxes are zero ($\frac{d\varphi_{ds}}{dt} = \frac{d\varphi_{qs}}{dt} = 0$). This leads to a clearer understanding of the relationship between stator and rotor currents, essential for effective control and estimation in various applications. Where the following equation presents the simplified stator equation voltages:

$$\begin{cases} V_{ds} = R_s I_{ds} - \omega_s L_s I_{qs} - \omega_s M I_{qr} \\ V_{qs} = R_s I_{qs} + \omega_s L_s I_{ds} + \omega_s M I_{dr} \end{cases} \quad (V.1)$$

By using the final electrical equation for the stator, the rotor currents I_{dr_est} and I_{qr_est} can be estimated as equation (V.2).

$$\begin{cases} I_{dr\_est} = \frac{1}{\omega_s M}\left(V_{qs} - R_s I_{qs} - \omega_s L_s I_{ds}\right) \\ I_{qr\_est} = \frac{-1}{\omega_s M}\left(V_{ds} - R_s I_{ds} + \omega_s L_s I_{qs}\right) \end{cases} \quad (V.2)$$

- **The Adjustable model**

The second model is an adjustable one, designed to estimate the rotor current components (in both *dq*-axes) by directly measuring the rotor currents using a current sensor and then transforming them from the *abc* to *dq* system using the Park transformation (equation V.3). The continuous feedback loop not only improves the estimation of the rotor position but also ensures the optimal performance of the DFIG system.

$$\begin{bmatrix} I_{dr\_adj} \\ I_{qr\_adj} \end{bmatrix} = \sqrt{\frac{2}{3}} \begin{bmatrix} cos(\theta) & cos(\theta - \frac{2\pi}{3}) & cos(\theta + \frac{2\pi}{3}) \\ -sin(\theta) & -sin\left(\theta - \frac{2\pi}{3}\right) & -sin(\theta + \frac{2\pi}{3}) \\ \frac{1}{\sqrt{2}} & \frac{1}{\sqrt{2}} & \frac{1}{\sqrt{2}} \end{bmatrix} \begin{bmatrix} I_{ar\_meas} \\ I_{br\_meas} \\ I_{cr\_meas} \end{bmatrix} \quad (V.3)$$

The following sections explain the key aspects of this process.

- **Error Calculation**:

The difference between the rotor currents that estimated from the reference model I_{qr_est} and the measured rotor current I_{qr_adj} from adjustable model. This error represents the discrepancy between the actual and estimated rotor current components.

$$\varepsilon_{Iqr} = I_{qr\_est} - I_{qr\_adj} \quad (V.4)$$

- **Adaptation Mechanism**:

Using the error ε_{Iqr} between the reference and the adjustable model, the PI regulator adjusts the parameters of the adjustable model. This mechanism works to reduce the error and make the

electrical estimated rotor speed ω_{r_est} converge toward the measured electrical rotor speed ω_r the following equation:

$$\omega_{r\_est} = \left(K_p + \frac{K_i}{s}\right)\varepsilon_{Iqr} \quad (V.5)$$

- **Rotor Speed Estimation**:

To obtain the mechanical speed of the DFIG rotor, the estimated electrical speed ω_{r_est} is divided by the number of pole pairs, as shown in the following equation:

$$\omega_{mec\_est} = \frac{\omega_{r\_est}}{p} \quad (V.6)$$

Through these steps, the MRAS technique efficiently estimates the rotor speed of the DFIG, offering an effective solution for sensorless operation and enhancing the performance of control systems in wind energy applications. The following figure provides a detailed illustration of the application of the Model Reference Adaptive System (MRAS) to a wind energy system based on the Doubly-Fed Induction Generator (DFIG) [8-14]:

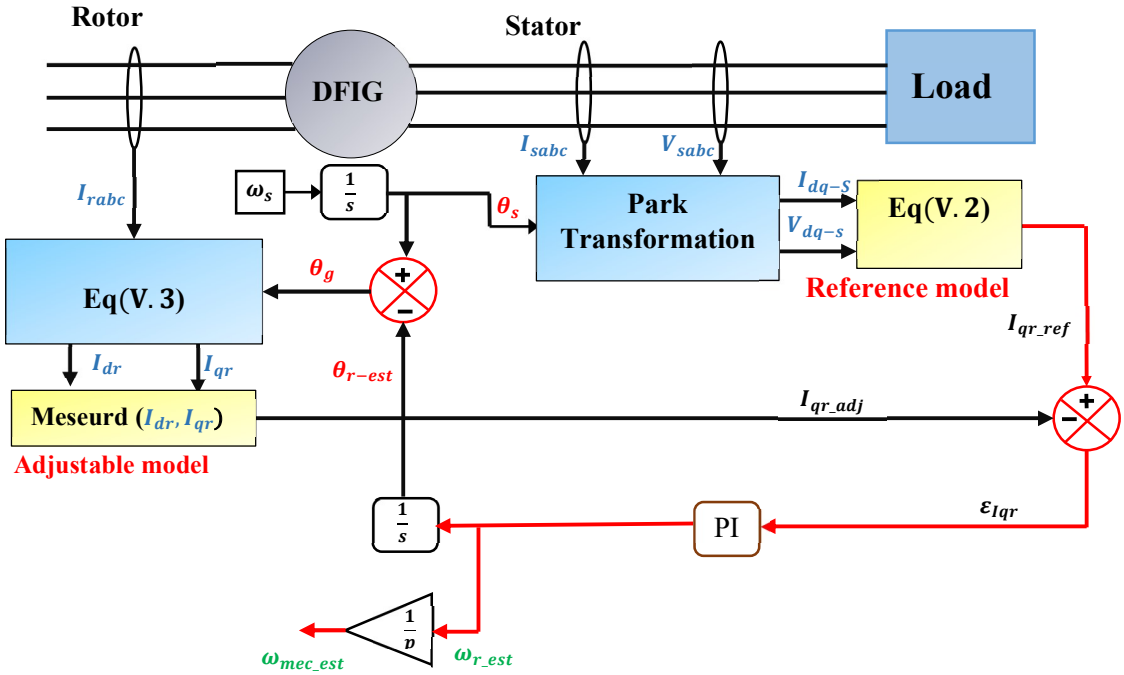

Figure V.2 Estimation the rotor speed of the standalone DFIG using Model Reference Adaptive System (MRAS).

V.3 Design of the MPC based control design for the stand alone DFIG

In this section, the application of Model Predictive Control (MPC) to the standalone Doubly-Fed Induction Generator (DFIG) system is detailed. The focus is on the design and implementation aspects, highlighting the control's effectiveness in addressing nonlinearity, optimizing dynamic response, and enhancing overall system performance.

V.3.1 Definition of MPC

Model Predictive Control (MPC) has emerged as a pivotal technique in modern control systems, particularly for its ability to manage complex dynamics and constraints that traditional methods, such as PID controllers, struggle to address. By utilizing a dynamic mathematical model, MPC forecasts future system behavior and optimizes control inputs over a defined time horizon, adapting in real-time to disturbances and changes. This adaptability is crucial for maintaining optimal performance across various applications, including industrial processes, robotics, and energy systems [15-18].

V.3.2 MPC History

Model Predictive Control (MPC) emerged in the 1960s as an advanced control technique based on optimal control theory. Early conceptualization was marked by Popov's work, which introduced model-based prediction using linear programming methods. In 1978, J. Richalet formalized the first industrial application of predictive control through Model Predictive Heuristic Control, later known as Model Algorithmic Control. By the 1980s, MPC became integral in the chemical process industry, where long time constants allowed sufficient computational time for solving the optimization problems. D.W. Clarke further popularized MPC in the late 1980s, broadening its application across industries. Rapid advancements in microprocessors and Digital Signal Processors (DSPs) eventually enabled MPC's application in fields with faster dynamics, including power electronics, where it has become vital for high-power systems operating at low switching frequencies [19-30].

V.3.3 Advantage

Model Predictive Control (MPC) offers several key advantages that make it a widely applicable and effective method in control systems, where the benefit of this control like follow [31-34]:

- One of the primary advantages of Model Predictive Control (MPC) is its capacity to manage multiple variables concurrently through a single cost function. This unique feature allows MPC to consider the interactions between various system parameters, optimizing control actions to achieve desired outcomes efficiently.
- MPC's design is conceptually intuitive and straightforward, making it easier for practitioners to understand and implement;
- This control approach is highly versatile, suitable for a wide range of systems, including multivariable, linear, and nonlinear systems;
- One of MPC's strengths is its ability to handle constraints on both manipulated and controlled variables, ensuring safe and reliable operation even under strict limitations;
- MPC can readily account for dead times and delays within the system, enhancing stability and accuracy in tracking reference signals;
- MPC is powerful in accommodating modifications and extensions tailored to specific application needs, which provides flexibility in its design and application;
- It allows for automatic adaptation in the presence of measurable disturbances, maintaining optimal performance by recalculating future control actions;
- In practical terms, MPC facilitates finite optimization over a given sampling period, ensuring real-time applicability and ease of integration into various industrial systems. Thus, the inclusion of MPC in control architectures enhances overall system performance, especially in cases where system demands and constraints are known in advance, ensuring both precision and adaptability;
- The main advantages of this control scheme are fast dynamic response and the possibility to use any modulation method such as PWM or space vector modulation (SVM).
- MPC is notably advantageous for its ability to regulate multiple variables while ensuring they remain within specified bounds. This capability allows MPC to handle complex systems where constraints on variables must be respected, enhancing system stability and performance.

V.3.4 Disadvantages

Model Predictive Control (MPC) is a powerful control strategy, yet it faces notable disadvantages [34], [35-39]:

- Particularly in complex systems like power converters;
- The computational demands can be significant, especially with high switching states and extended prediction horizons, leading to increased processing times;
- MPC's performance is heavily reliant on the accuracy of the system model discrepancies can severely impact control effectiveness;
- The selection of weighting factors further complicates the implementation; as optimal values are often not easily determined;
- Lastly, developing an appropriate system model can be resource-intensive, potentially resulting in high installation costs.

V.3.5 Principal of MPC

The Model Predictive Control (MPC) principle is based on predicting the future behavior of a system by utilizing an explicit numerical model of the system. The goal is to forecast the system's output over a finite time horizon, using available measurements up to the current time. The control strategy optimizes the system's actuation by minimizing a cost function, which considers both the current state of the system and the reference trajectory over the prediction horizon. This process is repeated at each sampling instant, where the most recent measurements are used to update the predictions and determine the optimal control action. MPC stands out for its ability to take into account future predefined trajectory information, enabling the system to adjust its behavior to align with a desired reference over the prediction horizon. This characteristic is particularly beneficial in systems where disturbances can be predicted, as the model can incorporate these disturbances into the optimization process. The result is a control system with significant dynamic potential, capable of adapting to both system behavior and external factors, making MPC a powerful tool for achieving precise control over complex systems with time-varying dynamics. Figure V.3 explains the MPC operating principle [31], [40-44].

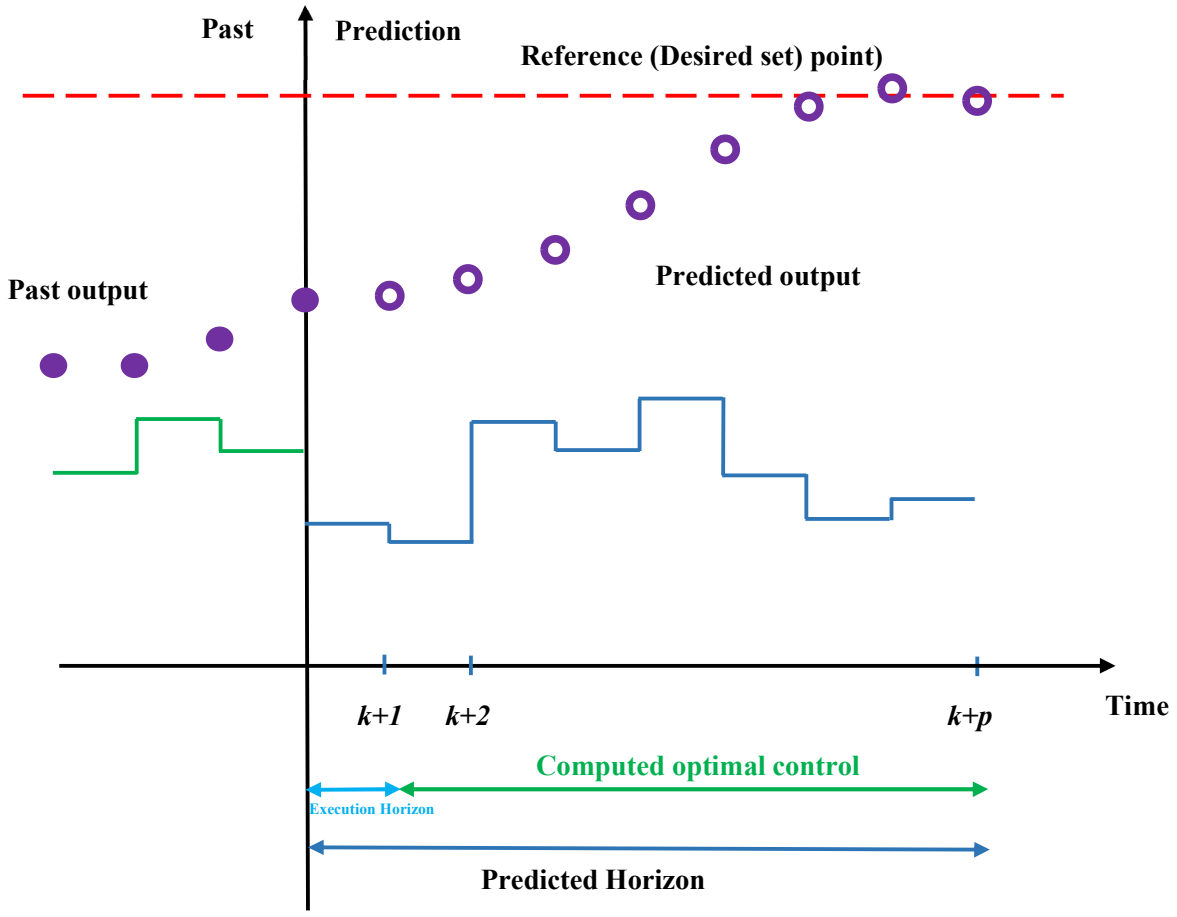

Figure V.3 Principle of Model Predictive Control, prediction horizon and control horizon.

V.3.6 Types of MPC

In the field of power electronics and electrical drives, two main types of Model Predictive Control (MPC) are applied: Generalized Predictive Control (GPC) and Finite-State Model Predictive Control (FS-MPC):

- **Generalized Predictive Control (GPC)** emerged in the mid-1980s as an advanced control technology. It is characterized by its ability to predict the future behavior of the system and optimize control actions accordingly. GPC has been widely used in various engineering applications, offering a powerful framework for handling multivariable systems and constraints.
- **Finite-State Model Predictive Control (FS-MPC)** gained significant attention in 2004, largely due to the pioneering work of the Chilean researcher J. Rodriguez and his team. FS-MPC has proven to be a highly effective alternative for numerically controlling power

supply systems, particularly in those that integrate power converters. This approach is appealing due to its ability to handle discrete states and manage switching actions efficiently, making it especially valuable in industrial and academic contexts. FS-MPC has found numerous applications in controlling power systems, offering improved performance in terms of stability and control accuracy [43], [45-46].

V.3.7 Application of FS-MPC on standalone DFIG system

The Finite Set Model Predictive Control (FSMPC) can be utilized to predict all rotor currents based on the proposed Finite Set Predictive Current Control (FSPCC) algorithm. This algorithm employs a dynamic system model to forecast the system's future behavior, aiming to optimize control inputs over a specified time horizon while accounting for system dynamics. A key feature of FSPCC is its use of a limited set of possible control actions, which are evaluated to predict and improve future system states. This enables the system to respond adaptively to changes and external disturbances, a capability crucial for managing complex systems that require precision and adaptability in their control strategies. In the specific application studied here, FS-PCC is applied to predict rotor currents one step ahead $I_{r\_(k+1)}$ using the Euler model. This approach allows for accurate and timely adjustments to control inputs based on the anticipated future behavior of the system. The predictive capability of FS-PCC is formulated through the following equation: $x(k)=x(kT_s)=x(t)$ with $\frac{dx(t)}{dt} = \frac{x_{(k+1)}-x_{(k)}}{T_s}$ for all $t \in [kT_s, (k+1)T_s]$ and $k \in IN \cup \{0\}$[47-48].

- **The currents predection**

The applied FSPCC on DFIG withe disecret time can be presented like follows:

$$\frac{dI_r}{dt} = \frac{I_{r\_(k+1)}-I_{r\_(k)}}{T_s} \quad (V.7)$$

So the the rotor predected currents in the $\alpha\beta$ reference demonstrated as follows:

$$I_{r(\alpha+\beta j)\_(k+1)} = \big(A\,(B + C) + A\,(D + E)\big)\,T_s + I_{r(\alpha+\beta j)_k} \quad (V.8)$$

Where;

$A = \frac{1}{L_s L_r \sigma}$; $B = (R_s M + j\omega_r M L_s) I_{s(\alpha+\beta j)\_(k)}$; $\sigma = 1\text{-}\frac{M^2}{L_s L_r}$;

$C = (-R_r L_s + j\omega_r L_r L_s - j\omega_s \sigma L_s L_r) I_{r(\alpha+\beta j)_k}$; $D = -M V_{s(\alpha+\beta j)_k}$;

$E = L_s V_{r(\alpha+\beta j)\_(k)}$;

$V_{r(\alpha+\beta j)\_(k)} = V_{bus}\, sw$; $sw = \frac{2}{3}\,(s(1) + a\,s(2) + a^2\,s(3))$; $a = \exp(\frac{j2\pi}{3})$;

$T_s = e^{-4} second(s)$.

- **Minimization of the Cost Function:**

In the application of the Finite-State Predictive Current Control (FS-PCC) strategy to a Doubly-Fed Induction Generator (DFIG), the cost function is fundamental in optimizing system performance by minimizing the current tracking error. Specifically, this approach reduces the difference between the reference current $I_{r(\alpha+\beta j)_{ref\_(k+1)}}$ and the predicted current $I_{r(\alpha+\beta j)\_(k+1)}$.The cost function serves as a selection criterion for the optimal rotor voltage vector, with the rotor voltage that minimizes the cost value being applied. Equation V. 8 illustrates this cost function as it is implemented [47], [49-50].

$$g = \left(I_{r\alpha\_ref_{(k+1)}} - I_{r\alpha\_(k+1)}\right)^2 + \left(I_{r\beta\_ref_{(k+1)}} - I_{r\beta\_(k+1)}\right)^2 \quad (V.9)$$

The selection of inverter voltage vectors in the FSPCC (Finite Set Predictive Current Control) framework is directed by a cost function, which enhances control performance by evaluating each possible switching state (8 vectors 2 from them are zero). The cost function predicts the future behavior of controlled variables in this case, the rotor current and minimizes its deviation from desired reference values over a specified prediction horizon. By assessing the impact of each switching state on the expected system response, the cost function identifies the optimal voltage vector that minimizes error while accounting for constraints such as switching frequency and system limits. This approach ensures accurate tracking, reduced losses, and improved dynamic performance of the electrical system. The Table 1 below shows the number and characteristics of the voltage vectors based on the switching states:

Table 1: The different voltage vectors and switching states of voltage source converter

Conducting Modes	Switching States			Output Voltage		Vectors Number
	S=[S_a	S_b	S_c]	U_α	U_β	
U_0	[0	0	0]	[0	0]	0
U_1	[1	0	0]	$[\frac{2vdc}{3}$	0]	1
U_2	[1	1	0]	$[\frac{vdc}{3}$	$\frac{\sqrt{3}vdc}{3}]$	2
U_3	[0	1	0]	$[-\frac{vdc}{3}$	$\frac{\sqrt{3}vdc}{3}$]	3
U_4	[0	1	1]	$[\frac{2vdc}{3}$	0]	4
U_5	[0	0	1]	$[-\frac{vdc}{3}$	$-\frac{\sqrt{3}vdc}{3}]$	5
U_6	[1	0	1]	$[\frac{vdc}{3}$	$\frac{\sqrt{3}vdc}{3}]$	6
U_7	[1	1	1]	[0	0]	7

V.4 Configuration of the Control-Observation design using FS-PCC and MRAS for Standalone DFIG

By eliminating the speed sensor and substituting the estimated speed from the MRAS observer in place of the rotor speed previously captured by the sensor and used in FSPCC control, the following form for the rotor currents at the next step $I_{r\_(k+1)}$ is obtained:

$$I_{r(\alpha+\beta j)\_(k+1)} = \left(A\,(B' + C') + A\,(D + E)\right) T_s + I_{r(\alpha+\beta j)_k} \quad (V.10)$$

Where:

$B' = (R_s M + j\omega_{r\_est} M L_s) I_{s(\alpha+\beta j)\_(k)}$; $C' = (-R_r L_s + j\omega_{r\_est} L_r L_s - j\omega_s \sigma L_s L_r) I_{r(\alpha+\beta j)\_(k)}$

Figure V.4 below provides a comprehensive explanation and description of the FSPCC-based MRAS control-observation approach applied to a standalone wind energy system based on a DFIG.

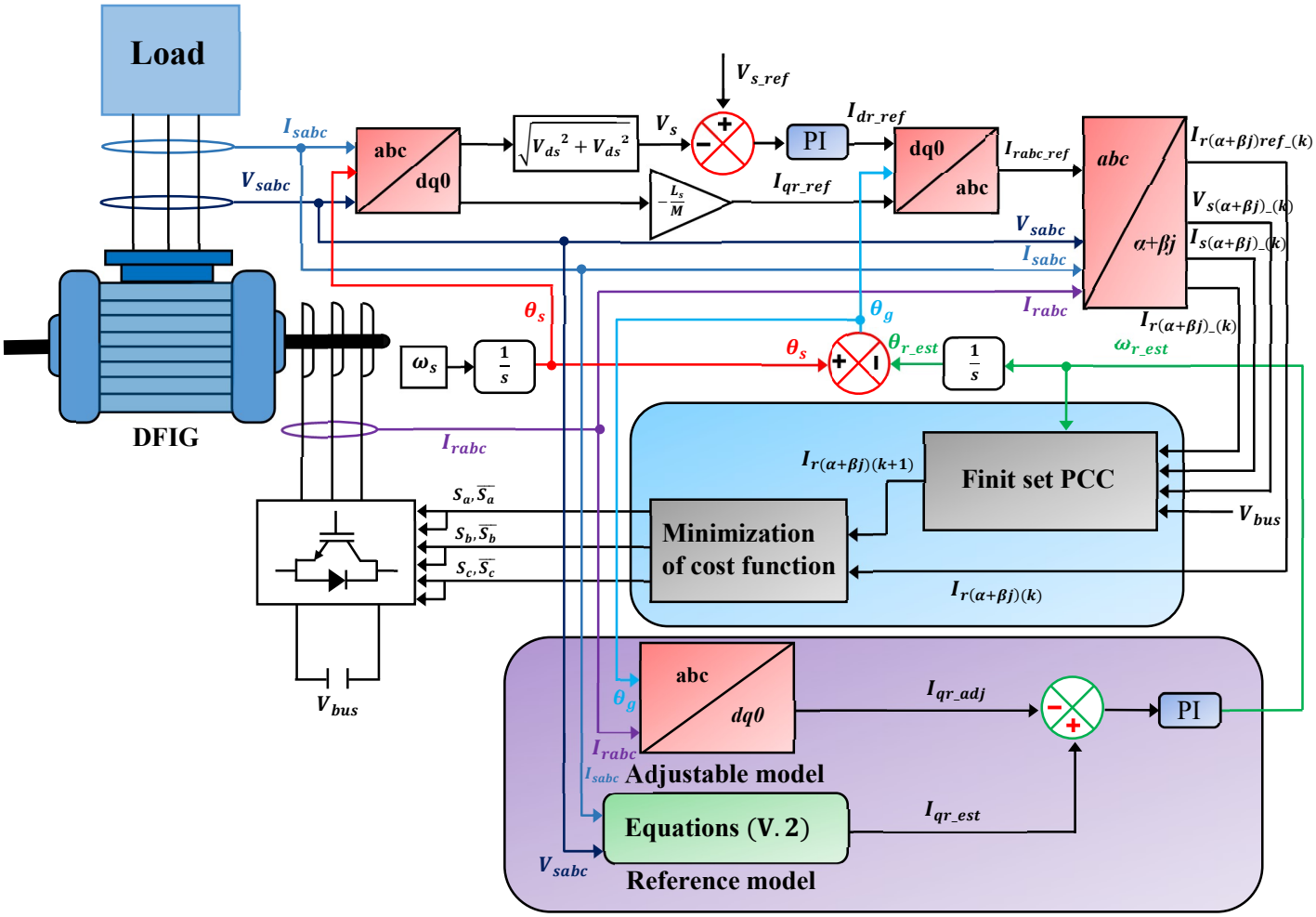

Figure V.4 Block diagram of Control- observation based on Sensor-less Finite set predictive current control applied on Standalone DFIG.

V.5 Simulation and Experimental Results with discussion

To validate and thoroughly assess the effectiveness of the proposed control-observation framework, which integrates Finite Set Predictive Control (FSPCC) with the Model Reference Adaptive System (MRAS) for speed estimation, a comprehensive study encompassing both experimental and simulation phases was undertaken. The experimental investigation was conducted in the Electrical Engineering Laboratory at the University of Biskra (LGEB), utilizing a 3 kW DC motor to emulate the turbine's mechanical input, coupled with a 3 kW Doubly-Fed Induction Generator (DFIG) connected to a 4 kW three-phase resistive load. The DFIG was operated in standalone mode, managed by a two-level IGBT inverter and controlled via a DS1004 board, as depicted in Figure V.5, which details the system's layout and interconnections.

For accurate control and continuous monitoring, a network of current and voltage sensors was deployed, allowing precise performance assessment and system stability tracking. The MRAS provided sensorless speed estimation, enhancing the design's practical feasibility. Alongside the experimental setup, a MATLAB-based simulation with identical parameters was developed, facilitating a comparative analysis between experimental and simulated outcomes for robust evaluation.

To assess the control strategy's robustness, stability, and overall effectiveness, multiple scenarios were created and applied in both the experimental and simulation contexts. These scenarios addressed varying operational conditions, such as sudden load variations, speed fluctuations, and the impact of external disturbances, providing a comprehensive view of the DFIG's dynamic response, speed tracking capabilities, and the predictive control scheme's adaptability.

This dual approach, incorporating both experimental validation and simulation, reinforces the theoretical foundation of the control-observation framework. The findings, presented in the subsequent sections, demonstrate the system's ability to achieve stable and efficient operation under demanding conditions, positioning the proposed control strategy as a suitable solution for advanced standalone renewable energy applications, particularly in the field of wind energy conversion.

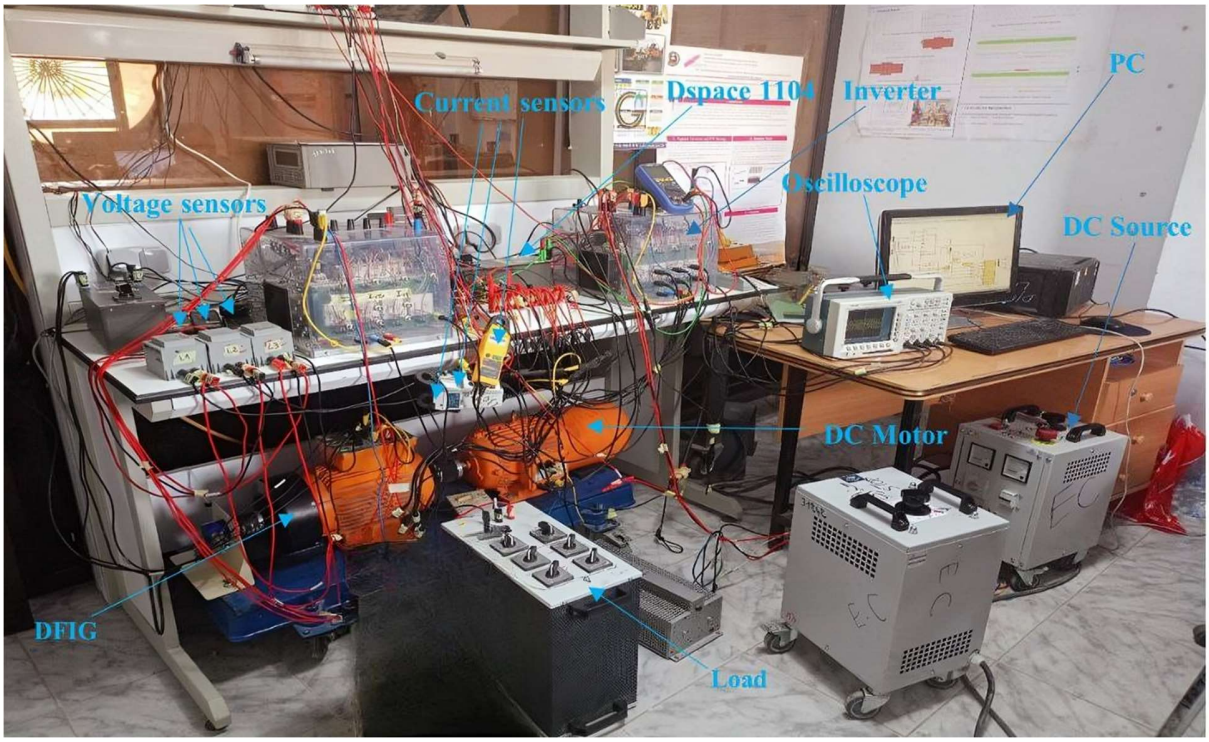

Figure V.5 Experimental setup.

In the first scenario, the turbine simulator a DC motor was operated at a fixed rotational speed to drive the DFIG under a constant load of 2 kW, with a reference voltage V_{s_ref}= 150 V was applied. This scenario was analyzed using both experimental and MATLAB simulation setups, conducted in the Electrical Engineering Laboratory at the University of Biskra (LGEB). Figures V. 6(a) through V.6(e) illustrate the MATLAB simulation results, while Figures V.6 (a') through V.6(e') display the corresponding experimental outcomes, highlighting the consistency between both setups.

Figure V.6(a) and V.6(a') compare the tracking performance of the mechanical speed ω_{mec} and the estimated speed ω_{mec_est}, obtained using the MRAS technique. The control-observation design achieved a close alignment between actual and estimated speeds, with both converging at 1200 RPM. The MRAS contributed to high-precision estimation by minimizing errors and reducing chattering effects, as observed in both simulation and experimental environment, which resulted in faster convergence and improved control smoothness.

Figures 6(b) and 6(b') examine the voltage regulation by comparing the reference voltage V_{s_ref} with the measured stator voltage V_s , showing consistent values at 150 V across both simulation

and experimental setups. This close match demonstrates the robustness of the control-observation design in maintaining a stable voltage with minimal deviations. The phase voltage V_{sa} and current I_{ra} show sinusoidal waveforms at 150 V and 9 A, respectively, in both environments, indicating low harmonic distortion and high power quality.

Figures 6(c) and 6(c') present the output current I_{sa}, , which maintains a stable sinusoidal form at 2 A in both cases (simulation and experimental) with minimizing tolerance bands and distortion, ensuring consistent current tracking.

Figures 6(d) and 6(d') display the reactive power Q_s, which hovers near zero with minimal ripple of ±5 Var in both simulation and experimental cases. This low reactive power ripple highlights the control strategy's effectiveness in stabilizing power flows and limiting reactive power exchanges, thus enhancing system performance and power factor quality.

Finally, Figures 6(e) and 6(e') compare the reference current I_{ra_ref} with the actual current I_{ra} , both showing excellent tracking at 9 A with negligible steady-state error in both setups. Active power P_s is stabilized at 500 W, and electromagnetic torque T_{em} remains at -5 Nm, with low torque ripple across both setups. These outcomes affirm the control scheme's capacity to maintain smooth mechanical performance and minimize stress on generator components, underscoring the close alignment of results achieved between simulation and experimental conditions.

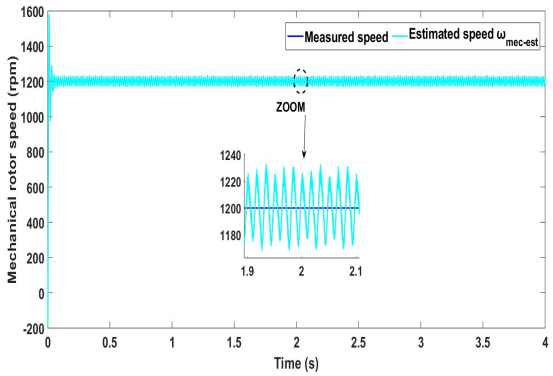

(a)

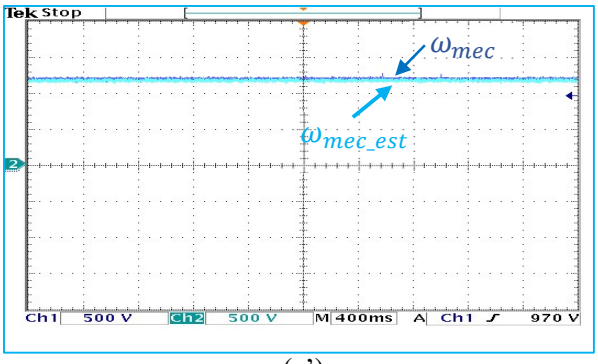

(a')

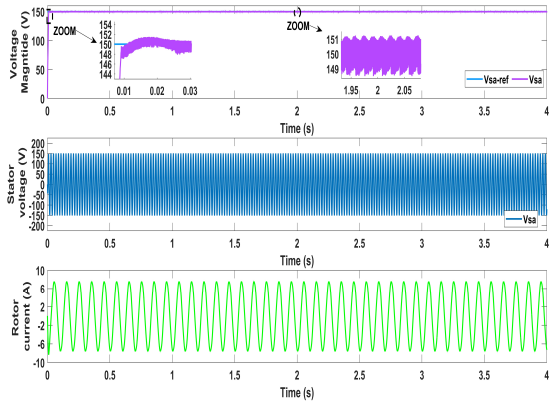
Voltage Magnitde (V)
ZOOM
ZOOM
Vsa-ref
Vsa
Time (s)
Stator voltage (V)
Vsa
Time (s)
Rotor current (A)
Time (s)

(b)

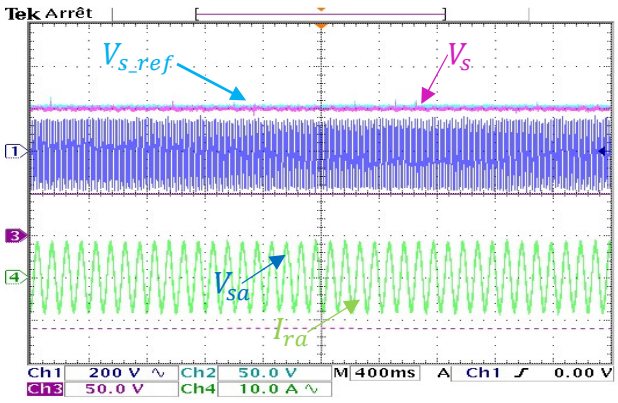
Tek Arrêt
V_{s_ref}
V_s
V_{sa}
I_{ra}
Ch1 200 V
Ch2 50.0 V
M 400ms
A Ch1 0.00 V
Ch3 50.0 V
Ch4 10.0 A

(b')

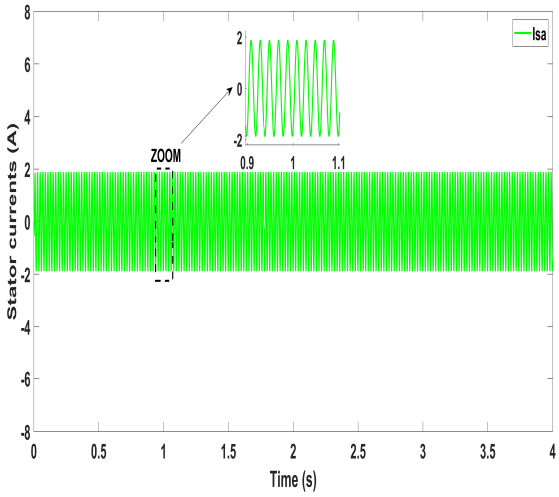
Isa
ZOOM
Stator currents (A)
Time (s)

(c)

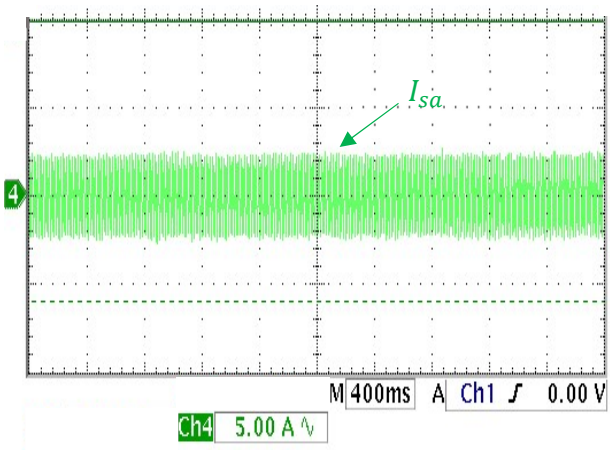
I_{sa}
M 400ms
A Ch1 0.00 V
Ch4 5.00 A

(c')

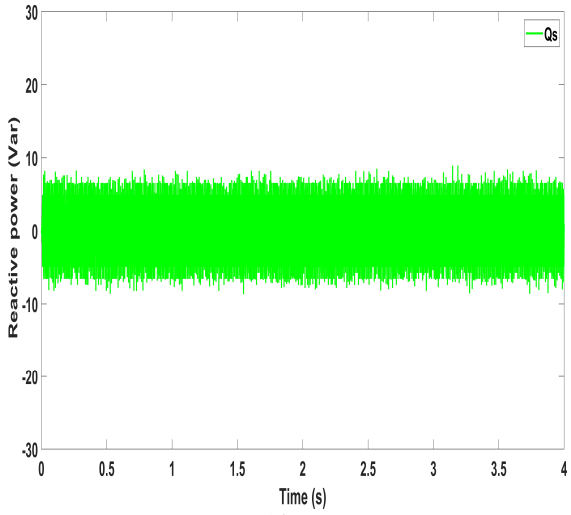
Qs
Reactive power (Var)
Time (s)

(d)

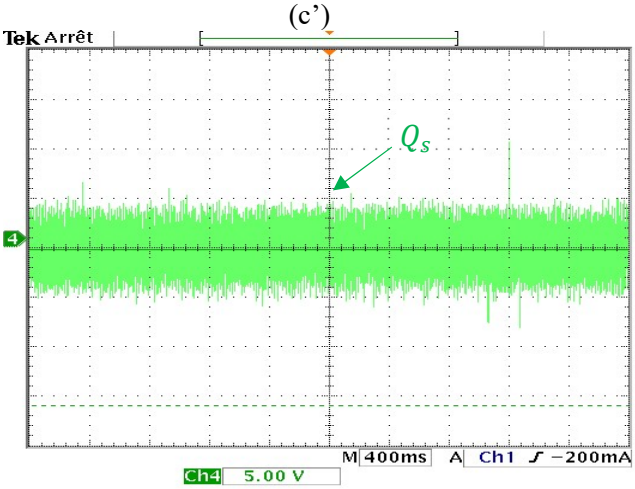
Tek Arrêt
Q_s
M 400ms
A Ch1 −200mA
Ch4 5.00 V

(d')

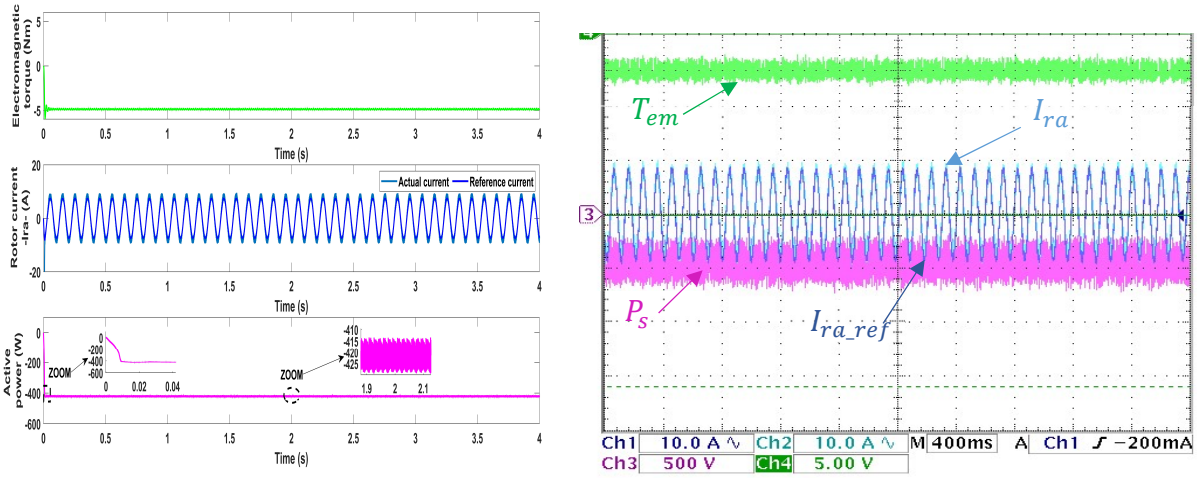

(e) (e')

Figure V.6 Performance of sensorless finite set predictive current control (FSPCC) applied to the system.

In the second scenario, we assessed the performance of the proposed control-observation approach on the system under abrupt changes in the reference voltage V_{s_ref}, while keeping the rotational speed constant at 1200 RPM and the load fixed at 2 kW. This evaluation was carried out through both MATLAB simulation and experimental. Figures 7(a) through 7(d) represent the MATLAB simulation results, while Figures 7(a') through 7(d') depict the experimental outcomes, showing a high degree of agreement between the two setups.

Figure V.7(a) and V.7(a') present the estimated rotational speed ω_{mec_est} of the DFIG, obtained through the MRAS technique. Both simulation and experimental data confirm that the control-observation approach achieved stable and accurate speed estimation, maintaining a steady 1200 RPM despite the abrupt change in voltage. The absence of speed chattering and overshoot (with minimal overshoot in simulation setup) during the voltage shift highlights the system's stability, with rapid rise times and minimal steady-state errors in both simulation and experimental setups.

Figures 7(b) and 7(b') examine the system's voltage response. Following an abrupt increase in the reference voltage from 150 V to 200 V at 2 seconds, the system responded immediately, achieving precise tracking with no overshoot in both simulated and experimental setups. This prompt response illustrates the control-observation strategy's superior voltage tracking capabilities. Additionally, the phase voltage V_{sa} increased smoothly from 150 V to 200 V, while the current I_{ra} rose proportionally from 9 A to 11 A, with sinusoidal waveforms consistent across both environments. These observations confirm the system's capacity to maintain a narrow current

tolerance band and reduce distortion, supporting improved efficiency and minimized generator stress during dynamic transitions.

Figures 7(c) and 7(c') display the output current I_{sa}, which increased from 2 A to 3 A following the voltage adjustment. The good sinusoidal shape of the current in both simulation and experimental setups demonstrates the control-observation design's robustness in managing sudden changes with a minimal tolerance band (TB), maintaining consistent current control.

Figures 7(d) and 7(d') highlight the response of the electromagnetic torque $T_{em}$and active power $P_s$to the voltage change. The torque increased smoothly from -5 Nm to -10 Nm, while the active power rose from 500 W to 800 W, both exhibiting minimal ripple in simulation and experimental tests. The precise match between the actual current I_{ra} and the reference current I_{ra_ref} during this transition, along with the stable adjustment of voltage, underscores the system's efficient torque and current regulation. The low ripple and smooth transition across both simulation and experimental results confirm the proposed control-observation strategy's capacity to handle sudden voltage changes while maintaining stable operation.

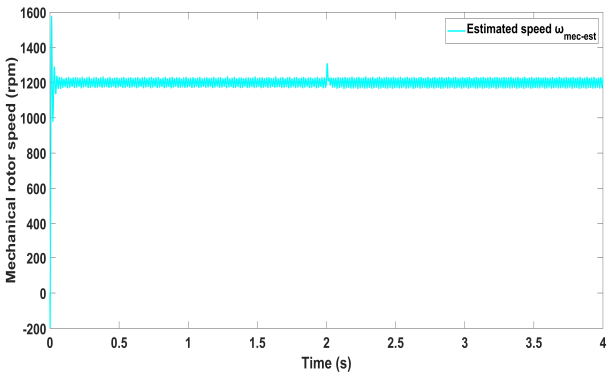

(a)

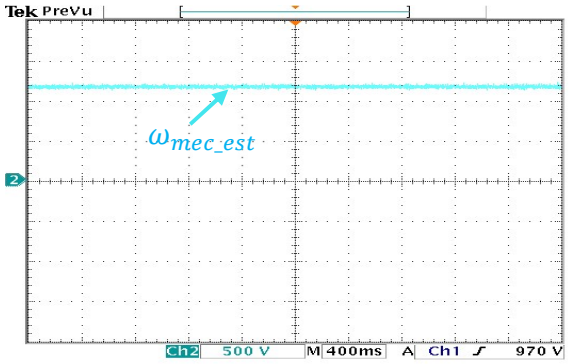

(a')

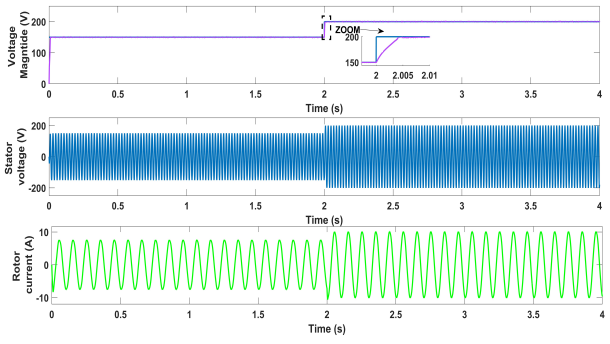

(b)

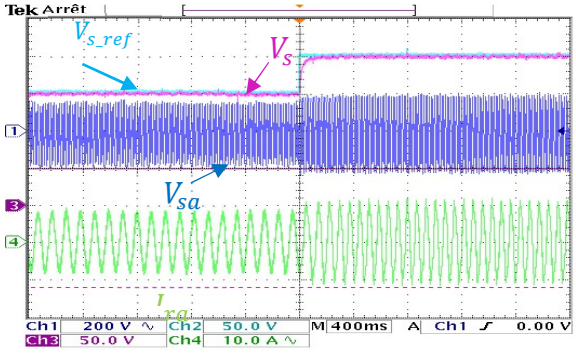

(b')

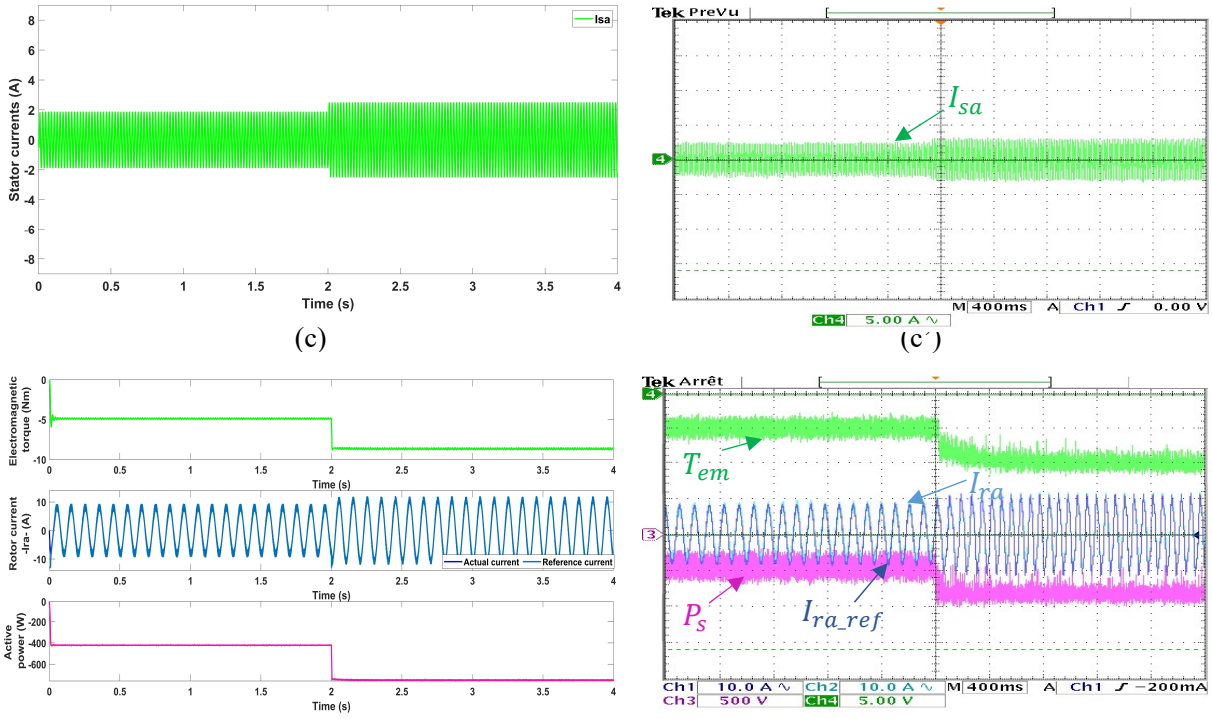

Figure V.7 Performance of sensorless finite set predictive current control (FSPCC) applied to the system during variations in the stator voltage reference value V_{s_ref}.

In the third scenario, the effectiveness of the proposed control-observation system was tested under conditions of sudden load changes, while maintaining a constant DFIG operating speed and a reference voltage V_{s_ref} of 150 V. Both MATLAB simulation and experimental tests. Where Figures 8(a) through 8(d) for simulation results, and Figures 8(a') through 8(d') for experimental results. The results displayed close alignment between the two setups, confirming the robustness and consistency of the control-observation system in handling load variations.

Figures 8(a) and 8(a') show the voltage response V_s in both simulation and experimental tests, where the system maintained precise tracking of the reference voltage V_{s_ref} at 150 V. When a sudden load increase from 2 kW to 3 kW at 2 seconds, a temporary voltage undershoot of approximately 20 V was observed. This minor undershoot, seen in both simulation and experimental data, reflects the system's flexibility to rapid load changes. However, the control-observation system quickly corrected the voltage back to the reference, demonstrating superior transient response and voltage regulation in both tests. The phase current I_{ra} also adjusted smoothly from 9 A to 12 A in response to the load change, maintaining a sinusoidal waveform that illustrates the system's resilience and adaptability under increased load demand.

Figures 8(b) and 8(b') depict the response of phase current I_{sa}, which increased from 2 A to 4 A in direct response to the load variation. Both simulation and experimental results confirm the system's ability to achieve a smooth, linear current adjustment without significant overshoot or current tolerance band (TB). This consistency highlights the control-observation strategy's advanced current regulation, ensuring high power quality and operational stability during dynamic load conditions.

Figures 8(c) and 8(c') analyze the reactive power Q_s, which remained steady at zero despite the additional load. Both the simulation and experimental results show a slight reactive power ripple of approximately from ±5 to ±7 VAR, attributed to the load shift. This minor fluctuation, mirrored in both settings, emphasizes the control-observation system's proficiency in minimizing reactive power disturbances, preserving stable voltage profiles, and enhancing overall DFIG system power quality even when sudden load changes occur.

Figures 9(d) and 9(d') focus on the impact of load change on electromagnetic torque T_{em}, which increased from -5 Nm to -11 Nm, resulting in an active power P_s increase from 500 W to 650 W. The system accurately tracked the reference current I_{ra_ref}, , with phase current I_{ra}, adjusting from 9 A to 12 A in perfect alignment. This precise current and torque tracking, seen in both simulation and experimental scenarios, underlines the control-observation system's capability to seamlessly manage current and torque adjustments under varying load conditions, contributing to stable torque and efficient active power regulation essential for optimal DFIG performance in dynamic environments.

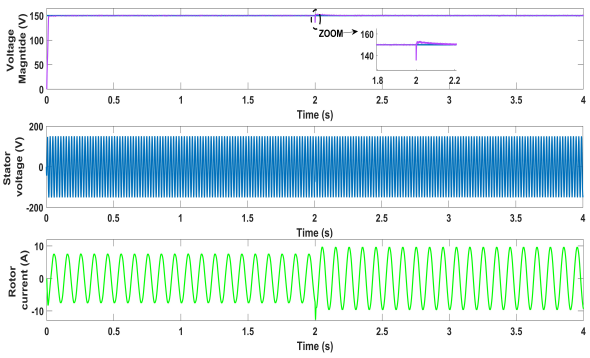

(a)

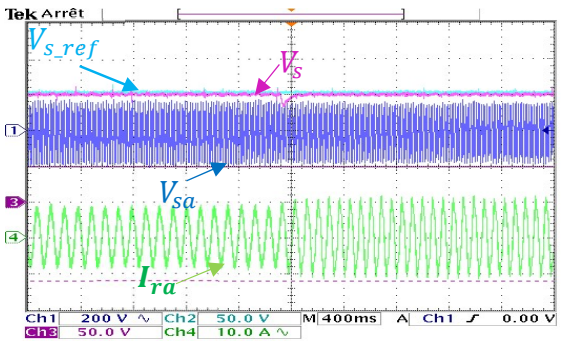

(a')

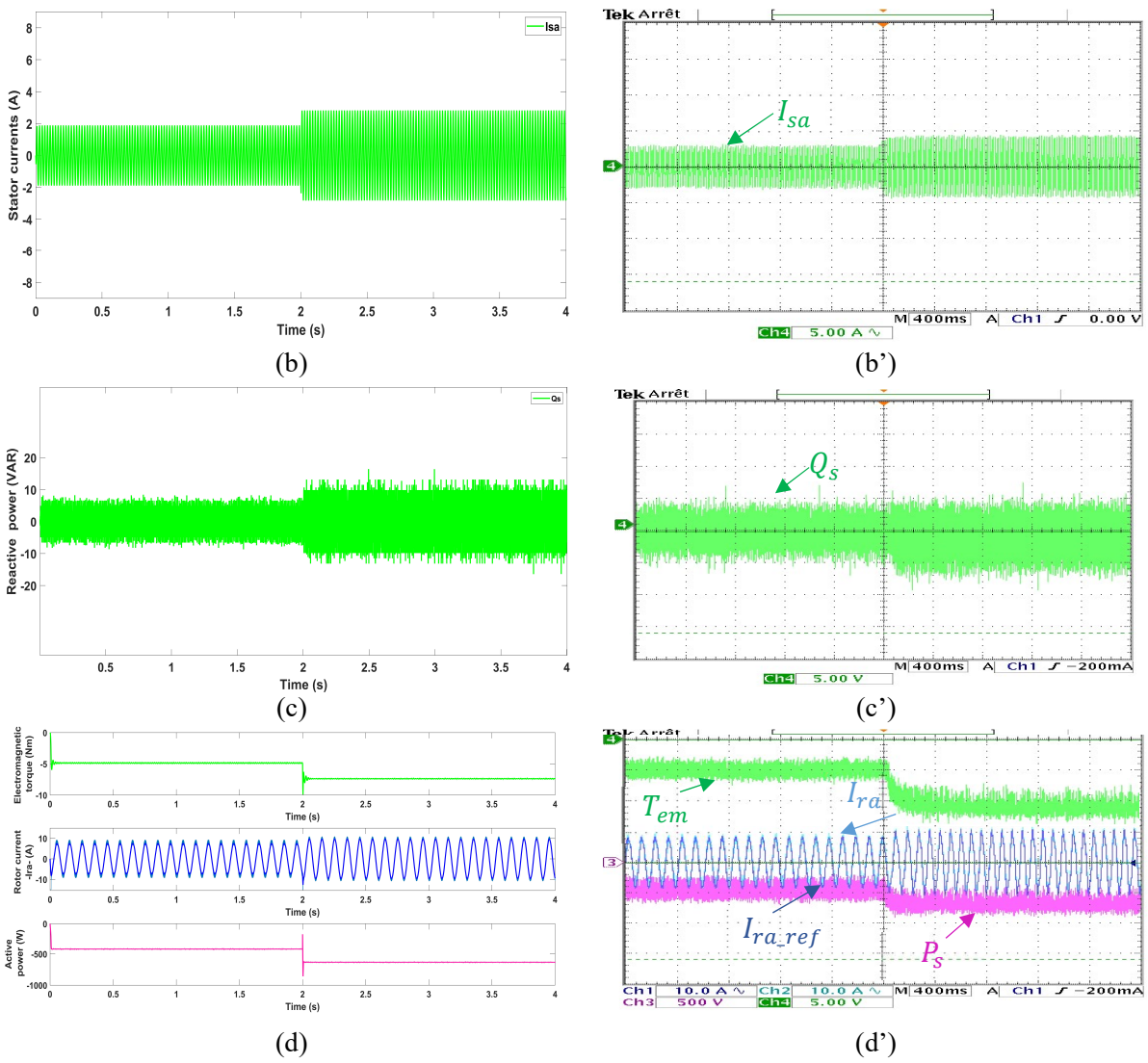

Figure V.8 Performance of sensorless finite set predictive current control (FSPCC) applied to the system under load variations.

In the final scenario, the behavior of the system was assessed under conditions of a sudden increase in the operating speed of the DFIG generator, aiming to evaluate the system's robustness and dynamic response to such changes. The turbine simulator initially operated at a constant speed, which was abruptly increased at 2 seconds, while the load remained fixed at 2 kW and the reference voltage V_{s_ref} was maintained at 150 V. Both simulation results in MATLAB and experimental data were analyzed, as depicted in Figures 9(a) through 9(e) for the simulation results and Figures 9(a') through 9(e') for the experimental results. The comparison between these two sets of results demonstrates close alignment, verifying the reliability and consistency of the proposed control-observation system.

Figure V.9(a) and Figure V.9(a') illustrate the estimated mechanical speed ω_{mec_est} of the DFIG obtained using Model Reference Adaptive System (MRAS) estimation. Both the simulation and experimental results show a sharp increase in operating speed from 1000 to 1200 RPM at 2 seconds, aligning with the intended speed change. The system tracked this abrupt speed shift with high accuracy in both the simulated and experimental environments, demonstrating the control-observation system's fast response time and precise speed estimation capabilities.

Figures 9(b) and 9(b') show that the stator voltage V_s in both the simulation and experimental setups remained stable and accurately tracked the reference voltage V_{s_ref} at 150 V despite the sudden speed change. This indicates the system's robustness in voltage regulation, decoupling voltage fluctuations from the speed variations. The phase voltage V_{sa} in both cases maintained a smooth sinusoidal waveform throughout, demonstrating the system's capability to preserve high-quality voltage signals even as the generator's speed changed. Additionally, the frequency of the rotor current I_{ra} increased proportionally with the speed, a natural consequence of the higher rotational frequency, as observed in both simulation and experimental results.

Figures 9(c) and 9(c') highlight the phase current I_{sa}, which remained constant at 2 A throughout the test in both the simulation and experimental results, unaffected by the change in generator speed. This constancy further emphasizes the effectiveness of the control system in maintaining steady current despite changes in operating conditions.

In Figures 9(d) and 9(d'), the reactive power Q_s remains close to zero with minimal ripple of ±5 VAR, both in simulation and experimental setups. This stability in reactive power during the sudden speed change reflects the efficiency of the control system in managing reactive power flows, minimizing disturbances, and maintaining stability.

Finally, Figures 9(e) and 9(e') present the electromagnetic torque T_{em} and active power P_s, which experienced only slight fluctuations following the speed increase but remained overall stable at -5 Nm and -500 W, respectively. The consistency of these values across both simulations and experiments demonstrates the control system's ability to manage torque and power dynamics efficiently, ensuring smooth transitions during speed changes. The alignment of the rotor current I_{ra} with the reference current I_{ra_ref} at 9 A further confirms the precise current tracking capabilities of the system.

The overall comparison between the simulation and experimental results in this scenario demonstrates that the proposed control-observation design is highly effective and reliable. The

system exhibited fast response times, precise voltage regulation, stable power and current control, and minimal reactive power ripple during sudden changes in speed. These findings highlight the robustness, adaptability, and precision of the control strategy, confirming its potential for applications in dynamic environments like wind energy conversion systems, where rapid changes in speed and load are common.

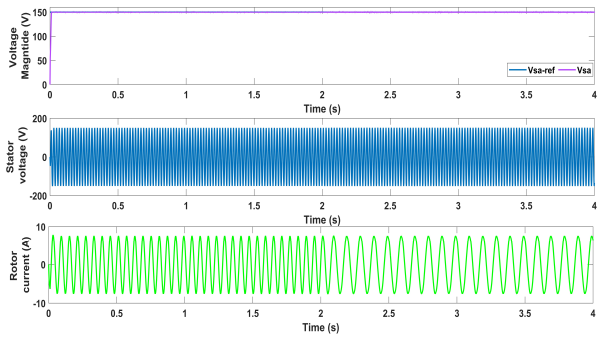

(a)

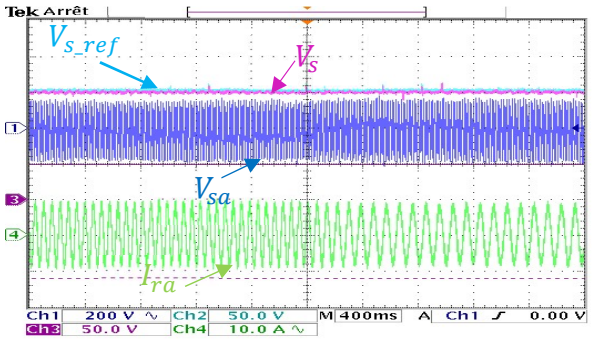

(a')

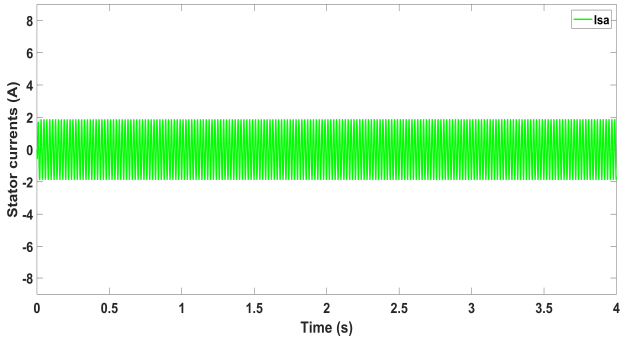

(b)

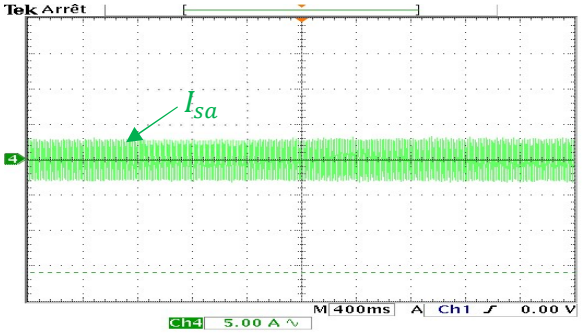

(b')

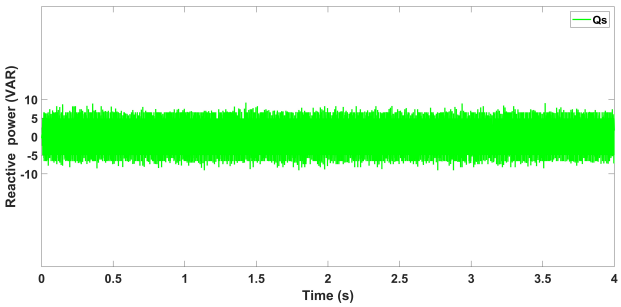

(c)

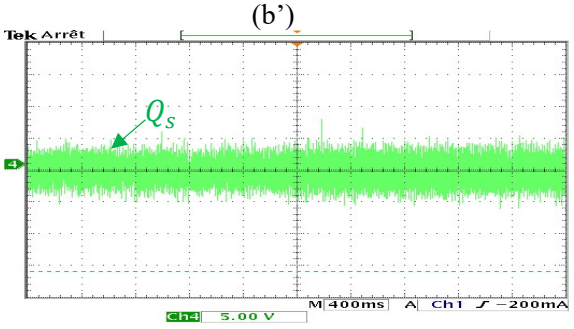

(c')

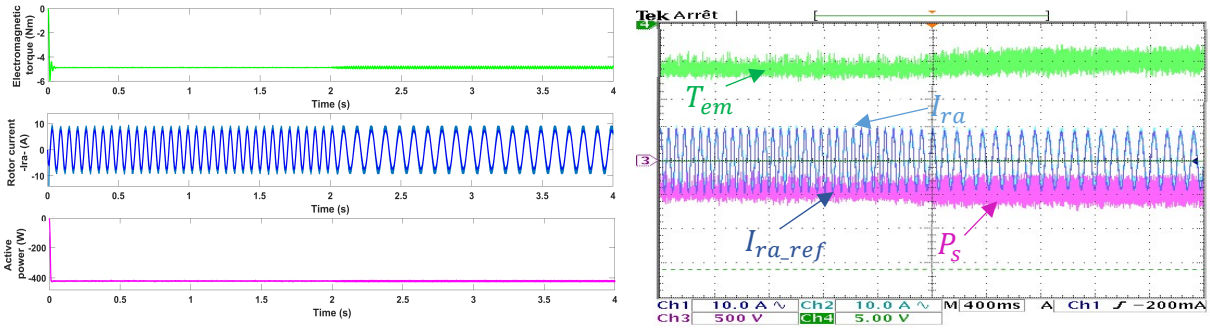

(d) (d')

Figure V.9 Performance of sensor-less finite set predictive current control applied to the system during speed variations.

V.5 Conclusion

This chapter has successfully demonstrated the design and implementation of an advanced control-observation system for standalone DFIGs, combining MRAS-based sensorless speed estimation with FS-MPC for precise and efficient operation. The proposed system addresses the unique challenges of standalone setups, such as the absence of grid support and the need for enhanced stability under dynamic conditions. By leveraging MRAS for accurate speed estimation and FS-PCC for robust current control, the system achieves a high level of precision, adaptability, and reliability.

The validation of the proposed design through both simulation and experimental testing highlights its robustness across various scenarios, including abrupt changes in speed, load, and voltage. The strong correlation between simulated and experimental results affirms the practical applicability of the control-observation framework, with minimal deviations and excellent dynamic response characteristics. This work sets a benchmark for the effective control of standalone DFIG systems, demonstrating its potential for applications in renewable energy systems, particularly standalone wind energy systems. The insights gained from this chapter lay the groundwork for future research aimed at further enhancing the efficiency and reliability of such systems.

REFERENCES BIBLIOGRAPHIQUES

[1] Gang, Tao. (2024). Adaptive Output Tracking Control with Reference Model System Uncertainties. doi: 10.48550/arxiv.2406.05580

[2] Yingli, Sang., Zhengqiang, Zhang. (2024). 2. Model Reference Adaptive Control for Multi-Variable Systems Using Available Signal for Feedback. doi: 10.1109/fasta61401.2024.10595173

[3] Xinkai, Zhao., Yahui, Nie., Hong, Bin. (2023). 3. Model Reference Adaptive System for Permanent Magnet Synchronous Motors. doi: 10.1109/ic2ecs60824.2023.10493807

[4] Hui-Yan, Chen., Renjie, Zhang., Shaopeng, Zhu., Jian, Gao., Rougang, Zhou. (2023). 4. Model Reference Adaptive Observer for Permanent Magnet Synchronous Motors Based on Improved Linear Dead-Time Compensation. Electronics, doi: 10.3390/electronics12244907

[5] Fang, Yan., Xiaorong, Hou., T., Tian. (2023). 5. Model reference adaptive control based on a novel scalar update law. International Journal of Robust and Nonlinear Control, doi: 10.1002/rnc.6689

[6] Xinkai, Zhao., Yahui, Nie., Hong, Bin. (2023). 2. Model Reference Adaptive System for Permanent Magnet Synchronous Motors. doi: 10.1109/ic2ecs60824.2023.10493807

[7] Hui-Yan, Chen., Renjie, Zhang., Shaopeng, Zhu., Jian, Gao., Rougang, Zhou. (2023). 3. Model Reference Adaptive Observer for Permanent Magnet Synchronous Motors Based on Improved Linear Dead-Time Compensation. Electronics, doi: 10.3390/electronics12244907

[8] Sanjeev, Kumar, Gagrai., Madhu, Singh. (2022). 5. Mathematical modelling and steady state analysis of doubly fed induction generator. doi: 10.26480/icpesd.01.2022.83.90

[9] Manuel, G., Satué., Manuel, R., Arahal., Manuel, G., Ortega., Daniel, R., Ramirez. (2022). 1. A simple rotor current estimation method for predictive control of multi-phase drives. International Journal of Circuit Theory and Applications, doi: 10.1002/cta.3394

[10] Yu-Ling, He., Mingzhe, Qiu., Meng, Jiang., Fuju, Zhou., David, Gerada., Xiao-Chen, Zhang., Xiaoyong, Du. (2022). 2. Stator current identification in generator among single and composite faults composed by static air-gap eccentricity and rotor inter-turn short circuit. Iet Electric Power Applications, doi: 10.1049/elp2.12260

[11] Cardenas, R., Pena, R., Proboste, J., Asher, G., & Clare, J. (2005). MRAS observer for sensorless control of standalone doubly fed induction generators. *IEEE Transactions on Energy conversion*, *20*(4), 710-718.

[12] Tao, Jiang., Yongchang, Zhang., Shengan, Zhang., Shengnan, Li. (2024). 1. Model-free predictive rotor current control of DFIGs based on an adaptive ultra-local model under nonideal power grids. Iet Renewable Power Generation, doi: 10.1049/rpg2.13053

[13] Mwana, Wa, Kalaga, Mbukani., M., N., Gitau., Raj, Naidoo. (2023). 3. An SMC-MRAS Speed Estimator for Sensor-Less Control of DFIG Systems in Wind Turbine Applications. Energies, doi: 10.3390/en16062633

[14] Abdelhak, Djoudi., NULL, AUTHOR_ID., Ahmed, Rennane. (2024). 2. New Algorithm to Support Adaptive Control of DFIG Currents and Fault Diagnosis of Speed Sensor. doi: 10.1109/iceeac61226.2024.10576265

[15] Bin, Ma., Xing, Guo., Penghui, Li. (2023). Adaptive energy management strategy based on a model predictive control with real-time tuning weight for hybrid energy storage system. Energy, doi: 10.1016/j.energy.2023.129128

[16] (2023). Reduced order model predictive control for parametrized parabolic partial differential equations. Applied Mathematics and Computation, 453:128044-128044. doi: 10.1016/j.amc.2023.128044

Michael, La, Corte. (2022). Introduction to Model Predictive Control. 53-67. doi: 10.1007/978-981-19-5852-6_4

[17] Peter, D., Aplan. (2022). Model Predictive Control. 207-231. doi: 10.1007/978-3-031-29754-0_8

[18] Maciej, Lawrynczuk. (2022). Special Issue "Model Predictive Control: Algorithms and Applications": Foreword by the Guest Editor. Algorithms, 15(12):452-452. doi: 10.3390/a15120452

[19] E. F. Camacho and C. Bordons, Model Predictive Control Springer Verlag, 1999.

[20] Garcia, C. E., Prett, D. M., & Morari, M. (1989). Model predictive control: theory and practice—a survey. Automatica, 25(3), 335-348

[21] J. M. Maciejowski, Predictive Control with Constraints. Englewood Cliffs, NJ: Prentice Hall, 2002

[22] Vazquez, S., Leon, J. I., Franquelo, L. G., Rodriguez, J., Young, H. A., Marquez, A., & Zanchetta, P. (2014). Model predictive control: A review of its applications in power electronics. IEEE industrial electronics magazine, 8(1), 16-31.

[23] G. C. Goodwin, M. M. Seron, and J. A. D. Dona, Constrained Control and Estimation – An Optimization Perspective. Springer Verlag, 2005.

[24] Clarke, D. W., Mohtadi, C., & Tuffs, P. S. (1987). Generalized predictive control—Part I. The basic algorithm. *Automatica*, *23*(2), 137-148.

[25] C. E. Garcia, D. M. Prett, and M. Morari, “Model predictive control: theory and practice – a survey,”

[26] Richalet, J. (1993). Industrial applications of model based predictive control. *Automatica*, *29*(5), 1251-1274.

[27] Richalet, J., Rault, A., Testud, J. L., & Papon, J. (1978). Model predictive heuristic control. *Automatica (journal of IFAC)*, *14*(5), 413-428.

[28] J. Holtz and S. Stadtfeld, "A predictive controller for the stator current vector of AC machines fed from a switched voltage source," in International Power Electronics Conference, IPEC, Tokyo, pp. 1665–1675, 1983.

[29] Merabet, A. (2007). *Commande non linéaire à modèle prédictif pour une machine asynchrone*. Université du Québec à Chicoutimi.

[30] Benchabane, A. (2022). *Nonlinear predictive control applied to physical multi-input multi-output system* (Doctoral dissertation).

[31] Rodriguez, J., & Cortes, P. (2012). *Predictive control of power converters and electrical drives*. John Wiley & Sons.

[32] Behrooz, F., Mariun, N., Marhaban, M. H., Mohd Radzi, M. A., & Ramli, A. R. (2018). Review of control techniques for HVAC systems—Nonlinearity approaches based on Fuzzy cognitive maps. *Energies*, *11*(3), 495.

[33] Pfeiffer, C. F., Skeie, N. O., & Perera, D. W. U. (2014). Control of temperature and energy consumption in buildings-a review

[34] D. KARBOUA, B. TOUAL, and A. KOUZOU, "Contribution to the control of three-phase permanent magnet synchronous based on advanced technique." Ph.D. dissertation, Ziane Achour University of Djelfa, 2024.

[35] Deepti, Khimani., Sammyak, Mate., Sharad, Bhartiya. (2023). Model Predictive Control: Trade-offs between Performance and Computation time. Advances in Control and Optimization of Dynamical Systems, 57:77-82. doi: 10.1016/j.ifacol.2024.05.014

[36] (2022). 5. A Practically Stabilizing Model Predictive Control Scheme for Switched Affine Systems. doi: 10.1109/lcsys.2022.3210368

[37] Salam, Ibrahim, Khather., Muhammed, A., Ibrahim., Abdullah, I., Abdullah. (2023). Review and Performance Analysis of Nonlinear Model Predictive Control—Current Prospects, Challenges and Future Directions. Journal européen des systèmes automatisés, doi: 10.18280/jesa.560409

[38] Rahul, Kumar, Jha. (2023). Model Predictive Control for Matrix Converters in Grid-Interactive Applications. December, doi: 10.36548/jeea.2023.4.003

[39] H.NOUAR, A. KOUZOU Contribution à la commande prédictive à base de modèle d'un convertisseur polyphasé, Ph.D. dissertation, Ziane Achour University of Djelfa,, 2020.

[40] BENCHIHA, A. S., & DIABATE, F. (2019). Commande prédictive du moteur à courant continu.

[41] M. C. LOZADA, " Sur les Modèle Flous Adaptatifs Dynamiques ", Thèse de doctorat, l'Institut National des Sciences Appliquées de Toulouse

[42] Bezzini, A. (2013). *Commande prédictive non linéaire en utilisant les systèmes Neuro-Flous et les algorithmes Génétiques* (Doctoral dissertation, Faculté des sciences et de la technologie UMKBiskra).

[43] Hayette, M. E. S. L. O. U. B. (2016). Commande DTC Prédictive D'une Machine Synchrone à Aimants Permanents. *Université Mohamed Khider, Biskra*.

[44] Tahir, S., Wang, J., Baloch, M. H., & Kaloi, G. S. (2018). Digital control techniques based on voltage source inverters in renewable energy applications: A review. *Electronics*, *7*(2), 18.

[45] CHEBAANI, mohamed (2020) *Contrôle prédictif directe du couple d'un moteur asynchrone.* Doctoral thesis, Université Mohamed Khider – Biskra.

[46] Lu, P. (1995). Optimal predictive control of continuous nonlinear systems. *International Journal of Control*, *62*(3), 633-649.

[47] Bouguenna, I. F., Tahour, A., Kennel, R., & Abdelrahem, M. (2021). Multiple-vector model predictive control with fuzzy logic for PMSM electric drive systems. *Energies*, *14*(6), 1727.

[48] Gao, X., Abdelrahem, M., Hackl, C. M., Zhang, Z., & Kennel, R. (2019). Direct predictive speed control with a sliding manifold term for PMSM drives. *IEEE Journal of Emerging and Selected Topics in Power Electronics*, *8*(2), 1258-1267.

[49] Bao, G., Qi, W., & He, T. (2020). Direct torque control of PMSM with modified finite set model predictive control. Energies, 13(1), 234.

[50] Samithas, D., Balachandran, P. K., & Selvarajan, S. (2024). Experimental analysis of enhanced finite set model predictive control and direct torque control in SRM drives for torque ripple reduction. Scientific Reports, 14(1), 16805.

GENERAL CONCLUSION

This thesis focused on studying and analyzing wind energy systems based on the Doubly Fed Induction Generator (DFIG), with emphasis on system modeling, advanced control strategies, and sensor fault detection and compensation. The work was structured into five interrelated chapters, each addressing a fundamental aspect of wind energy system operation and control, providing a comprehensive framework for improving system performance and reliability.

Firstly, an overview of wind energy was presented, covering its historical development, environmental impact, and wind characteristics in Algeria. The classification of wind turbines based on their operational design and applications, whether in standalone or grid connected systems, was also discussed. Additionally, the concept of electromechanical energy conversion was introduced to establish a fundamental understanding of DFIG operation.

Next, a detailed mathematical modeling of the DFIG based wind energy system. This included wind dynamics, turbine modeling, and generator equations, with a focus on the Maximum Power Point Tracking (MPPT) technique to optimize energy extraction under different operating conditions. This modeling was essential for designing effective control strategies to ensure optimal system performance.

To enhance system performance, a chapter was dedicated to controlling the active and reactive power of the stator using advanced control strategies. The study implemented the BSC-LQR approach, which combines Backstepping Control (BSC) with Linear Quadratic Regulator (LQR) to achieve stable dynamic response and mitigate power fluctuations during sudden wind speed variations.

Furthermore, the impact of current sensor failures on system performance was investigated. An Extended Kalman Filter (EKF) was proposed to estimate rotor and stator currents in the presence of sensor faults, ensuring continuous operation and improving system reliability. Additionally, a fault detection method was developed to identify the faulty sensor, contributing to enhanced system performance and reducing maintenance requirements.

The final chapter focused on reducing operational costs and improving system reliability by eliminating the speed sensor and implementing an advanced control approach. A combination of Finite Set Predictive Current Control (FS-PCC) and Model Reference Adaptive System (MRAS) was applied for speed estimation. This strategy proved effective in improving system response

while minimizing reliance on additional sensors, thereby enhancing overall system efficiency and reducing maintenance costs.

Overall, this thesis provides a comprehensive framework for improving the efficiency and stability of DFIG based wind energy systems by integrating precise mathematical modeling, advanced control strategies, and intelligent sensor fault detection and compensation techniques. These findings contribute to the development of self-sustaining wind energy systems, enhancing their reliability and operational efficiency in dynamic and changing environmental conditions.

APPENDEX

Table 1: Parameters of the DFIG

Parameters	**Value**	**Unit**
Nominal power (Pn)	3	Kw
Stator frequency (F)	50	Hz
Nominal Voltage (Vs)	220	V
Nominal speed ($\boldsymbol{\omega_n}$)	1450	RPM
Stator inductance (Ls)	0.255	H
Rotor inductance (Lr)	0.255	H
Mutual inductance (Lm)	0.180	H
Stator resistance (Rs)	1.6	Ω
Rotor resistance (Rr)	1.8	Ω
Number of pairs poles (p)	2	
Gains for BSC	K1=3000, k2=900, k3=3000, k4=400	
Gains for BSC-LQR	K1=3000, k3=3000, $Q=0.01\begin{bmatrix}1&0&0&0\\0&1&0&0\\0&0&1&0\\0&0&0&1\end{bmatrix}$ $R=0.1\begin{bmatrix}1&1&1&1\\1&1&1&1\\1&1&1&1\\1&1&1&1\end{bmatrix}$	
PI regulator Gains for FSPCC	$K_p = 0.6 \;\; K_i = 6$	
PI regulator Gains for MRAS	$K_p = 100 \;\; K_i = 0$	
Turbine parameters	C_1=0.5176 C_2=116 C_3=0.4 C_4=5 C_5=21 C_6=0.0068 C_{p_max}=0.48 $\lambda_{opt} = 8.1$	

Abstract

With the increasing reliance on wind energy for electricity generation, researchers have conducted extensive studies to enhance power quality and maximize energy extraction. Among the various generator technologies, the Doubly-Fed Induction Generator (DFIG) has gained significant attention due to its ability to operate at variable speeds, making it well-suited for a wide range of wind conditions. This thesis provides a comprehensive study of wind energy, beginning with an overview of wind power generation, turbine operation, and the Maximum Power Point Tracking (MPPT) strategy for optimal power extraction. It also explores the process of electromechanical energy conversion through generators and presents an in-depth analysis of advanced control strategies and their classifications. A hybrid control approach integrating Backstepping Control (BSC) with the Linear Quadratic Regulator (LQR) is implemented to enhance system stability and performance. Additionally, the thesis investigates the impact of current sensors on control implementation and system operation. To address sensor failures, the Extended Kalman Filter (EKF) is utilized for current estimation and fault detection, ensuring continuous and reliable system performance. The final part of the study focuses on an advanced control strategy, Finite Set Predictive Current Control (FSPCC), combined with a sensorless approach using the Model Reference Adaptive System (MRAS) observer to eliminate the speed sensor. This approach not only reduces operational costs but also enhances system efficiency, making it a viable solution for real-time wind energy applications. By integrating precise system modeling, advanced control techniques, and sensor fault compensation strategies, this research contributes to the improvement of DFIG-based wind energy systems, enhancing their reliability, efficiency, and cost-effectiveness in practical applications.

Keywords: Wind energy, DFIG, MPPT, advanced control, BSC, LQR, EKF, FSPCC, MRAS.

Résumé

Avec la montée en puissance de l'énergie éolienne dans la production d'électricité, des recherches approfondies ont été menées pour améliorer la qualité de l'énergie et maximiser son extraction. Parmi les différentes technologies de génération, le générateur asynchrone à double alimentation (GADA) a suscité un grand intérêt en raison de sa capacité à fonctionner à vitesse variable, ce qui le rend adapté à un large éventail de conditions éoliennes. Cette thèse présente une étude complète de l'énergie éolienne, en commençant par une analyse théorique de la production d'énergie, du

fonctionnement des éoliennes et de la stratégie de suivi du point de puissance maximale (MPPT) pour une extraction optimale. Elle examine également le processus de conversion électromécanique à l'aide des générateurs, ainsi qu'une analyse approfondie des stratégies de commande avancées et de leurs classifications. Une approche de commande hybride combinant la commande Backstepping (BSC) avec le régulateur quadratique linéaire (LQR) a été mise en œuvre pour améliorer la stabilité et la performance du système. En outre, cette étude explore l'impact des capteurs de courant sur l'application des stratégies de commande et la performance du système. Pour pallier les pannes des capteurs, le filtre de Kalman étendu (EKF) a été utilisé pour estimer les courants et détecter les défauts, garantissant ainsi un fonctionnement fiable et continu. La dernière partie de cette recherche se concentre sur une stratégie de commande avancée, la commande prédictive de courant à ensemble fini (FSPCC), associée à l'observateur adaptatif à modèle de référence (MRAS) pour éliminer le capteur de vitesse. Cette approche permet de réduire les coûts opérationnels tout en améliorant l'efficacité du système, ce qui en fait une solution viable pour les applications pratiques des systèmes éoliens.

En combinant une modélisation précise, des techniques de commande avancées et des stratégies de compensation des défauts de capteurs, cette étude contribue à l'amélioration des performances des systèmes GADA, en renforçant leur fiabilité et leur efficacité opérationnelle dans des environnements dynamiques.

Mots-clés : Energie éolienne, GADA, MPPT, commande avancées, BSC, LQR, EKF, FSPCC, MRAS.

ملخص:

مع تزايد الاعتماد على طاقة الرياح في توليد الكهرباء، أجرى الباحثون دراسات مكثفة لتحسين جودة الطاقة وتعظيم استخراجها. ومن بين تقنيات التوليد المختلفة، حظي المولد الحثي مزدوج التغذية (DFIG) باهتمام واسع نظرًا لإمكانية تشغيله بسرعات متغيرة، مما يجعله مناسبًا لمجموعة واسعة من ظروف الرياح. تقدم هذه الأطروحة دراسة شاملة حول طاقة الرياح، بدءًا من الشرح النظري لعملية إنتاج الطاقة الريحية، وآلية تشغيل التوربين، واستراتيجية تتبع نقطة الاستطاعة القصوى (MPPT) لاستخراج أقصى قدرة ممكنة. كما تستعرض عملية التحويل الكهروميكانيكي للطاقة باستخدام المولدات، إلى جانب تحليل مفصل لاستراتيجيات التحكم المتقدمة وتصنيفاتها. تم تنفيذ نهج تحكم هجين يجمع بين التحكم بالتراجع (BSC) ومنظم LQR للتحكم في الاستطاعة الفعالة والردية وذلك لتعزيز استقرار النظام وأدائه. بالإضافة إلى ذلك، تتناول الدراسة تأثير حساسات التيار في تطبيق استراتيجيات التحكم وأداء النظام. وللتعامل مع أعطال المستشعرات، تم استخدام مرشح كالمان الممتد (EKF) لتقدير التيارات وتحديد مواقع الأعطال، مما يضمن استمرارية التشغيل وتحسين موثوقية النظام.

يركز الجزء الأخير من البحث على تطبيق استراتيجية تحكم متقدمة، وهي التحكم التنبئي بالتيارات ذات المجموعة المحدودة (FSPCC)، إلى جانب استخدام المراقب التكيفي ذو المرجعية النموذجية (MRAS) للتخلص من حساس السرعة. يساهم هذا النهج في تقليل تكاليف التشغيل مع تحسين كفاءة النظام، مما يجعله خيارًا فعالًا للتطبيقات العملية في أنظمة طاقة الرياح.
من خلال الجمع بين النمذجة الدقيقة، واستراتيجيات التحكم المتطورة، وأساليب تعويض أعطال المستشعرات، تسهم هذه الدراسة في تحسين أداء أنظمة DFIG وتعزيز موثوقيتها وكفاءتها التشغيلية في البيئات المتغيرة.
كلمات مفتاحية: طاقة الرياح , مولد الحثي مزدوج التغذية (DFIG), تتبع نقطة الاستطاعة القصوى (MPPT), استراتيجيات التحكم المتقدمة, التحكم بالتراجع (BSC), منظم LQR, مرشح كالمان الممتد (EKF), التحكم التنبئي بالتيارات ذات المجموعة المحدودة (FSPCC), مراقب التكيفي ذو المرجعية النموذجية (MRAS).